2014

Modeling and simulation of hydrokinetic composite turbine system

Haifeng Li

Department: Mechanical and Aerospace Engineering

MODELING AND SIMULATION

OF HYDROKINETIC COMPOSITE TURBINE SYSTEM

by

HAIFENG LI

A DISSERTATION

Presented to the Faculty of the Graduate School of the

MISSOURI UNIVERSITY OF SCIENCE AND TECHNOLOGY

In Partial Fulfillment of the Requirements for the Degree

DOCTOR OF PHILOSOPHY

in

MECHANICAL ENGINEERING

2014

Approved
K. Chandrashekhara, Advisor
Xiaoping Du
Joshua L. Rovey
Jonathan W. Kimball
Steve E. Watkins

PUBLICATION DISSERTATION OPTION

This dissertation has been prepared in the form of three papers for publication as follows:

Pages 7-63 have been submitted to Ocean Engineering

Pages 64-104 have been submitted to Engineering Optimization

Pages 105-139 are intended for submission to International Journal of Electrical Power & Energy Systems

ABSTRACT

The utilization of kinetic energy from the river is promising as an attractive alternative to other available renewable energy resources. Hydrokinetic turbine systems are advantageous over traditional dam based hydropower systems due to “zero-head” and mobility. The objective of this study is to design and analyze hydrokinetic composite turbine system in operation. Fatigue study and structural optimization of composite turbine blades were conducted. System level performance of the composite hydrokinetic turbine was evaluated. A fully-coupled blade element momentum-finite element method algorithm has been developed to compute the stress response of the turbine blade subjected to hydrodynamic and buoyancy loadings during operation. Loadings on the blade were validated with commercial software simulation results. Reliability-based fatigue life of the designed composite blade was investigated. A particle swarm based structural optimization model was developed to optimize the weight and structural performance of laminated composite hydrokinetic turbine blades. The online iterative optimization process couples the three-dimensional comprehensive finite element model of the blade with real-time particle swarm optimization (PSO). The composite blade after optimization possesses much less weight and better load-carrying capability. Finally, the model developed has been extended to design and evaluate the performance of a three-blade horizontal axis hydrokinetic composite turbine system. Flow behavior around the blade and power/power efficiency of the system was characterized by simulation. Laboratory water tunnel testing was performed and simulation results were validated by experimental findings. The work performed provides a valuable procedure for the design and analysis of hydrokinetic composite turbine systems.

ACKNOWLEDGMENTS

I would like to express my sincere gratitude to Dr. K Chandrashekhara for his valuable guidance, assistance and encouragement during my graduate study at Missouri University of Science and Technology. I will never forget the countless hours of discussion he spent with us. Thank him for generous support of providing excellent working environment and teamwork. It has been a great pleasure working with him.

I also want to extend my genuine appreciation to my advisory committee members, Dr. Xiaoping Du, Dr. Joshua L. Rovey, Dr. Jonathan W. Kimball, and Dr. Steve E. Watkins for their valuable time and advice in the review of this dissertation.

Great appreciation goes to Dr. Jian Chen for his important guidance and valuable training he provided prior to and during this research. I also wish to thank the assistance from my fellow colleagues, Dr. V. G. K. Menta, Dr. R. Vuppalapati, Mr. V. Bheem Reddy, Mr. Z. Huo, Mr. J. R. Nicholas, Mr. M. Mohamed, Mr. A. M. Abutunis, Mr. G. A. Taylor, Mr. S. Anandan and Mr. X. Wang.

I would like to acknowledge the financial support from Office of Naval Research in the form of graduate research assistantship and from Department of Mechanical and Aerospace Engineering at Missouri University of Science and Technology for a graduate teaching assistantship.

Finally, I wish to express my deepest gratitude to my family, and my friends for their company, understanding, and encouragement. Without their support, especially my wife, I would not be able to accomplish and fulfil my dreams.

TABLE OF CONTENTS

LIST OF ILLUSTRATIONS

Page

LIST OF TABLES

Page

SECTION

1. INTRODUCTION

Hydrokinetic turbine systems are zero-head hydropower systems which utilize kinetic energy from flowing water to generate power. The blade is a critical component in a hydrokinetic turbine system which governs the performance of the turbine system. Operating life of the blade is mainly depending on varying hydrokinetic loadings, water/mud corrosion and impact from floaters and fish schools. To create a successful blade design, interconnected parameters for load identification, geometry/structural design, static and fatigue failure evaluation require detailed investigation (Shokrieh and Rafiee, 2006). Distinctive characteristics of composites, in terms of light weight and corrosion resistance, make composite materials superior for river applications, as compared to metallic materials. Also, the high strength/stiffness and design flexibility of composites enable an optimal blade structural design with a complex geometric layout and improved load-carrying capacity with significantly less weight.

The application and installation of hydrokinetic turbine systems in rivers, tides, ocean currents and waves is quite promising. The potential hydroelectric power sites at the United States' rivers and estuaries are capable of providing up to 130, 000 gigawatt-hours per year, which is amount to half of the yearly dam-based electricity production (Sofge, 2009). While characterizing turbine performance, power output and power efficiency are the two key parameters of interest (Bahaj et al., 2007). Flow velocity and turbine rotor configurations such as pitch angle will significantly influence the power output and efficiency of the system. Parametric studies at various flow velocity, tip speed ratio (TSR), and blade pitch angle on the performance of the composite turbine system are essential (Cecile et al., 2009). A high-fidelity simulation tool is a key to characterize the hydrokinetic composite turbine system (McCann et al. 2006). Experimental study on a prototype level hydrokinetic turbine system is also important in terms of parametric study and validation of the simulation tool developed.

2. LITERATURE REVIEW

The manufacturing process of composite structures is quite complex. Specifically composite hydrokinetic turbine blades, various parameters in terms of fiber/matrix type, reinforcement structure, laminate stacking sequence, environmental conditions, and loading conditions (Degrieck and Paepegem, 2001) can influence the fatigue behavior of composite blades. These factors will accumulate damage to the composite blade and either independently or interactively affects the fatigue life. As a result of the booming of wind industry, the fatigue life of composite structures with application to wind turbine has been studied considerably, especially turbine blades. A fatigue database regarding composite materials for wind turbine blades (Mandell and Samborsky, 2010) was established under the joint effort from Department of Energy and Montana State University. Detailed fatigue results for composite materials used for wind turbine under constant/variable amplitude fatigue loadings were included. Sutherland and Mandell (2005a, 2005b) evaluated the damage of wind turbine blades due to the effects of mean stress and an optimized constant-life diagram. Samborsky et al. (2008) studied delamination at thick ply drops in both carbon and glass fiber laminates subjected to the fatigue loading. Unlike commercialized wind turbine systems, detailed studies on composites for hydrokinetic/tidal applications are very few. There is a certain degree of statistical variability regarding fatigue loads. These factors include material uncertainty, variable water velocity, and scattered S-N data. Young et al. (2010) investigated the effect of material and operational uncertainties on the performance of self-adaptive marine rotors using reliability based design and optimization methodology. Lange (1996) revealed that fatigue reliability is highly dependent on the model chosen. In flatter S-N curves, the spread in failure probabilities for a given turbine life increased. Also, due to the complexity of composite manufacturing processes, blade-to-blade variation has been rarely investigated (Nijssen, 2006). It is indicated that the reliability based analysis is a must for the fatigue analysis of composite blades.

In last decades, limited work has been done for hydrokinetic turbine blades, although extensive research on structural design and analysis of wind turbine blades. Zhu and Rustamov (2012) conducted structural finite element analysis on a 750-kW wind

turbine composite blade. The stacking of the blade lay-up was optimized to reduce the blade tip deflection and stress with respect to design operating condition. Poulose and Hu (2010) performed finite element strength analysis of a wind turbine blade. Three blade configurations of different fiber orientations were investigated. Based on stress, deflection and major factor failure criteria, a best orientation was selected. Forcier and Joncas (2012) studied the introduction of ribs to improve the structural rigidity while reducing the blade shell thickness. However, detailed lay-up specification and sequence are yet to be studied. For the emerging hydrokinetic applications, Bir et al. (2011) designed a horizontal-axis tidal turbine composite blade with optimal location of webs and minimum thickness while satisfying the ultimate-strength and buckling-resistance criteria. In these design processes, the trial and error method was used based on existing baseline designs. Significant amount of time was required and results might not be satisfactory.

A number of systemic studies on hydrokinetic turbine systems have been performed using combined experiment and simulation techniques. McCann et al. (2006) described a European design tool for tidal current turbines (GH Tidal Bladed) derived from wind industry. Tidal device modeling and standard development were discussed. Bahaj et al. (2007) conducted experimental performance evaluation of a 800 mm diameter turbine in a cavitation tunnel and a towing tank to validate the code. A set of data obtained from experiment was compared with GH-Tidal Bladed results regarding the shaft power and thrust generated by the turbine at different blade pitches and speeds. The experimental results demonstrated that the numerical code is capable of predicting the turbine performance. Clarke et al. (2007) investigated a contra-rotating tidal current turbine. The comparison of power coefficient between simulation (modified blade element modeling theory) and experiment shows a good agreement. Also, the concept of ducted turbine was potentially improving power coefficient. A power coefficient of 55% was obtained at a tip speed ratio (TSR) of 7 (Cecile et al., 2009). However, the study on hydrokinetic turbine systems using composites is limited; also the mechanism of hydrokinetic turbine systems is still not fully understood.

A survey of the literature indicates that although composite blades for wind turbine application have been studied extensively, the application on hydrokinetic

turbines is rare. Also, mainly the trial and error method is used for design and analysis of composite blades. Previous studies on composite hydrokinetic turbine are very limited at system level as well. Therefore, this work studied composite hydrokinetic turbine systems at both component and system level. The present work is divided into three parts: In the first part, a blade element momentum – finite element method (BEM-FEM) coupled model was developed to predict the behavior of the composite blade subjected to varying hydrokinetic loads. The model was implemented to study the reliability-based fatigue life of a medium-scale composite hydrokinetic turbine blade. In the second part, structural optimization of laminated composite hydrokinetic turbine blade was performed using particle swarm optimization (PSO), aiming for less weight and better load-carrying capability. In the third part, the model was extended to design and evaluate the performance of a horizontal axis hydrokinetic composite turbine system. Water tunnel experiments were conducted and the results were used to validate the numerical model developed.

3. SCOPE AND OBJECTIVES

This dissertation comprises three papers corresponding to the following problems.

The first paper is titled "**Reliability-based Fatigue Life Investigation for a Medium-scale Composite Hydrokinetic Turbine Blade**." In this paper, a reliability-based fatigue life analysis methodology was developed for a medium-scale hydrokinetic turbine blade. The finite element method coupled with the blade element momentum theory (FEM-BEM) was used to find the spontaneous stress response of the turbine blade. Stress-critical zones were monitored to study the fatigue behavior of the blade. Random load cases were calculated based on the rate-of-occurrence of the flow pattern of the Missouri river. The allowable fatigue strengths, specifically S-N curve, were generated from the MSU/DOE fatigue database. Linear Goodman diagram with the modified stress ratio was developed for coefficient derivation based on the required design life. A metamodel of stress response was constructed depending on simulations at specified design points. A reliability analysis method, accounting for uncertainties in material properties and the S-N curve, was employed to predict the fatigue life distribution of the composite hydrokinetic turbine blade.

The second paper is titled "**Particle Swarm based Structural Optimization of Laminated Composite Hydrokinetic Turbine Blades**." In this paper, detailed lay-up optimization was performed for laminated composite hydrokinetic turbine blades using particle swarm optimization (PSO) technique. A two-step online automated optimization methodology was developed including weight targeted particle swarm optimization and stacking sequence optimization to improve load-carrying capacity. In the first step, independent parameters in terms of layer numbers, ply thickness and ply orientations were optimized to minimize weight of the blade while satisfying failure evaluation. BEM-FEM coupled model was implemented to predict stress behavior of the blade under hydrokinetic loadings. Three composite failure criteria (maximum stress, Tsai-Hill and Tsai-Wu criteria) were utilized to design the most conservative blade design. In the second step, discrete combinatorial optimization of blade stacking sequence was conducted to maximize out-of-plane load-carrying capacity of the blade using a novel permutation discrete particle swarm optimization model. To improve the efficiency of the

algorithm, concepts of valid/invalid exchange and memory checking were introduced. A final optimized composite blade with significant material saving and improved structural performance was presented.

The third paper is titled "**Design and Performance Evaluation of a Hydrokinetic Composite Turbine System**." In this paper, a three-blade horizontal axis hydrokinetic composite turbine system was designed, manufactured and tested in a water tunnel. To characterize wake flow behind the chosen hydrofoil, computational fluid dynamics (CFD) simulation was performed and the result was validated with particle image velocimetry (PIV) measurements. A numerical simulation model based on the modified blade element momentum (BEM) theory was developed to predict the power and power coefficient of the manufactured composite turbine system. Experiments monitoring performance of the composite turbine system in a water tunnel were conducted. Tip-speed ratio, torque and corresponding power output of the turbine system at various blade pitch settings and water velocities were investigated. The effect of pitch angle, water velocity and tip-speed ratio on the performance of the turbine system was evaluated and compared with parametric numerical simulation. The developed simulation methodology was validated by water tunnel experimental findings. This study provides useful guidelines for the design and performance evaluation of hydrokinetic composite turbine systems.

PAPER

I. RELIABILITY-BASED FATIGUE LIFE INVESTIGATION FOR A MEDIUM-SCALE COMPOSITE HYDROKINETIC TURBINE BLADE

H. Li[1], Z. Hu[1], K. Chandrashekhara[1], X. Du[1] and R. Mishra[2]

[1] *Department of Mechanical and Aerospace Engineering*

Missouri University of Science and Technology, Rolla, MO 65409

[2] *Department of Material Science and Engineering*

University of North Texas, Denton, TX 76203

ABSTRACT

As the most important, expensive component of the hydrokinetic turbine system, the composite turbine blade must achieve a long operating life (10-20 years). The investigation of fatigue life for the composite turbine blade is essential when designing a cost-effective hydrokinetic composite turbine system intended for safe, long-term operation. A reliability-based fatigue life analysis methodology was developed for a medium-scale, horizontal axis, hydrokinetic turbine blade. Finite element method, coupled with the blade element momentum theory, was used to find the stress response on the turbine blade. The fatigue behavior of the blade was studied in stress-critical zones. Random load cases were weighted by rate-of-occurrence from stream patterns of the Missouri river. The allowable fatigue strengths were determined from the MSU/DOE fatigue database for the S-N curve. Coefficients were derived from linear Goodman diagram with the modified stress ratio and the required design life. A metamodel was constructed for the stress response according to simulations at specified design points. Accounting for uncertainties in material properties and the material S-N curve, the reliability analysis method was employed to estimate the fatigue life distribution of the

hydrokinetic turbine blade. The probability of fatigue failure of the composite blade was most sensitive to the composite material S-N data. Transverse modulus E_{22} of the composite material imposed more sensitivity relating to the matrix cracking (fatigue failure mode), as compared to other directional properties.

1. INTRODUCTION

Hydrokinetic turbines are zero-head hydropower. The turbines use hydrokinetic power from flowing water to generate power. In many ways, hydrokinetic turbines resemble wind turbines. The most notable difference is in density; the density of water is approximately 850 times greater than the density of air. Thus, more energy is expected from a hydrokinetic turbine . Due to the vast resources of hydrokinetic/tidal energy on the earth, research into hydrokinetic/tidal turbine systems, as an alternative renewable energy, has been booming in recent years (Khan et al., 2009; Schwartz et al., 2006).

The blade is the key component in a hydrokinetic turbine system; it determines the performance of the turbine system. A hydrodynamic profile design of the turbine blade is required to extract the maximum energy from water flow. Environmental conditions must be considered when designing the blade. Varying hydrokinetic loadings, water/mud corrosion and impact from floaters and fish schools each has a significant effect on the blade's operating life. From a structural point of view: 1) the hydrokinetic turbine blade is long and flexible; 2) there are possibilities of vibrations in the resonant mode; 3) the randomness of water velocity causes the randomness of load spectra; 4) low maintenance is expected during operating under water with different conditions (Shokrieh

and Rafiee, 2006). Load identification, geometry/structural design, static failure, and fatigue failure all need to be addressed to create a successful blade design.

Typical fatigue loads on hydrokinetic turbine blades include stochastic hydrodynamic loadings from water streams, weight and buoyancy of the composite blade, and induced centrifugal and coriolis force (Nijssen, 2006). The stochastic hydrokinetic loadings include the flapwise loads and the edgewise loads. The flapwise loads originate, primarily from the water load. This load acts perpendicular to the rotor plane. The edgewise loads originate, primarily from the blade weight, buoyancy forces from water volumes occupied by the blade body, and also the torque loads that drive the rotor. The loading direction for edgewise loads changes twice during a revolution.

As per materials, attractive characteristics of composites, like light weight, high strength/stiffness, design flexibility and corrosion resistance (as compared to metallic materials), make composite materials an advantageous option for river applications. Based on these characteristics of composites, Manufacturing using composites is capable of achieving a structural design with a complicated geometric layout and adequate load-carrying capacity, while achieving significant weight reduction.

The manufacturing process for composite structures is quite complex. As a result, various parameters can influence the fatigue behavior of composites in terms of fiber/matrix type, reinforcement structure, laminate stacking sequence, environmental conditions (both temperature and moisture), and loading conditions (stress ratio, frequency) (Degrieck and Paepegem, 2001). The damage accumulation of composites from these factors may either independently or interactively affect fatigue life. Over the last several decades, various fatigue damage models of fiber reinforced composite

materials have been developed. These models can be mainly categorized into three sections: 1) S-N curves/Goodman diagrams incorporating fatigue failure criterion with no degradation mechanisms, 2) Phenomenological models based on residual stiffness/strength, and 3) progressive damage models utilizing damage variables to characterize different damage mechanisms (e.g. matrix cracks and delamination). Detailed discussions on the development of fatigue damage models of fiber-reinforced composite materials can be found in review papers (Degrieck and Paepegem, 2001; Post et al., 2008).

The fatigue life of composites for wind turbine blade applications has been studied considerably as a result of the rapid growth in the wind industry. A Department of Energy/Montana State University (DOE/MSU) composite material fatigue database for wind blades (Mandell and Samborsky, 2010) was established under sponsorship of Sandia National Laboratories (SNL). The database includes detailed fatigue results for composite materials under constant/variable amplitude fatigue loadings. Sutherland and Mandell (2005a, 2005b) studied the effect of both mean stress and an optimized constant-life diagram on the damage of wind turbine blades. Samborsky et al. (2008) investigated the fatigue loading effect on delamination at thick ply drops in both carbon and glass fiber laminates. Comparatively, study regarding composites used for hydrokinetic/tidal applications is still much less. Some preliminary studies can be seen in (Mahfuz and Akram, 2011; Kennedy et al., 2011; Li et al. 2012).

Fatigue loads on hydrokinetic turbine blades have a certain degree of statistical variability. These factors comprise material variability, variable water velocity, and scattered S-N data. Young et al. (2010) quantified the influence of material and

operational uncertainties on the performance of self-adaptive marine rotors. A reliability based design and optimization methodology for adaptive marine structures was developed. Lange (1996) found fatigue reliability is significantly dependent on the type of model chosen. An increasing spread in failure probabilities for a given turbine life was observed in flatter S-N curves. Blade-to-blade variation has been characterized very little due to the complexity of composite manufacturing processes (Nijssen, 2006). Hence, the reliability method should be introduced into the fatigue analysis of composite blades.

The study on composite blades for hydrokinetic applications is very limited and there is a lack of complete characterization of factors' effect (material, flow, and fatigue data) on the fatigue life. The purpose of this paper is to quantify both the effects of material, loading uncertainties on the stress response and fatigue data on the fatigue life distribution of a medium-scale hydrokinetic composite turbine blade. The optimized composite turbine blade is intended to be deployed in Missouri River. A fully-coupled blade element momentum-finite element method (BEM-FEM) was used to compute the stress response of the turbine blade. Modeling uncertainties were conducted with Hashin failure initiation model to correlate with the fatigue failure mode of the turbine blade. The fatigue model was based on both MSU/DOE experimental S-N data and the residual strength approach to cumulative damage. The probability of fatigue failure was evaluated. The effects of the river flow velocity model were investigated on the fatigue probability distribution of the turbine blade.

2. STRUCTURAL DESIGN OF THE COMPOSITE BLADE

2.1 Hydrodynamic profile

The composite blade was designed for three-blade, horizontal axis, hydrokinetic turbine systems. It has a length of 1 m, and varying cross sections with an 8 degree twist angle. The circular root section was designed for easy mounting on the hub. The blade consisted of eight blade stations, as shown in Fig. 1. The blade profile was based on the hydrofoil Eppler 395. The hydrofoil provides a high ratio of C_l/C_d . Detailed identification of both the hydrodynamic profile and the corresponding hydrodynamic loadings on the blade surface, with varying tip speed ratio (TSR), is illustrated in Section 3.

2.2 Facesheet and core materials

Hydrokinetic turbine systems operating under water experience highly repetitive hydrodynamic loadings. Also, bio-fouling and corrosion issues need to be addressed properly. The hydrokinetic turbine blade facesheet made of composite materials with a high modulus and strength provides excellent static failure resistance. Corrosion issues can also be effectively prevented with the use of composite materials (Anyi and Kirke, 2010). Widely used carbon fibers normally cost 10 to 20 times as much as glass fibers. Carbon fibers do, however, provide a much higher modulus and weight reduction. An E-glass/epoxy material was selected as a compromise between price and performance. Initial work on the blade design was conducted, based on both trial and error and numerical optimization methods (Li and Chandrashekhara, 2012). In the current study, E-glass/epoxy laminates with $[0_2/90_2/0_2/90_2]$ ply orientations were used to form the facesheet of the hydrokinetic turbine blade. Each ply thickness was 0.356 mm.

Various blade core configurations (Fig. 2) were evaluated to obtain an optimal blade internal structural layout (Berry, 2007): hollow, solid foam, composite shear web, and both foam and shear web. Blades with a facesheet only tend to provide the lightest solution when operating under water. Water impermeability is prevented as water is prone to intrude the cavity of the blade. The water intrusion causes extra dynamic loadings when the blade is rotating and significantly reduces the fatigue life of the blade. The core material selected requires high buckling resistance, water impermeability, and high strength to weight ratios. Divinycell HCP 100 was selected to provide excellent hydraulic compressive properties, a closed cell structure with very low buoyancy loss, and water absorption under long-term loading conditions. Moreover, HCP 100 offers excellent ductile characteristics; it is suitable for hydrokinetic turbine blades which experience either impact or slamming loads from floaters and schools of fish. Given the water impermeability of the turbine blade, the weight of the turbine blade tends to be offset by neutral buoyancy. The buoyancy from the core material is beneficial for a fatigue load reduction of the rotor and a higher power extraction from water. However, it seems insufficient with only solid foam to withstand shear loading. Thus, the concept of a shear web was introduced. Therefore, solid foam, combined with a shear web, was adopted for the blade core design to provide water impermeability and maintain a shear loading capacity.

2.3 Failure mode of the composite blade

An appropriate damage initiation model must be chosen to evaluate the failure mode of the composite blade. Unlike maximum stress/strain, Tsai-Hill and Tsai-Wu criterion, Hashin damage considers four different failure modes: fiber tension, fiber compression, matrix tension, and matrix compression. Failure in the ply thickness

direction is ignored. Hashin damage predicts the dominating factor that influences the cracking/failure of the composite blade. Predictions from Hashin damage were used in this study to provide both the critical material points and the corresponding failure modes necessary for fatigue failure evaluation. The initiation criteria (Hashin, 1980) used was as follows:

- Fiber tension ($\hat{\sigma}_{11} \geq 0$): $F_f^t = (\frac{\hat{\sigma}_{11}}{X^T})^2 + \alpha(\frac{\hat{\tau}_{12}}{S^T})^2$
- Fiber compression ($\hat{\sigma}_{11} < 0$): $F_f^c = (\frac{\hat{\sigma}_{11}}{X^C})^2$
- Matrix tension ($\hat{\sigma}_{22} \geq 0$): $F_m^t = (\frac{\hat{\sigma}_{22}}{Y^T})^2 + (\frac{\hat{\tau}_{12}}{S^L})^2$
- Matrix compression ($\hat{\sigma}_{22} < 0$): $F_m^c = (\frac{\hat{\sigma}_{22}}{2S^T})^2 + \left[\left(\frac{Y^C}{2S^T}\right)^2 - 1\right]\frac{\hat{\sigma}_{22}}{Y^C} + (\frac{\hat{\tau}_{12}}{S^L})^2$ (1)

where F represents the typical failure initiation prediction (a value greater than 1 indicates failure); superscript t/T and c/C represent tension and compression, respectively, subscript f and m represent fiber and matrix, respectively; X, Y and S represent the longitudinal, transverse and shear strength separately; S^L and S^T represent the longitudinal and transverse shear strength, respectively; α is the coefficient that determines the contribution of the shear stress to the fiber tensile initiation criterion; and $\hat{\sigma}_{11}, \hat{\sigma}_{22}$, and $\hat{\tau}_{12}$ are components of the effective stress tensor.

Stress from each ply through the blade thickness was calculated to identify structural failure of the composite blade under applied hydrodynamic loadings. The Hashin failure criterion was then applied based on current stress conditions. The first ply failure (FPF) was regarded as the structural failure initiation of the hydrokinetic turbine blade (Zhang and Yang, 2009). The composite blade of the current design should not experience stress higher than FPF. Detailed implementation of the methodology in the

finite element model of composite blades is illustrated in detail in Section 3. Table 1 lists the structural performance of the composite blades under specified hydrodynamic loadings. Three blade configurations were evaluated at a water velocity 2.47 m/s. Figure 3 illustrates the critical stress spots within the turbine blades. The maximum Hashin failure index the blade experienced was reduced by 38.2% when foam was present; the critical stress spot was transformed to stations 5-6. The complete design of the blade (with foam) greatly relieved stress at the root section, though it added more weight to the entire rotor system. This weight, however, was alleviated by the buoyancy the foam provided. Both the hollow blade and the blade with solid foam only tended to have high stress values in the region between station 4 and station 6. The existence of a shear web significantly reduced the stress level at the outer bound of the blade; it effectively prevents buckling/breakage of the blade at outer bound.

3. BEM-FEM COUPLED METHOD

The BEM-FEM coupled method determines the stress response of the composite turbine blade at any given hydrokinetic loading condition. Computational fluid dynamics (CFD) analysis tends to give more detailed and accurate fluid effect on the turbine blade. However, the BEM-FEM coupled method proposed in this paper is capable of yielding faster and more efficient solutions at any specified blade geometry/structure configurations. Parametric studies of reliability-based fatigue analysis could be achieved in significantly less time. It is especially time-saving under the circumstance that significant sampling points are required to construct the stress response of the blade.

Figure 4 illustrates the flowchart of the BEM-FEM coupled method developed. The method uses Xfoil to obtain the hydrodynamic coefficients of hydrofoils at different stations. With the input from real time flow velocity and the blade geometric configuration, the real time hydrodynamic forces were calculated using the BEM method in MATLAB. The forces were the input to the finite element model using ABAQUS. Based on the existing blade structural lay-up, structural response of the blade was obtained. The stress analysis results of ABAQUS were then transferred back to MATLAB for post-processing. During the next step of the analysis, water velocity model will be called again for an updated flow velocity. Every data point obtained from the analysis was processed in MATLAB as well (input to the fatigue reliability computational block).

3.1 Hydrodynamic performance of hydrofoils

The baseline blade construction was based on hydrofoil Eppler 395, as shown in Fig. 5. Fully hydrodynamic performance of Eppler 395, namely lift/drag coefficients, needs to be characterized at specified angle of attacks/Reynolds numbers. The smooth geometric transition between blade root section and tip indicates hydrodynamic characteristic variation at different blade cross sections as well. Xfoil (Drela, 2006), which is widely accepted as an effective tool for low Reynolds number airfoil design was used to address this issue. Xfoil combines second order panel method and fully-coupled viscous/inviscid interaction. The software is capable of simulating small to medium flow separation and yielding acceptable results for large flow separation. Coefficients of drag/lift both at the Reynolds number of turbine operation and a low range of angle of attack [0, 15] degree were calculated to obtain accurate results.

Inputting BEM, however, requires a complete hydrofoil dataset at each cross-section over a [-180,180] degree range angle of attack. The hydrofoil table from Xfoil was extended to large angle of attacks using the Viterna method (Viterna and Janetzke, 1982):

$$C_{D_{max}} = 1.11 + 0.018AR$$

$$C_D = C_{D_{max}} \sin^2 \alpha + B_2 \cos \alpha$$

$$C_L = \frac{C_{D_{max}}}{2} \sin 2\alpha + A_2 \frac{\cos^2 \alpha}{\sin \alpha} \quad (2)$$

where $B_2 = \frac{C_{D_s} - C_{D_{max}} \sin^2 \alpha_s}{\cos \alpha_s}$, $A_2 = (C_{D_s} - C_{D_{max}} \sin \alpha_s \cos \alpha_s) \frac{\sin \alpha_s}{\cos^2 \alpha_s}$, s denotes the value at the stall angle, and AR is the blade aspect ratio. A smooth, geometric transition exists between the root section and the blade tip. Thus, unknown hydrodynamic characteristics from transitional cross-sections (blend hydrofoil) are obtained by weighting. Figures 6 and 7 illustrate the typical lift coefficient and drag coefficient, respectively, including all 8 stations in the range [-180,180] after interpolation and weighting.

3.2 Hydrokinetic loadings on the turbine blade

The BEM theory is an extension of the actuator disk theory. This theory combines the conservation of momentum theory with the blade element theory (Buckland et al., 2010). No-radial-dependency is assumed. As stated, BEM, compared to CFD analysis, is capable to give time-efficient and reliable solutions at any given blade geometry, pitch angle, angular velocity and river velocity. Fatigue analysis would also be an intensive calculation process due to the variability of the water velocity model and uncertainties within the materials. BEM was adopted in this study to calculate the loads on the blade

surface. Prandtl tip loss, Glauert correction and hub loss was incorporated in BEM to improve solution accuracy (Sale et al., 2009).

Figure 8 illustrates the induced velocity field around a hydrofoil. The induced velocity in the axial direction is specified with the axial induction factor a as aV_o, where V_o is the undisturbed water velocity. The induced tangential velocity in the rotor wake is specified with the tangential induction factor a' as $a'\omega r$. Variable ω represents the angular velocity of the rotor, and r is the radial distance from the rotational axis. Variable ϕ is the flow angle, θ is the sectional pitch angle, and α is the local angle of attack. Variable α is used to interpolate from hydrofoil table to get the corresponding C_l and C_d.

The Prandtl tip loss model corrects the assumption of an infinite number of blades. The model estimates the vortices influence, which shed from the blade tips, on the induced velocity field in the rotor plane. Equations accounting for the blade tip loss, hub loss, and their combined effect are given by:

$$F_{tip} = \frac{2}{\pi}\cos^{-1}[e^{-\frac{B\,(L-r)}{2r\sin\phi}}]$$

$$F_{hub} = \frac{2}{\pi}\cos^{-1}[e^{-\frac{B\,(r-R_{hub})}{2R_{hub}\sin\phi}}]$$

$$F = F_{tip}F_{hub} \tag{3}$$

where L is the blade length, R_{hub} is the radius of the hub, and B is the number of blades.

With a known section angle of attack, both the lift coefficient (C_l) and the drag coefficient (C_d) were extracted from the hydrofoil table at every iteration.

BEM is typically an iterative process. The thrust coefficient is an indicator to update both a and a' at each iteration with

$$C_T = \frac{\sigma(1-a)^2(C_l \cos\phi + C_d \sin\phi)}{\sin^2\phi} \tag{4}$$

where σ is the blade element solidity.

Both a and a' are then updated for the next iteration, when $C_T \leq 0.96F$:

$$a = \left[1 + \frac{4F\sin^2\phi}{\sigma(C_l \cos\phi + C_d \sin\phi)}\right]^{-1} \tag{5}$$

If $C_T > 0.96F$, the blade element is highly loaded and operating in a turbulent wake state. A modification to the Glauert empirical relation was applied (Buhl, 2004). Variable a is instead updated with

$$a = \frac{18F - 20 - 3\sqrt{C_T(50-36F)+12F(3F-4)}}{36F-50} \tag{6}$$

Meanwhile, a' is updated with

$$a' = \left[\frac{4F\sin\phi\cos\phi}{\sigma(C_l \sin\phi - C_d \cos\phi)} - 1\right]^{-1} \tag{7}$$

Once the iterative process converges, and the induction factors have been obtained at every blade element, the relative water velocity can be obtained with $V_{rel} = \frac{\omega r(1+a')}{\cos(\phi)}$. As the lift and drag coefficients (C_l and C_d) were extrapolated from the hydrofoil table, the lift (L) and drag (D), per station length, can be computed with

$$L = \frac{1}{2}\rho V_{rel}^2 c C_l$$

$$D = \frac{1}{2}\rho V_{rel}^2 c C_d \tag{8}$$

Both the force normal and tangential to the rotor plane, as shown in Fig. 9, can then be obtained with

$$F_N = L\cos\phi + D\sin\phi$$

$$F_T = L\sin\phi - D\cos\phi \tag{9}$$

These loads serve as the input to the finite element model.

The hydrodynamic loadings obtained from MATLAB simulation were validated with Bladed Tidal (G.H. Ltd., 2012) for the demo blade provided by the software. The validation ensures fidelity of the hydrodynamic load input to the finite element model of the blade. The demo blade was intended for a three-blade tidal turbine system. It was 10.5 m long with an 8.5° twist. It operated at a tidal velocity of 3 m/s and a fixed pitch of 0°. The tip speed ratio (TSR) was equal to 3 (i.e., rotational velocity was 7.54 rpm). Numerical analysis solutions were obtained from both the in-house code and Blade Tidal. A verification of the results in terms of normal/tangential forces, axial/tangential induction factors, and lift/drag coefficient along the blade was conducted. Figure 10 demonstrates the comparison of normal (out-of-plane) and tangential (in-plane) forces for the specific case between two codes.

3.3 Finite element model of the turbine blade

Finite element method was used to identify the turbine blade's critical stress spots. It was also used to evaluate the blade's structural failure. The commercial software package ABAQUS 6.10 (Dassault Systèmes, 2010) was used for the stress analysis of the composite blade. Table 2 lists the material properties of the E-glass/epoxy lamina used in the simulation. The BEM code's output was in-plane/out-of-plane hydrokinetic loadings, per unit length, on the blade's surface. These loadings were integrated over adjacent blade stations. Each station span (8 in total) was applied with concentrated hydrodynamic forces on the blade surface using the multi-point constraint (MPC) technique. Concentrated loads were applied on reference nodes sets along the pitch axis of the turbine blade. Structural distributing coupling was adopted to interconnect degrees of freedom between the control point and the certain blade station surface. The structural

coupling method couples the translation and rotation of the reference node to the translation and the rotation motion of the coupling nodes, respectively. This method is well-suited for bending problems of composite blade; the coupling constraint covers small sections of nodes, and the reference node is very close to the constrained surface.

The composite blade was treated as an encastre beam with all degrees of freedom fixed at the root section. Loadings including the weight of the composite blade $\{F_w\}$, the buoyancy force $\{F_b\}$ due to water, the induced centrifugal force $\{F_{ce}\}$, and the coriolis force $\{F_{co}\}$ were each considered when fully characterizing the turbine blade's loading condition during the operation (Young et al., 2010). The structural analysis of the rotating blade-fixed coordinate system was formulated as:

$$[K]\{u\} = \{F_h\}+\{F_w\} + \{F_b\} + \{F_{ce}\} + \{F_{co}\} \quad (10)$$

where $\{u\}$ is the structural nodal displacement vector, $[K]$ is the stiffness matrix and $\{F_h\}$ is the hydrodynamic force. Figure 11 depicts the finite element model of the composite blade (S4R shell elements). Each lay-up was modeled individually using S4R shell elements. All the forces were applied through ABAQUS load module. $\{F_h\}$ was the output from the BEM model. $\{F_w\}$, $\{F_b\}$, $\{F_{ce}\}$ $\{F_{co}\}$ were applied in forms of periodic gravity, body force, rotational body force, and Coriolis force, respectively. The low-cycle calculation of the rotating composite blade was conducted in ABAQUS. Figure 12 illustrates the simultaneous stress variation with time of the stress concentration spot, at the root section of the blade, under five normalized loading cycles. The stress was extracted from the surface layer (0°) of the composite blade in transverse direction.

4. FATIGUE LIFE OF THE COMPOSITE BLADE

4.1 Water velocity model

The river flow velocity, which governs the fatigue life of the turbine blade, is a stochastic process. River velocity varies at different time instants due to natural variability. The design of hydrokinetic turbine systems is a relatively new research topic. Thus, no close form is available to describe the distribution of river flow velocity. There are some researchers have devoted efforts in the modeling of statistical distribution of river flow velocity (Beersma and Buishand, 2004； Hu and Du, 2012). However, in this paper, three common distributions were used to describe the river velocity since not enough data is available to determine the optimal for the Missouri river. The three distributions used include the normal, lognormal, and Weibull distributions. At the beginning, samples were generated for the river flow velocity for the fatigue life analysis of the composite hydrokinetic turbine blade.

The Expansion Optimal Linear Estimation method (EOLE) (Sudret, 2008) was used to generate samples for the stochastic process of river flow velocity over a time interval $[0, t_s]$. The time interval $[0, t_s]$ was divided into s time points: $(t_i)_{i=1,2,\cdots,s} = (t_0, t_1, t_2, \ldots, t_s)$. After the discretization, the non-Gaussian distribution of river velocity $V(t)$ was transformed into a function of a standard Gaussian stochastic process, as bellows:

$$V(t) = F_V(U(t)) \tag{11}$$

Based on the transformation and discretization, the correlated stochastic samples of $U(t)$ was then generated using the following formula:

$$U(t)=\sum_{i=1}^{p}\frac{U_i}{\sqrt{\eta_i}}\varphi_i^T\rho_U\left(t,t_i\right) \tag{12}$$

where U_i ($i=1,2,\cdots,p\le s$) are independent, standard, normal, random variables. Variables η_i and φ_i^T are the eigenvalues and eigenvectors of the correlation matrix ($\sum$), respectively, in the form of $\Sigma\varphi_i=\eta_i\varphi_i$. $\sum$ is given as follows:

$$\sum=\begin{pmatrix}\rho_U\left(t_1,t_1\right) & \rho_U\left(t_1,t_2\right) & \cdots & \rho_U\left(t_1,t_S\right)\\ \rho_U\left(t_2,t_1\right) & \rho_U\left(t_2,t_2\right) & \cdots & \rho_U\left(t_2,t_S\right)\\ \vdots & \vdots & \ddots & \vdots\\ \rho_U\left(t_S,t_1\right) & \rho_U\left(t_S,t_2\right) & \cdots & \rho_U\left(t_S,t_S\right)\end{pmatrix}_{s\times s} \tag{13}$$

It should be noted that the eigenvalues are sorted in decreasing order. $p\le s$ is the number of terms in the summation, corresponding to the p largest eigenvalues.

The ELOE method is an effective approach to generating samples for stochastic processes. River velocity samples were generated for the fatigue life analysis of the composite turbine blade with Eq. (11)-(13). Figure 13 displays a sample water velocity versus time.

4.2 Fatigue stress cyclic counting

The transient simultaneous stress response of the turbine blade was obtained via BEM-FEM coupled method with the aid of metamodel construction (see Section 5). The random nature of the time dependent stress spectrum requires an appropriate cycle counting algorithm. The algorithm was used to reduce the variable amplitude stress cycles into a series of simple constant stress amplitude cycles or half cycles. When compared to other counting methods (e.g., level crossing and range-mean), rainflow counting is a much better method as the mean (or R value) information is retained. In the current study, the rainflow counting algorithm which follows the ASTM standard was

used (ASTM standard, 1985). Data extracted includes stress cycles with stress amplitude, mean stress and cycle numbers. Figure 14 illustrates both the typical mean value and the amplitude distribution of stress cycles after applying the rainflow cyclic counting algorithm under the sample river flow velocity. Most of the cycles fall into the stress region with low mean and amplitude.

4.3 Constant-life diagram

S-N data is required to estimate the number of cycles to failure, at any specified stress amplitude, of the hydrokinetic turbine blade. The fatigue behavior of the composite blade material is, typically, fully presented as a constant-life diagram (CLD). S-N data are plotted as a function of mean stress and amplitude along lines of R values in the CLD. In the current numerical study, the normalized S-N curve of cross-ply E-glass/epoxy laminates used (R=0.1) was derived from the MSU/DOE composite fatigue database (Mandell and Samborsky, 2010):

$$\frac{\sigma_{max}}{\sigma_o} = 1.0 - 0.1 \times \mathrm{Log^N} \tag{14}$$

The calculated stress cycle ratio from individual stress cycle indicates very high mean stresses. Thus, a linear Goodman equation was used to correct the mean stress effect (Nijssen, 2006):

$$\frac{\sigma_a}{\sigma_{N_f}} + \frac{\sigma_m}{\sigma_0} = 1 \tag{15}$$

where σ_{N_f} is the stress amplitude for finite fatigue life N_f under fully reversed (R=-1) loading conditions and σ_a is the alternating stress amplitude with respect to the mean stress σ_m. R is defined by:

$$R = \frac{\sigma_{min}}{\sigma_{max}} = \frac{\sigma_m - \sigma_a}{\sigma_m + \sigma_a} \tag{16}$$

where σ_{min} and σ_{max} are the minimum and maximum stress of a typical stress cycle, respectively.

A full CLD was constructed based on above calculation (Fig. 15). Less stress cycles to failure were expected for stress with either high mean or high alternative stress.

4.4 Damage accumulation model

A non-linear residual strength model (Sutherland and Mandell, 2005a, 2005b) was adopted in this study to calculate damage accumulation that leads to blade fatigue failure. The non-linear residual strength model has the form:

$$(\sigma_R)_i=\sigma_0-(\sigma_0-\sigma_i)\left(\frac{n_i}{N_{f_i}\left(\sigma_{m_i},\sigma_{a_{ij}}\right)}\right)^v \quad (17)$$

where n_i is the number of applied cycles, N_{f_i} is the number of cycles to failure at a specified stress state $\left(\sigma_{m_i},\sigma_{a_i}\right)$, $(\sigma_R)_i$ is the residual strength after step i, σ_i is the peak stress amplitude of the hydrokinetic loading at step i, σ_0 is the static strength, and v is the nonlinear degradation parameter. Failure occurs when the applied hydrokinetic loadings cannot be withstood by the residual strength of the composite blade.

5. RELIABILITY-BASED FATIGUE LIFE DISTRIBUTION

Uncertainties in the process of the fatigue life investigation were analyzed in this section. A metamodel was then constructed for the stress response of turbine blades. The fatigue life distribution, sensitivities of random variables, and effect of rive velocity model on fatigue life were then studied using the first order reliability method.

5.1 Uncertainties involved in fatigue life estimation

Uncertainties that may affect the design fatigue life of turbine blades can be divided into two categories: 1) the uncertainties in laminate properties of the composite material and 2) the uncertainties in parameter of S-N curve.

5.1.1 Uncertainties in laminate properties

Important parameters that influence the fatigue performance of the composite blade could be attributed to a probability of both fiber misalignment and a statistic variation of fiber/resin stiffness. Hence, six variables for material stiffness and four variables for ply-orientation were assigned with probability distributions. These variables include the elastic modulus E_{11}, $E_{22}(E_{33})$ and the shear modulus $G_{12}(G_{13})$, G_{23}. As mentioned in section 2, the hydrokinetic turbine blade was made of E-glass/epoxy laminates with $[0_2/90_2/0_2/90_2]$ configurations. Hence, variation was also assigned to each of the ply orientations. Normally distributed and a 2% coefficient of variation (ratio of the standard deviation to the mean of a random variable) were assumed to the stiffness (Young et al., 2010). A 2° variation of ply orientation to the composite material was also assumed (Table 3).

5.1.2 Scatter in S-N data

Variation in both static strength and fatigue life is unavoidable; composite coupons tested under fatigue loadings would not be in the exact same condition. Typically, the values of static strength scatter in glass/epoxy composites are within 10% of the mean value. The static scatter is inherently attributed to the material production (Nijssen, 2006). The scatter in fatigue strength can be related to scatter in static strength. In the current study, static data was included in S-N data. This data assumed that static data indicates failure in the first load cycle of material specimens. Therefore, the fatigue

behavior of the chosen material can be described by static strength and a slope parameter. A conservative variation in static strength (2%) and the slope of S-N curve were assumed to characterize the scatter in fatigue data to avoid uncertainty overlapping with laminate properties (Fig. 16).

5.2 Construction of the metamodel

There are many kinds of metamodel techniques available, such as the response surface method, the Kriging model method (Jones, 1998), support vector machine (Burges, 1998), and polynomial chaos expansion (PCE) method (Xiu and Karniadakis, 2002). To account for the uncertainties in laminate properties as well as the river flow loading, herein, the PCE method was employed to construct the metamodel of stress response. Training points of input variables were generated according to their probability distributions. BEM-FEM analyses were then performed at the training points. After that, the metamodel was constructed using the PCE method and the accuracy of metamodel was verified by checking the coefficients of determination. More details about the PCE method can be found in (Hosder, Walters and Balch, 2010). In the subsequent subsections, detailed implement procedure was explained.

5.2.1 Sampling of random variables

Samples of random variables were generated to construct metamodels. These samples were generated according to both the distribution of random variables and their bases for expansion. To evenly generated samples over the design space, the Hammersley sampling method was employed to generate training samples (Chen et al. 1995). The number of variables intended to be expanded required a number of 265 samplings. Typical samples with both distributed material properties and lay-up information are presented in Fig. 17.

5.2.2 Stress response

BEM-FEM coupled analysis was performed at the training points. Structural evaluation of the composite turbine blade was conducted to obtain the failure mode of the blade under varying hydrokinetic loadings (see Section 2). Matrix cracking in the transverse direction on the top layer was found to be the most dominate fatigue failure indicator. Based on these studies, a stress response, with respect to the matrix crack failure mode, was developed with the Polynomial Chaos Expansion (PCE) method. In the PCE method, the river velocity was expanded using the Legendre polynomials and the other uncertain variables which follow Gaussian distribution were expanded using the Hermit polynomials. Figure 18 depicts the stress values of the matrix in tension (from samplings versus the metamodel prediction). Results indicate the metamodel predicts stress response very well. The metamodel is capable of yielding stress response of the blade under specified water velocities. The stress response as a function of random variables is depicted in Fig. 19.

5.3 First order reliability method (FORM)

The first order reliability method (FORM) was employed to perform the reliability-based fatigue life investigation to account for uncertainties in the design process. A generalized limit-state function is in the form of $G = g(\mathbf{X})$ with a vector of random variables $\mathbf{X} = [X_1, X_2, \cdots, X_n]$. The probability of failure has the form of $p_f = \Pr\{G = g(\mathbf{X}) < 0\}$. The following integral needs to be solved to estimate the failure probability:

$$p_f = \Pr\{G = g(\mathbf{X}) < 0\} = \int_{g(\mathbf{X})<0} f_{\mathbf{X}}(\mathbf{X}) d\mathbf{X} \tag{18}$$

where $f_{\mathbf{X}}(\mathbf{X})$ represents for the joint PDF of random variables $\mathbf{X}$.

The integral in Eq. (18) is usually a high-dimensional integration. This integration is very difficult to solve directly. Ten random variables were involved in the reliability-based fatigue life analysis of turbine blades. The integral was, therefore, ten-dimensional.

FORM, the most commonly used reliability analysis method, has been applied in various areas where uncertainties are presented (Hu et al., 2012). The FORM approximates the limit-state function $G = g(\mathbf{X})$ by the first order Taylor expansion method. The integral in Eq. (18) then was estimated in the standard Gaussian space by linearizing the limit-state function at the most probable point (MPP).

Random variables $\mathbf{X}$ were transformed into standard Gaussian random variables $\mathbf{U}$ before applying FORM, as follows:

$$\Phi(U_i) = F_{X_i}(X_i) \tag{19}$$

and

$$U_i = \Phi^{-1}(F_{X_i}(X_i)) \tag{20}$$

in which $\Phi(\cdot)$ is the CDF of a standard Gaussian random variable, $F_{X_i}(\cdot)$ is the CDF of the random variable X_i, and U_i is the standard Gaussian random variable corresponding to random variable X_i.

After the transformation, the limit-state function becomes $G = g(T(\mathbf{U}))$, where $T(\cdot)$ is the operator used to transform $\mathbf{U}$ to $\mathbf{X}$. The MPP point, where the joint PDF $f_{\mathbf{X}}(\mathbf{X})$ has the highest probability density, was then obtained by solving the following optimization model:

$$\begin{cases} \min \|\mathbf{u}\| \\ \mathbf{u} = [u_1, u_2, \cdots, u_n] \\ x_i = F_{X_i}^{-1}(\Phi(u_i)), i = 1, 2, \cdots, n \\ G = g(\mathbf{x}) = 0 \end{cases} \tag{21}$$

Once the MPP $\mathbf{u}^*$ is obtained, the probability of failure in Eq. (11) was approximated with (Du and Chen, 2000)

$$p_f = \Pr\{G = g(\mathbf{X}) < 0\} = \Phi(-\beta) \tag{22}$$

where β is the reliability index. The index is given by

$$\beta = \left\|\mathbf{u}^*\right\| \tag{23}$$

5.4 Fatigue life distribution

A detailed numerical procedure (summary of the numerical implementation above), is shown in Fig. 20. A brief description of the flowchart according to the sequence of dataflow is illustrated, as follows:

i. Blade hydrodynamic/structural design: design the blade shape and structural lay-out;

ii. Sampling/ BEM-FEM simulation: analyze using BEM-FEM coupled method and obtain blade stress at sampling points;

iii. Metamodel construction/fatigue investigation: Using the metamodel, investigate fatigue of the composite blade at any given random variables;

iv. Parameter sensitivity/effect of water velocity model: Study the sensitivities of random variables and effect of water velocity models on the fatigue performance of the blade.

The stall-regulated, horizontal axis, hydrokinetic turbine system consists of three composite blades. Fatigue study was conducted on a blade-to-blade basis. The

hydrokinetic loadings, however, were evaluated from a turbine point of view. The stall-regulated turbine system always operates under a fixed rotational speed (60 rpm). The probabilities of failure with respect to different design fatigue lives were analyzed using FORM. Figure 21 displays the obtained probability of fatigue failure with respect to expected fatigue life ranges (lognormal distribution). The probability that the fatigue life the turbine blade is less than the designed life (i.e. 20 years) is 5.0684×10^{-4}.

Sensitivity factors (Hu et al., 2012) were used to quantify the relative importance of random variables to the probability of fatigue failure. The sensitivity factor was computed using the MPP:

$$\alpha_i = -u_i^* / \beta \tag{24}$$

where α_i is the sensitivity factor of random variable *i*.

Results indicate that the two parameters of the S-N curve have the highest sensitivity factors, which are -0.6961 and -0.7362, respectively. The result implies that the uncertainties in the S-N curve will affect the fatigue life design significantly. The sensitivity factors of composite material parameters were also compared to analyze the importance of composite material properties. Figure 22 depicts sensitivity factors for the eight random variables of composite material.

From Fig. 22, both G_{12} and E_{11} contributed negatively to the failure probability; other parameters contributed positively. E_{22}, second ply, and third ply were each more important than other parameters. E_{22} is corresponding to the failure mode in terms of the matrix cracking in transverse direction. Second ply and third ply, as the core of the composite lay-up, contribute more than the surface (First ply) and bottom layer (Fourth ply).

The probability of turbine blade failure, for these three distributions, was analyzed to study the effect of river velocity model on the estimation of fatigue life. Figure 23 plots the fatigue probability of failure with respect to different river velocity distribution models. The fatigue life distribution was found to be only slightly affected by the river velocity model.

6. CONCLUSION

A methodology for the reliability-based fatigue life investigation of a median scale composite hydrokinetic turbine blade was proposed and studied. The BEM-FEM coupled method was adopted and applied to determine not only the real-time hydrokinetic loadings but also the stress distribution of the composite turbine blade. The model was based on fatigue data from the MSU/DOE fatigue database; constant life diagram was developed for modified stress ratios and the required fatigue life. A metamodel with respect to stress response was established, addressing the natural variability of material properties/lay-up information. Scatter in S-N data on fatigue life distribution and sensitivity of random variables, in terms of stiffness and ply orientation, on probability of fatigue failure were studied. Studies were also performed on the effect of the water velocity model on blade fatigue failure reliability. The probability that the blade fatigue life was less than 20 years is 5.0684×10^{-4}. The probability of failure of the composite would increase with time until CDF reached 1. The fatigue failure mode determined the sensitivity of fatigue life to E_{22} (the blade transverse direction). All of the plies contributed positively to the probability of fatigue failure. The second ply and third ply

were more important. Although the river velocity model did influence fatigue life distribution, it only slightly influenced the fatigue failure probability. This study suggests the need for a more detailed composite material characterization for hydrokinetic applications. The study provides a complete set of reliability-based fatigue life evaluation methodology for composite blades intended for hydrokinetic applications and can be extended to other fatigue dominant composite structural applications.

REFERENCES

American Society for Testing and Materials (ASTM), "Standard Practices for Cycle Counting in Fatigue Analysis," E1049– 85, ASTM subcommittee E08.04, June 1985 (Reapproved 2011)

Anyi, M. and Kirke, B., "Evaluation of Small Axial Flow Hydrokinetic Turbines for Remote Communities," Energy for Sustainable Development, Vol. 14(2), pp. 110-116, June 2010.

Buhl, M. "A New Empirical Relationship between Thrust Coefficient and Induction Factor for the Turbulent Windmill State," NREL/TP-500-36834. Golden, CO: National Renewable Energy Laboratory. Sept. 2004.

Beersma, J.J. and Buishand, T.A., "Joint Probability of Precipitation and Discharge Deficits in the Netherlands," Water Resources Research, Vol. 40, pp. 1-11, 2004.

Berry, D., "Design of 9-Meter Carbon-Fiberglass Prototype Blades: CX-100 and TX-100," Sandia National Lab report: 2007-0201, September, 2007.

Buckland, H., Masters, I., Chapman, J. and Orme, J., "Blade Element Momentum Theory in Modeling Tidal Stream Turbines," 18th UK Conference on Computational Mechanics, Association of Computational Mechanics in Engineering, Southampton, UK, March 29-31, 2010.

Burges, Christopher J.C., "A Tutorial on Support Vector Machines for Pattern Recognition," Data mining and knowledge discovery, Vol. 2(2), pp. 121-167, 1998.

Chen, W., Tsui, K-L, Allen, J.K. and Mistree, F., "Integration of the Response Surface Methodology with the Compromise Decision Support Problem in Developing A General Robust Design Procedure," Proceedings of the American Society of Mechanical Engineers Technical Conference, pp. 17-20, 1995.

Du, X. and Chen, W., "Methodology for Managing Uncertainty in Simulation-Based Systems Design," AIAA Journal, Vol. 38(8), pp. 1471-1478, 2000.

Degrieck, J. and Paepegem, W.V., "Fatigue Damage Modeling of Fibre-reinforced Composite Materials: Review," Applied Mechanics Reviews, Vol. 54(4), pp. 279-300, 2001.

Drela, M., Xfoil 6.96 for Win32, http://web.mit.edu/drela/Public/web/xfoil/, May 3, 2006.

Dassault Systèmes, ABAQUS Version 6.10 User Documentation, 2010.

Garrad Hassan & Partner Ltd., Tidal Bladed Theory and User Manual (version 4.3), Aug., 2012.

Hashin, Z., "Failure Criteria for Unidirectional Fiber Composites," Journal of Applied Mechanics, Vol. 47, pp. 329-334, 1980

Hosder, S., Walters, R. W., and Balch, M., "Point-collocation Nonintrusive Polynomial Chaos Method for Stochastic Computational Fluid Dynamics," AIAA journal, Vol. 48(12), pp. 2721-2730, 2010.

Hu, Z., Li, H., Du, X., and Chandrashekhara, K., "Simulation-Based Time-Dependent Reliability Analysis for Composite Hydrokinetic Turbine Blades," Structural and Multidisciplinary Optimization, Vol. 47 (5), pp. 765-781, 2012.

Hu, Z. and Du, X., "Reliability Analysis for Hydrokinetic Turbine Blades," Renewable Energy, Vol. 48, pp. 251–262, 2012.

Jones, D. R., Schonlau, M., and Welch, W. J., "Efficient Global Optimization of Expensive Black-Box Functions," Journal of Global Optimization, Vol. 13(4), pp. 455-492, 1998.

Khan, M.J., Bhuyan, G.,Iqbal, M.T. and Quaicoe, J.E., "Hydrokinetic Energy Conversion Systems and Assessment of Horizontal and Vertical Axis Turbines for River and Tidal Applications: A Technology Status Review," Applied Energy, Vol.86 (10), pp. 1823-1835, October 2009.

Kennedy, C.R., Leen, S.B. and Bradaigh, M.O., "A Study on the Fatigue Life of Glass Reinforced Polymer Composites for Tidal Turbine Blades," on Ocean, Offshore and Arctic Engineering, OMAE 2011, ASME, Rotterdam, The Netherlands, June 19-24, 2011.

Lange, C. H., "Probabilistic Fatigue Methodology and Wind Turbine Reliability," Sandia National Laboratory report: SAND96-1246, 1996.

Li, H., Chandrashekhara, K. and Mishra, R. S., "Fatigue Life Investigation for a Medium Scale Composite Hydrokinetic Turbine Blade," Society for the Advancement of Material and Process Engineering (SAMPE), Baltimore, Maryland, May 21-24, 2012.

Li, H. and Chandrashekhara, K., "Structural Optimization of Laminated Composite Blade Using Particle Swarm Optimization," Proceedings of ASME 2012 International Mechanical Engineering Congress & Exposition (IMECE 2012). Houston, Texas, November 9-15, 2012.

Mandell, J.F. and Samborsky D.D., "DOE/MSU Composite Material Fatigue Database," Sandia National Laboratories, SAND97-3002, Vol. 19, http://windpower.sandia.gov, March 31, 2010.

Mahfuz, H. and Akram, M.W., "Life Prediction of Composite Turbine Blades under Random Ocean Current and Velocity Shear," In Oceans, 2011 IEEE-Spain, pp. 1-7, IEEE, 2011.

Nijssen, R.P.L., "Fatigue Life Prediction and Strength Degradation of Wind Turbine Rotor Blade Composite," Graduate Thesis, November, 2006.

Post, N.L., Case, S.W. and Lesko, J.J., "Modeling the Variable Amplitude Fatigue of Composite Materials: A Review and Evaluation of the State of the Art for Spectrum Loading," International Journal of Fatigue, Vol. 30(12), pp. 2064-2086, December 2008.

RESOLVE, Inc., Schwartz, S.S., ed., "Proceedings of the Hydrokinetic and Wave Energy Technologies Technical and Environmental Issues Workshop," Washington, DC., October 26-28, 2005, http://hydropower.inl.gov/hydrokinetic_wave/, prepared on March 24, 2006.

Sudret, B., and Der Kiureghian, A., "Stochastic finite element methods and reliability: a state-of-the-art report," Department of Civil and Environmental Engineering, University of California, 2000.

Soden, P., Hinton, M. and Kaddour, A. "Lamina Properties, Lay-up Configurations and Loading Conditions for a Range of Fiber-reinforced Composite Laminates," Composite Science and Technology, Vol. 58, pp. 1011-1022, 1998.

Sutherland, H.J. and Mandell, J.F., "Optimized Constant-Life Diagram for the Analysis of Fiberglass Composites Used in Wind Turbine Blades," Journal of Solar Energy Engineering, Vol. 127, pp. 563-569, November 2005a.

Sutherland, H.J. and Mandell, J.F., "The Effect of Mean Stress on Damage Predictions for Spectral Loading of Fibreglass Composite Coupons," Wind Energy, Vol. 8, pp. 93-108, 2005b.

Shokrieh, M.M. and Rafiee, R., "Simulation of Fatigue Failure in a Full Composite Wind Turbine Blade," Composite Structures, Vol. 74, pp. 332-242, 2006.

Samborsky, D.D., Wilson, T.J., Agastra, P. and Mandell, J.F., "Delamination at Thick Ply Drops in Carbon and Glass Fiber Laminates Under Fatigue Loading," Journal of Solar Energy Engineering, Vol. 130, pp. 031001-1-8, August 2008.

Sale, D., Jonkman, J. and Musial, W., "Hydrodynamic Optimization Method and Design Code for Stall-Regulated Hydrokinetic Turbine Rotors," ASME 28th International Conference on Ocean, Offshore, and Arctic Engineering. American Society of Mechanical Engineers (ASME), NREL/CP-500-45021, Honolulu, Hawaii, May 31-June 5, 2009.

Viterna, L.A. and Janetzke, "Theoretical and Experimental Power from Large Horizontal-Axis Wind Turbines," NASA TM-82944, Washington, DC: National Aeronautics and Space Administration, September, 1982.

Xiu, D., and Karniadakis, G. E., "The Wiener-askey Polynomial Chaos for Stochastic Differential Equations," SIAM Journal on Scientific Computing, Vol. 24(2), pp. 619-644, 2002.

Young, Y. L., Baker, J.W. and Motley, M.R., "Reliability-based Design and Optimization of Adaptive Marine Structures," Composite Structures, Vol. 92(2), pp. 244-253, January 2010.

Zhang, Y.X. and Yang, C.H., "Recent Developments in Finite Element Analysis for Laminated Composite Plates," Composite Structures, Vol. 88, pp. 147-157, 2009.

Table 1 Static stress evaluation for different blade configurations

Blade configuration	Hollow	Foam	Shear web
Weight (kg)	2.07	5.62	2.66
Buoyancy (N)	-	86.9	-
Deflection under hydrodynamic loadings (m)	0.025	0.022	0.021
Maximum Hashin failure index	0.4638	0.2865	0.4405
Location	Root section	Station 5-6	Root section

Table 2 Material properties of E-glass/epoxy lamina (Soden et al., 1998)

Property	Value
Young's modulus (GPa)	E_1=45.6, E_2= E_3=16.2
Poisson's ratio	ν_{12} =ν_{13}= 0.278, ν_{23}=0.4
Shear modulus (GPa)	G_{12}=G_{13}= 5.83, G_{23}=5.786
Density (kg/m^3)	ρ=2000
Longitudinal tensile strength (MPa)	X^T=1280
Longitudinal compressive strength (MPa)	X^C=800
Transverse tensile strength (MPa)	Y^T=40
Transverse compressive strength (MPa)	Y^C=145
Inplane shear strength (MPa)	S^T=S^L=73

Table 3 Probability distributions of variables from the composite laminate

Variable	Mean	(Coefficient of) variation	Distribution type
Young's modulus	E_{11}=45.6 GPa	0.02	Gaussian
	E_{22}=E_{33}=16.2 GPa	0.02	
Shear modulus	G_{12}= G_{13} =5.83 GPa	0.02	
	G_{23}=5.786 GPa	0.02	
Ply orientation	First ply=0°	2°	
	Second ply=90°	2°	
	Third ply=0°	2°	
	Forth ply=90°	2°	

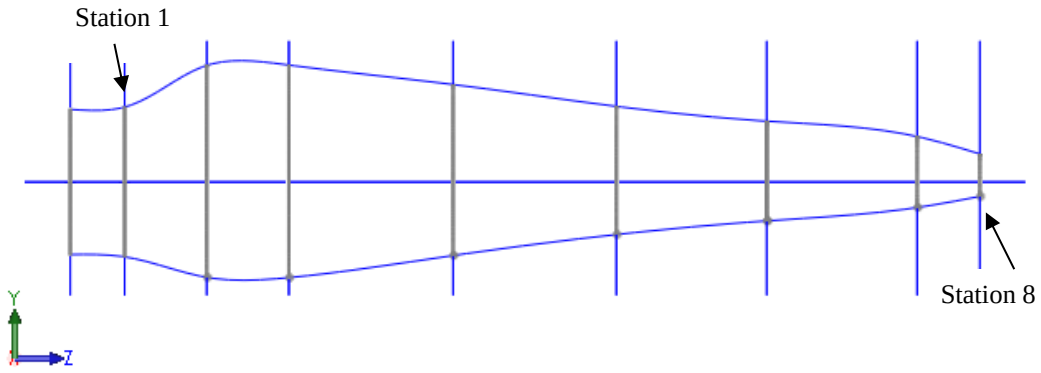

(a) longitudinal view of the blade stations

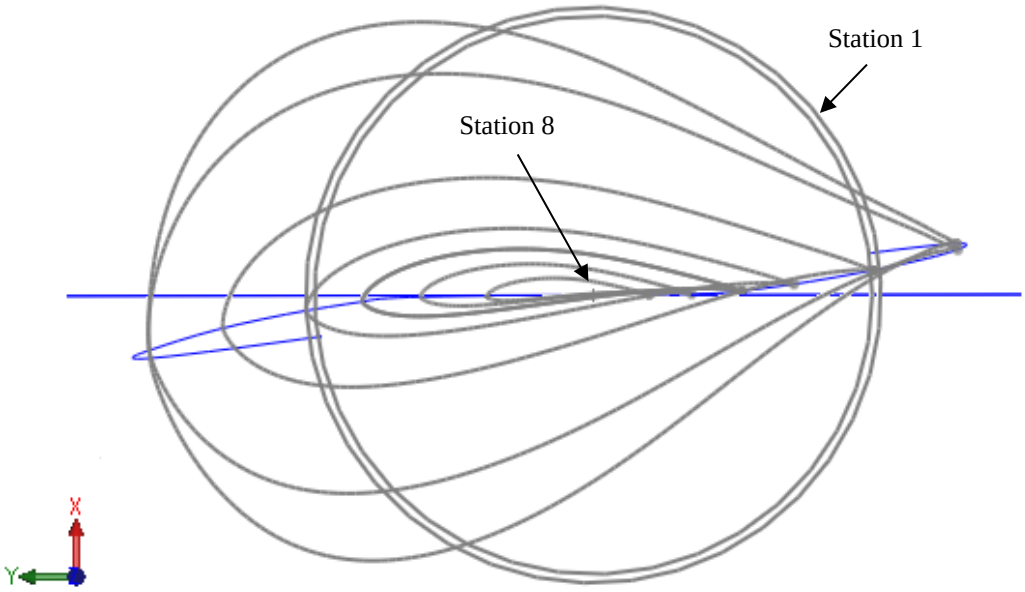

(b) Cross-sectional view of the blade stations

Fig. 1 Hydrodynamic profile of the hydrokinetic composite blade

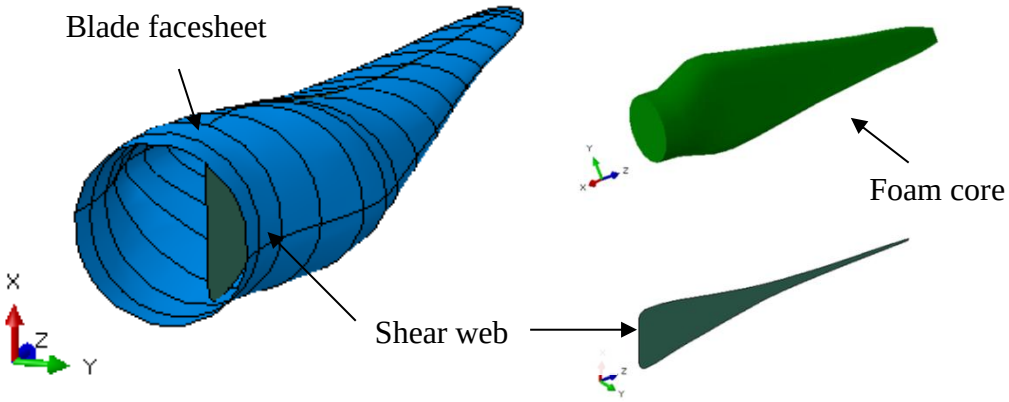

Fig. 2 Configurations of the composite blade structure

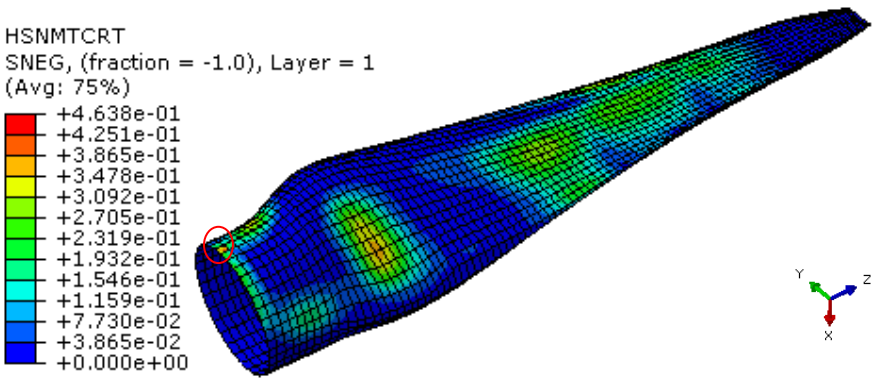

(a) Hollow blade (at the root)

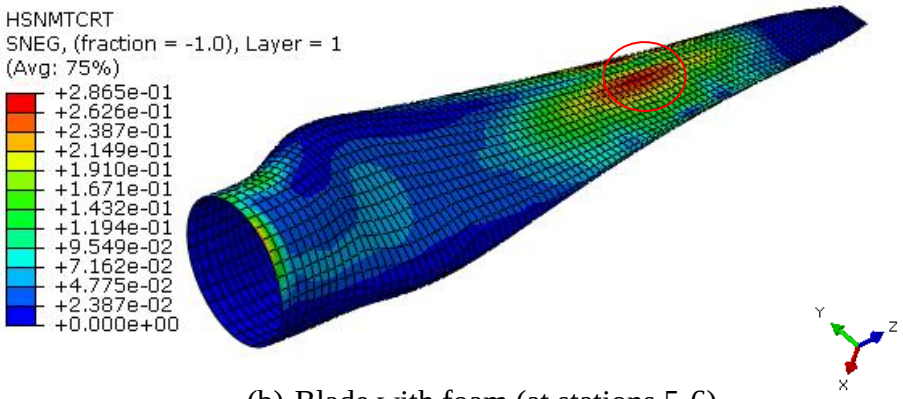

(b) Blade with foam (at stations 5-6)

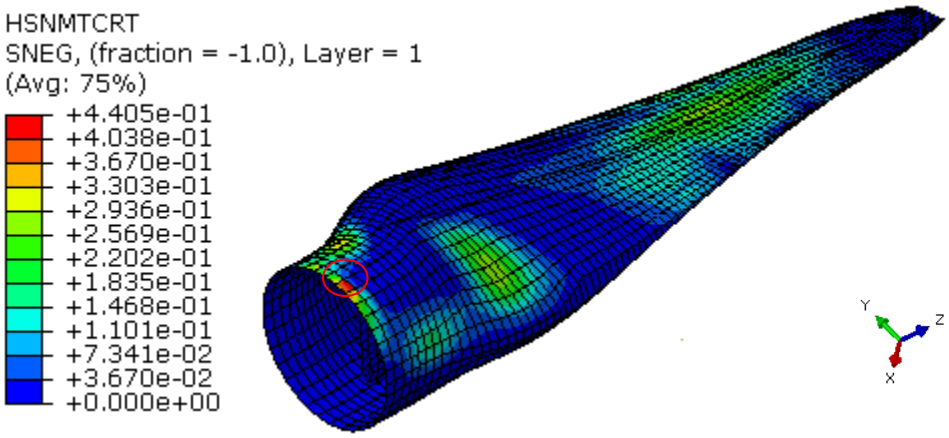

(c) Blade with a shear web (at the root)

Fig. 3 Critical position of stress concentration for different blade configurations

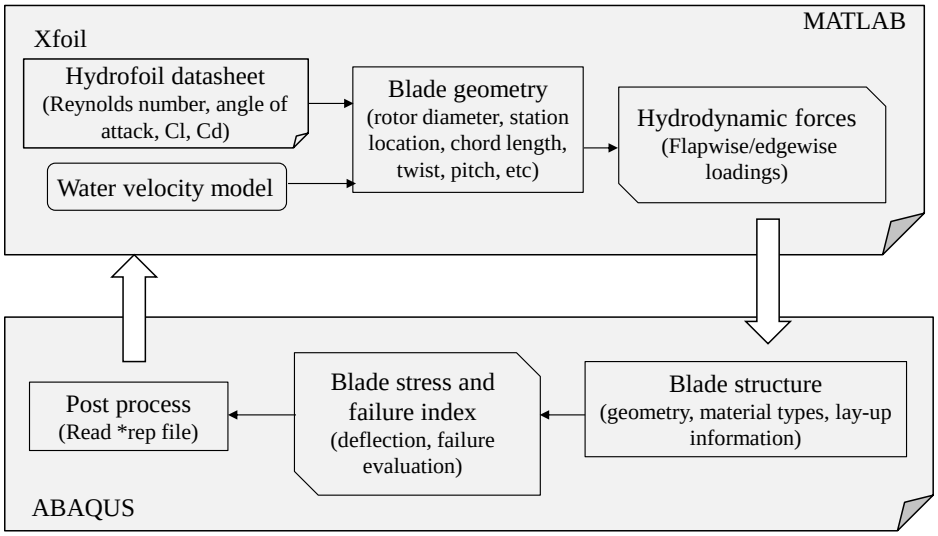

Fig. 4 Flowchart of the BEM-FEM coupled model

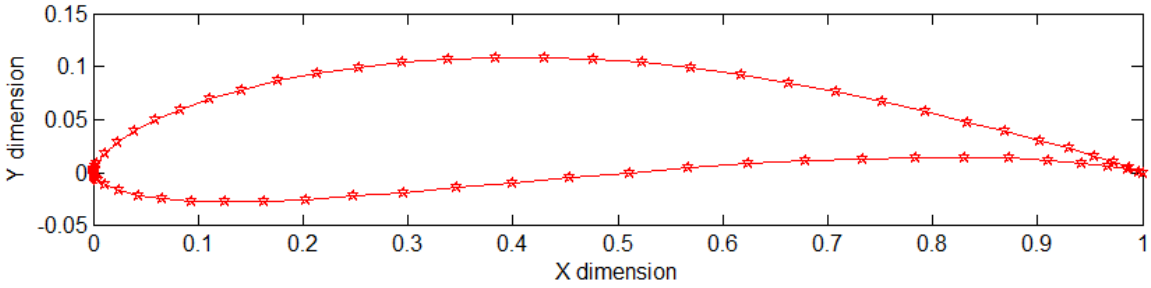

Fig. 5 Geometry profile of Eppler 395

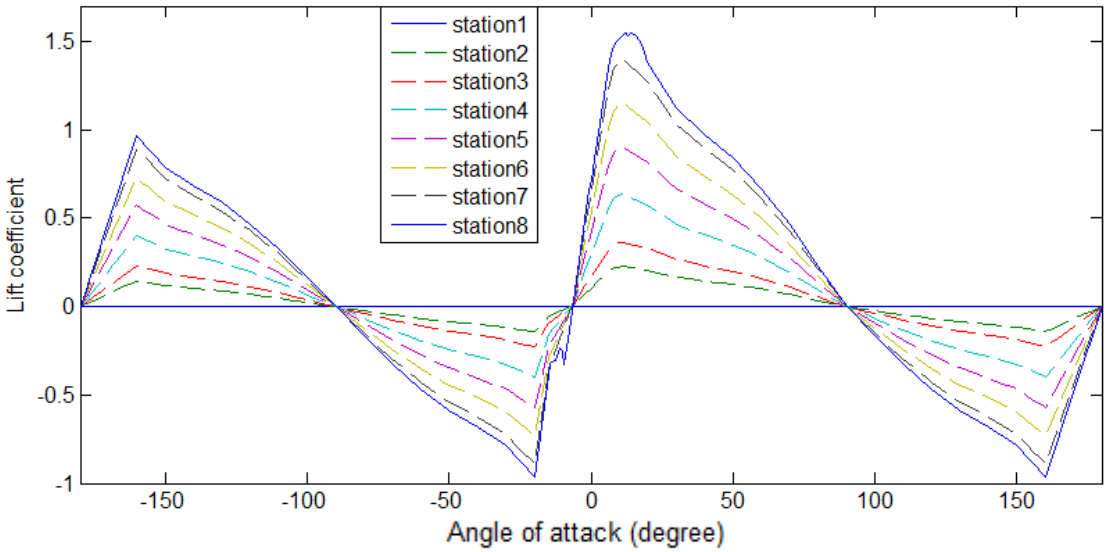

Fig. 6 Lift coefficient with angle of attack at each station

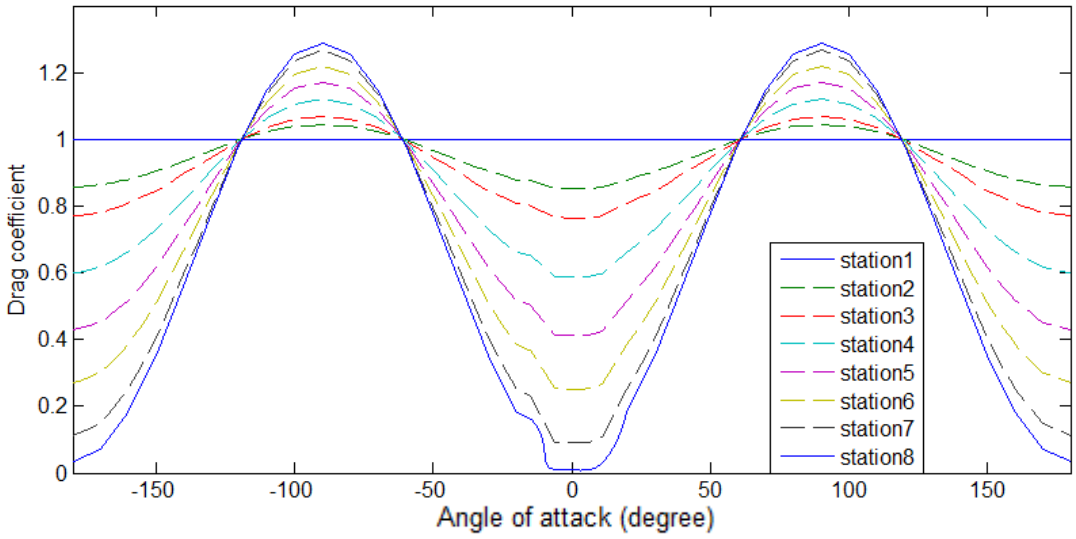

Fig. 7 Drag coefficient with angle of attack at each station

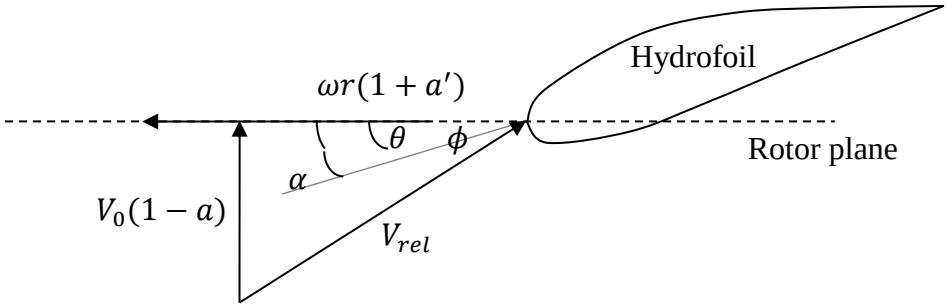

Fig. 8 Velocity vectors around a certain blade station

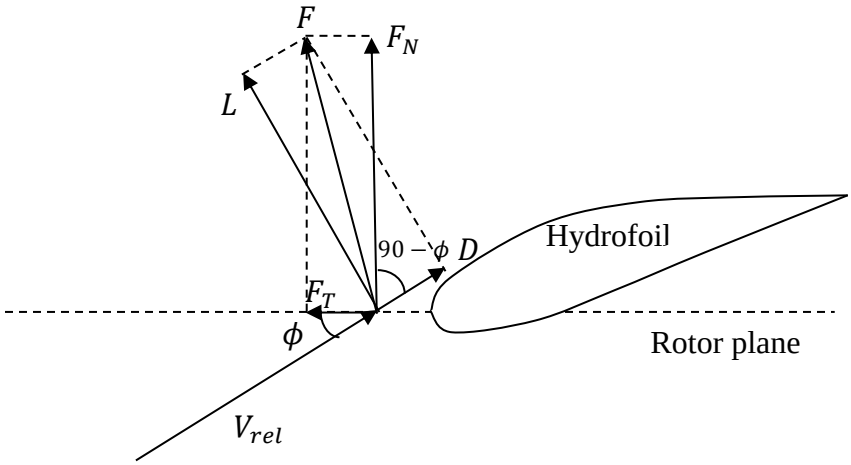

Fig. 9 Load integration on a typical hydrofoil

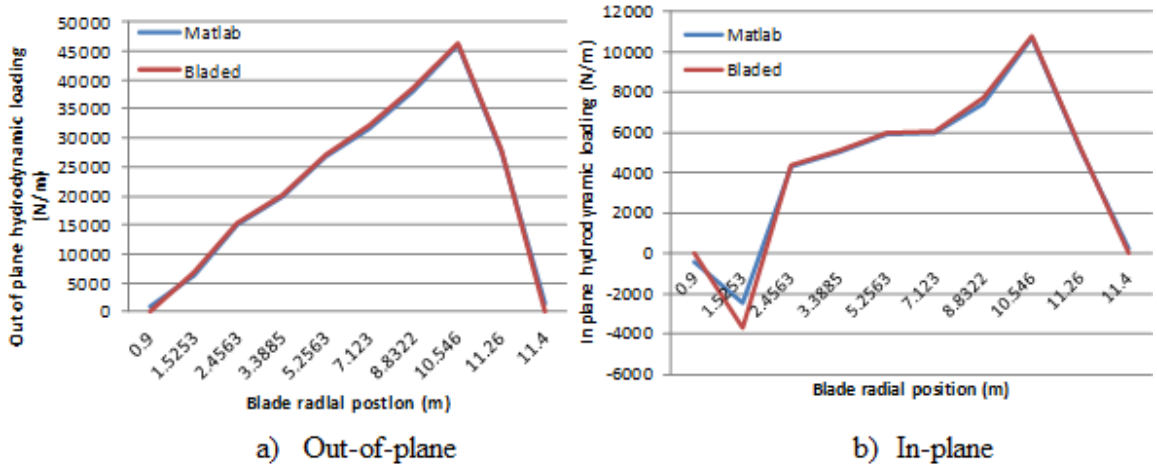

a) Out-of-plane b) In-plane

Fig. 10 Comparison of hydrodynamic loadings on the composite blade between the in-house MATLAB code and Blade Tidal

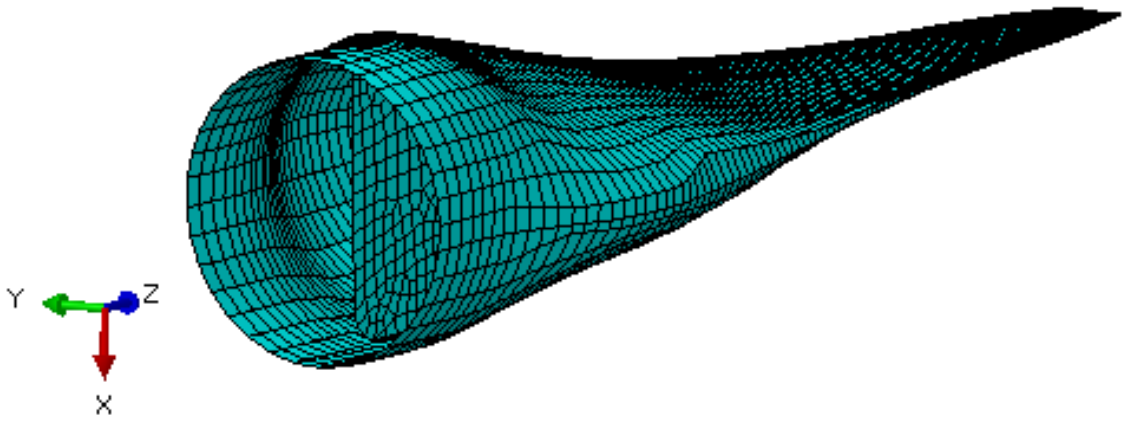

Fig. 11 Finite element model of the composite blade

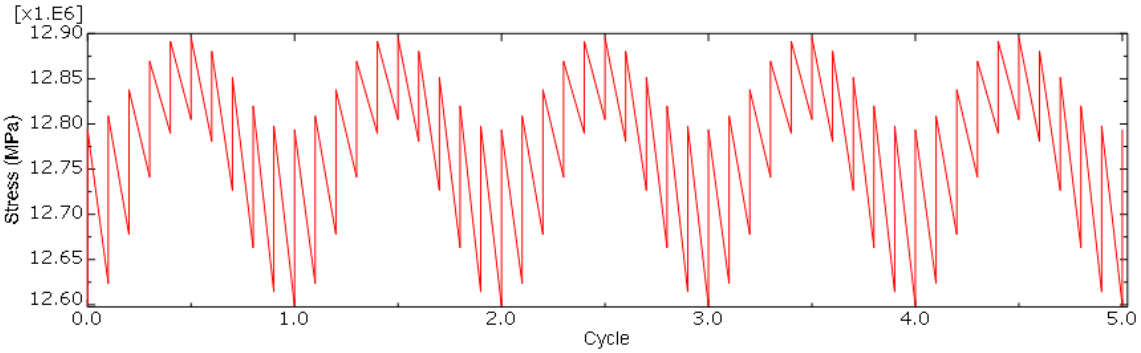

Fig. 12 Stress variation with time (stress concentration spot, root) of the optimal composite blade under cyclic loadings

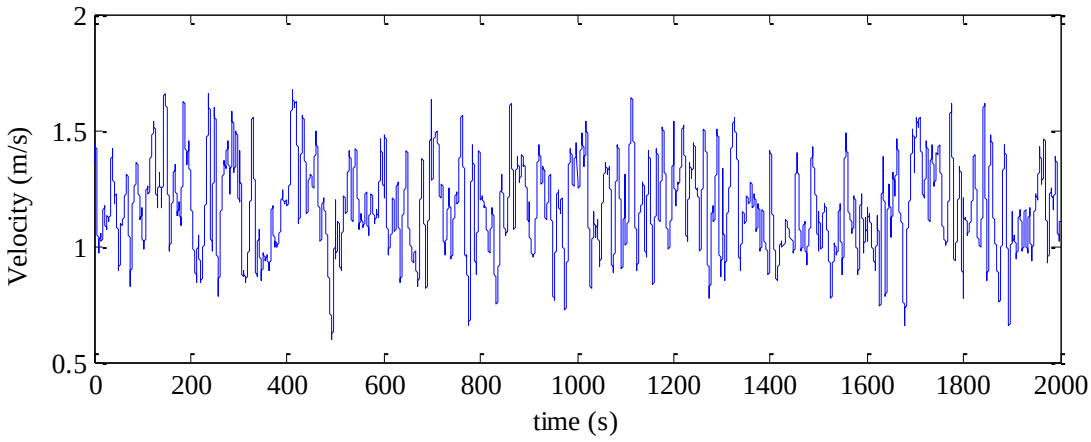

Fig. 13 A sample time history of river flow velocity (T=2000s)

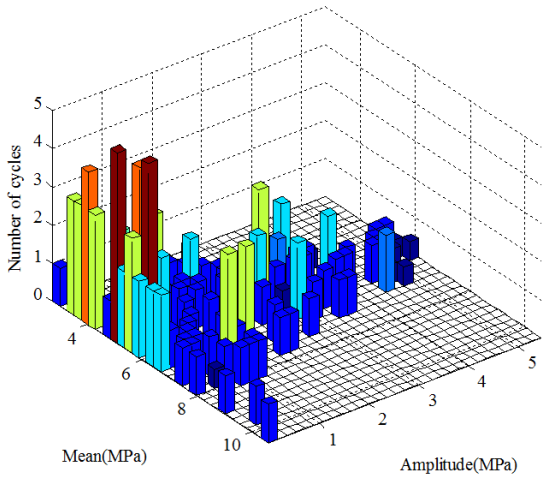

Fig. 14 Histogram of both stress amplitude and mean stress distribution

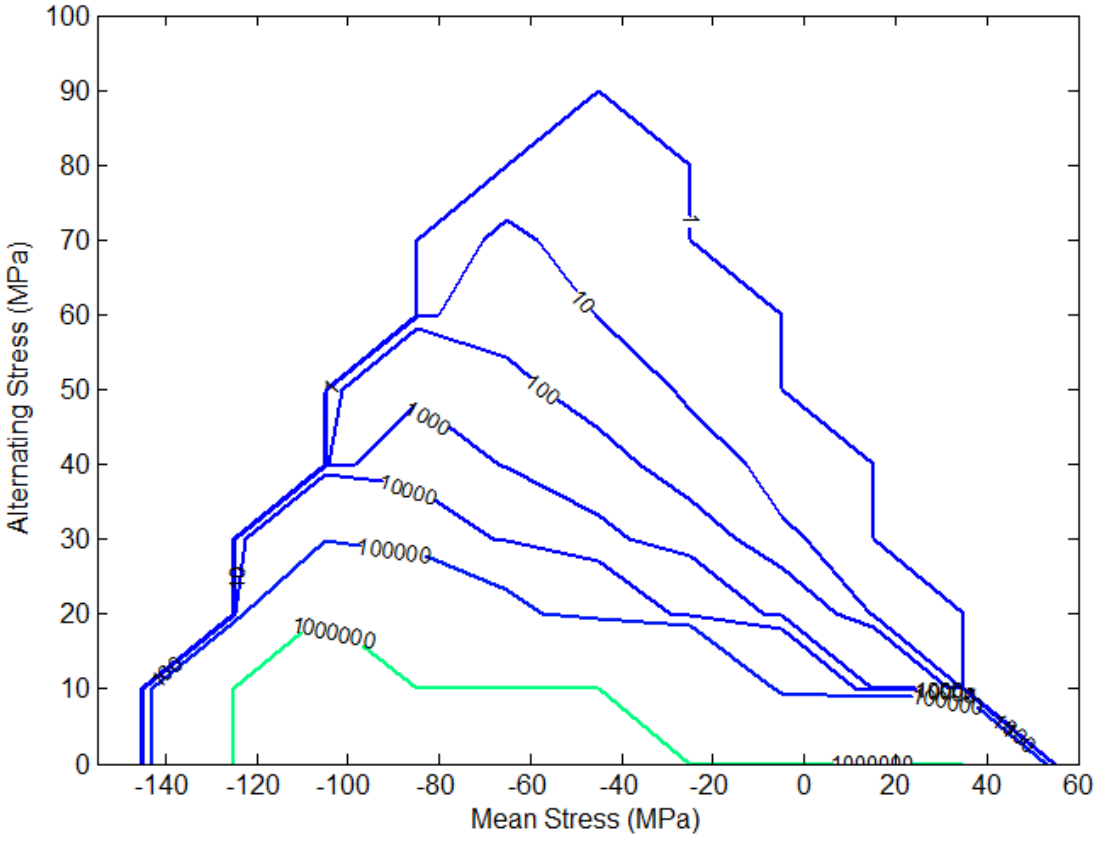

Fig. 15 Mean CLD for composite material, E-glass/epoxy [0 ℃90 ℃]

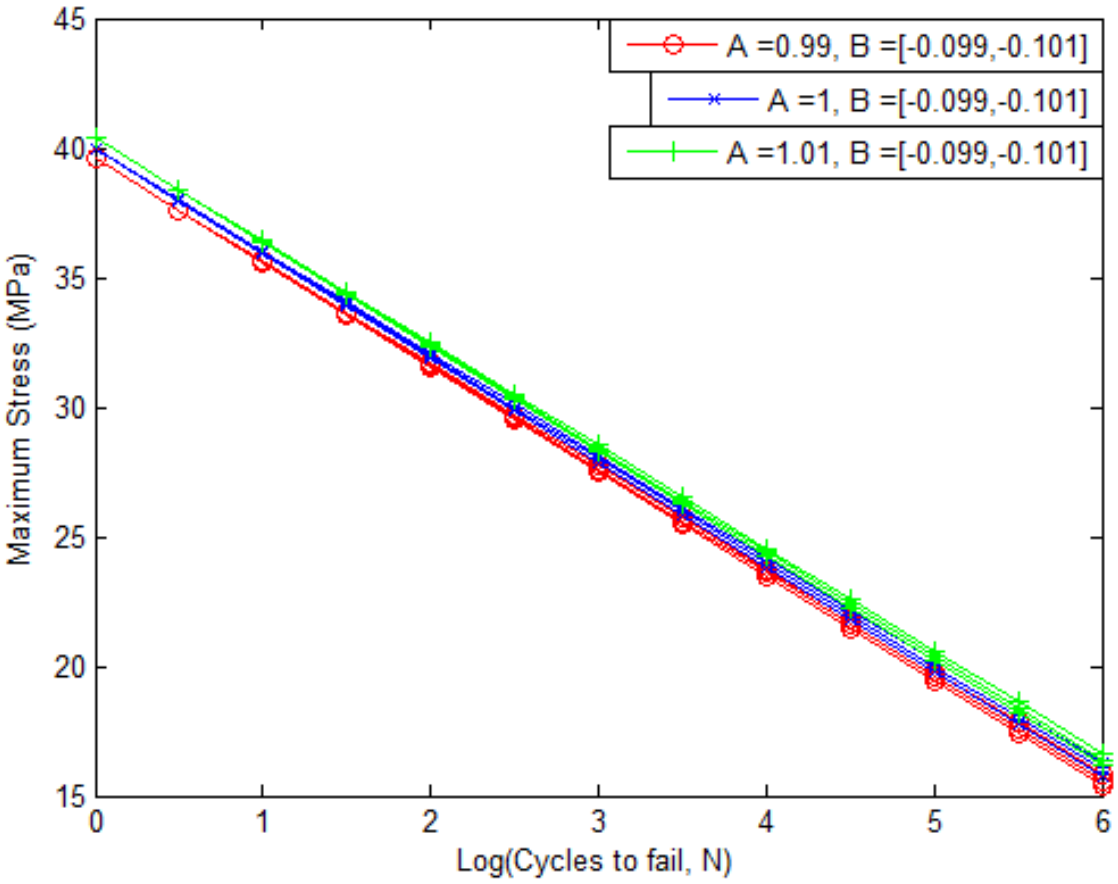

Fig. 16 scatter of S-N data (R=0.1)

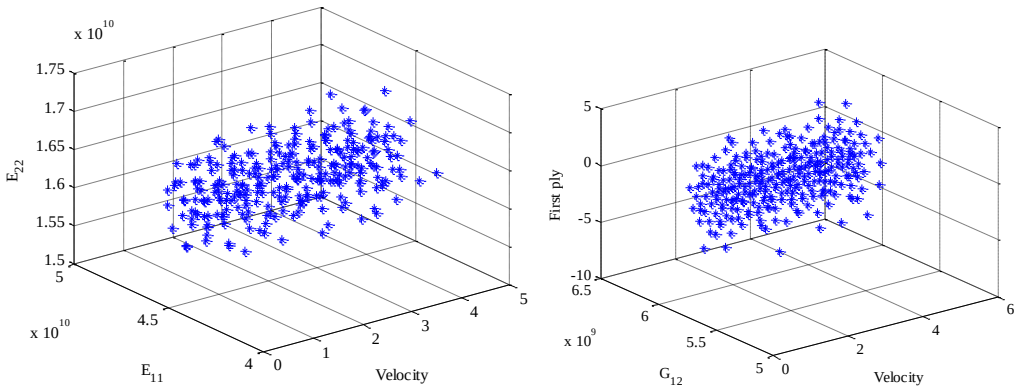

(a) E_{11}, Velocity and E_{22} (b) G_{12}, Velocity and First ply

Fig. 17 Samples of random variables regarding both material properties and ply-orientation

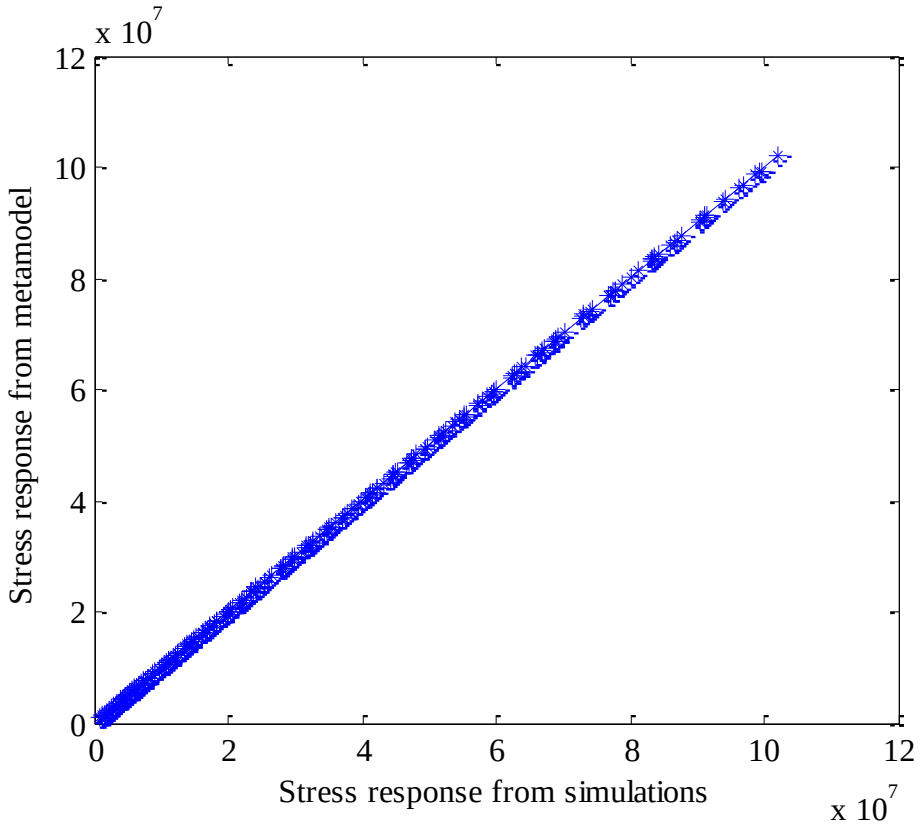

Fig. 18 Predicted stress values compared to solution from sampling points

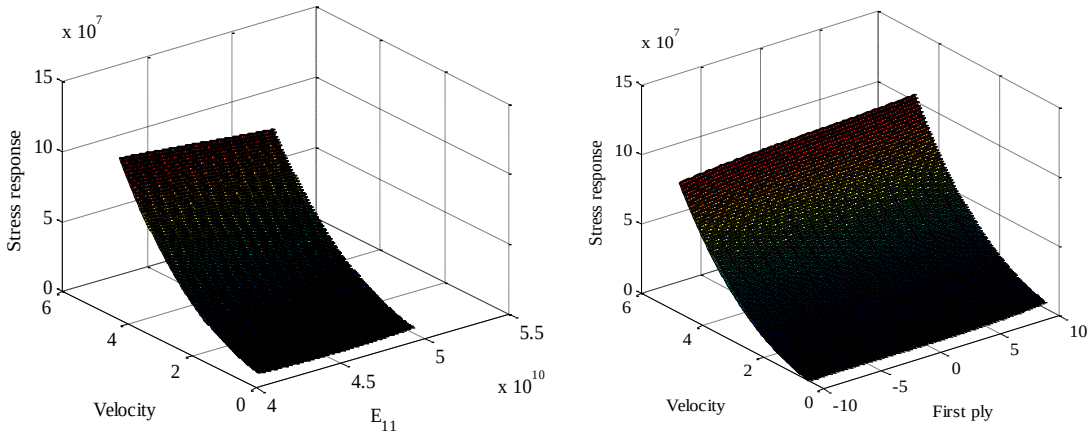

(a) Velocity, E_{11} and Stress response (b) Velocity, First ply and Stress response

Fig. 19 Response surface of matrix tensile stress

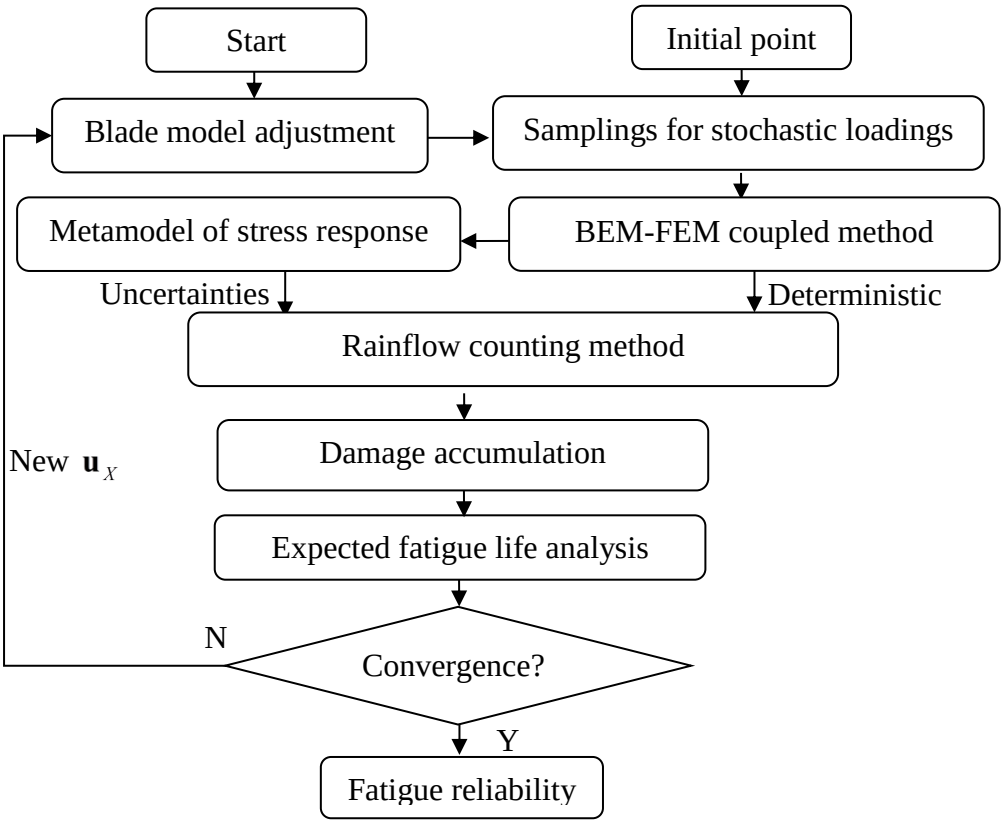

Fig. 20 Fatigue reliability analysis of hydrokinetic turbine blade

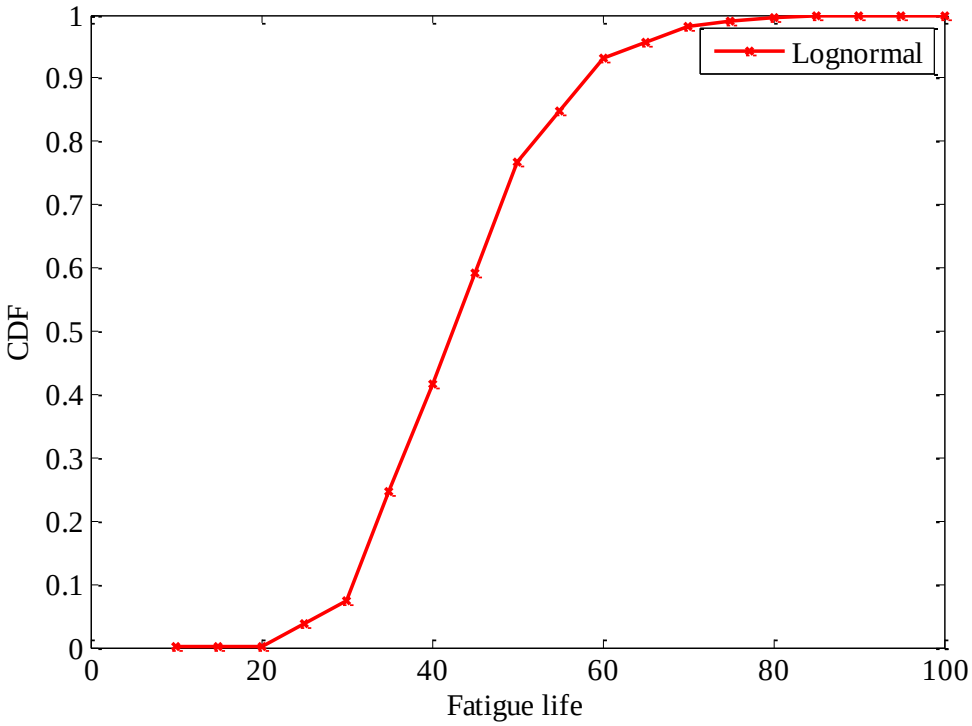

Fig. 21 Probability of fatigue failure with intended fatigue life.

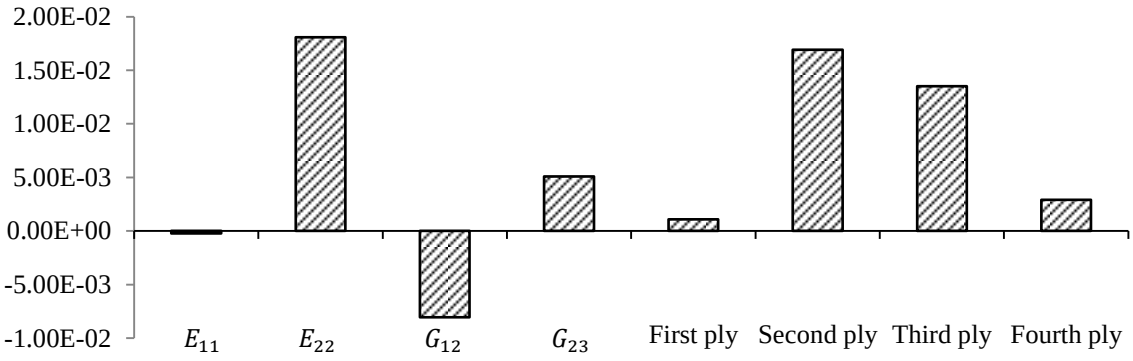

Fig. 22 Sensitivity factors of composite materials

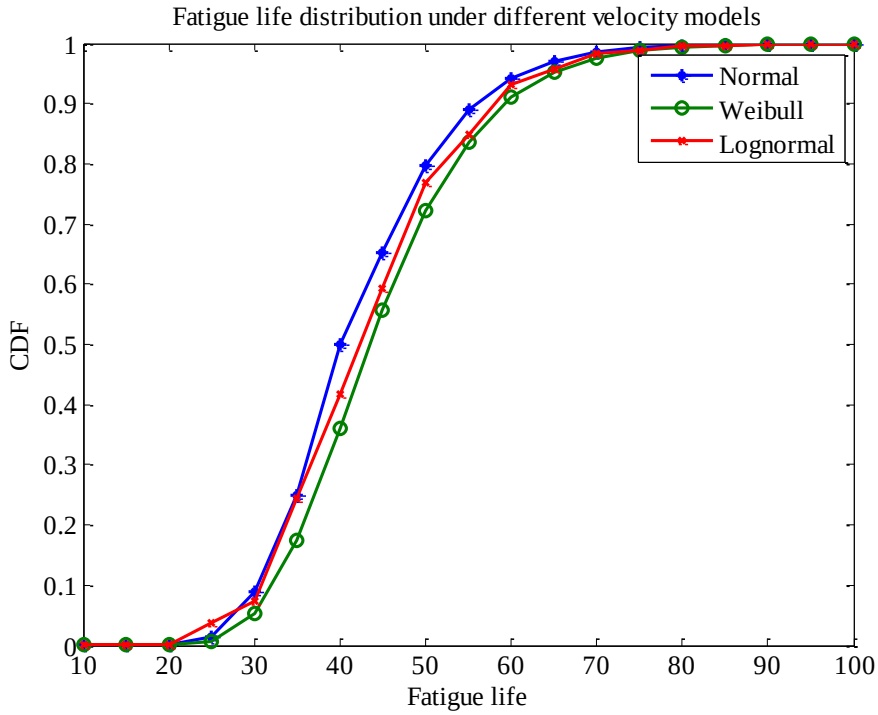

Fig. 23 Fatigue life distribution under different river velocity distribution models

II. PARTICLE SWARM BASED STRUCTURAL OPTIMIZATION OF LAMINATED COMPOSITE HYDROKINETIC TURBINE BLADES

H. Li and K. Chandrashekhara

Department of Mechanical and Aerospace Engineering

Missouri University of Science and Technology

Rolla, MO, USA

ABSTRACT

Hydrokinetic composite blades operating underwater experience hostile environment and complicated loadings. A composite blade for river applications with robust design should be able to withstand varying loading conditions and satisfy conservative failure evaluations. Composite blade manufacturing is quite complex and requires extensive optimization studies in terms of material selection, number of layers, stacking sequence, ply thickness and orientation. To avoid repetitive trial and error method process, particle swarm optimization technique was used to perform detailed blade structural lay-up optimization. Layer numbers, ply thickness and ply orientations were optimized using standard particle swarm optimization to minimize weight of the composite blade while satisfying failure evaluation. A modified blade element momentum-finite element method coupled model was developed to predict stress behavior of the blade under hydrokinetic loadings. Three composite failure criteria, namely maximum stress, Tsai-Hill and Tsai-Wu criteria were applied to generate the most conservative blade design. To address the discrete combinatorial optimization problem of blade stacking sequence, a novel permutation discrete particle swarm optimization model was also developed to maximize the out-of-plane load-carrying capability of the composite blade. The concepts of valid/invalid exchange and memory

checking were introduced to improve the efficiency of the algorithm. A final composite blade design with significant material saving and improved performance was presented. The proposed methodology offers an alternative and efficient design solution to composite structural optimization which involves complex loading conditions and multiple discrete and combinatorial design parameters.

1. INTRODUCTION

Hydrokinetic turbines are regarded as zero-head hydropower which utilizes hydrokinetics instead of potential energy of river flow. The greater density of water (850 times), as compared to air density, implies significant higher power output from a hydrokinetic turbine compared to a wind turbine for a fixed flow stream (Sale et al., 2009). However, turbines operating under water suffer harsher environment conditions. Varying hydrokinetic loadings, floater/fish school impacts and corrosion will impair the performance of hydrokinetic turbines. Composite materials, unlike traditional metallic materials, have superior properties in terms of light weight, high strength/stiffness to weight ratio and excellent anti-corrosion capability. The great design flexibility of composites will offer a blade structural design with complicated hydrodynamic profile, and sufficient load-carrying capability with significant weight reduction (Agarwal et al., 2006; Pierson, 2009).

Nevertheless, design of composite blades with satisfactory performance requires intensive study in terms of geometry design, load identification and structural optimization based on failure evaluation. In last decades, extensive research work has

been done on design, analysis for wind turbine blades, but very few for hydrokinetic turbine blades. Zhu and Rustamov (2012) performed structural analysis on a medium scale (750 kW) composite wind turbine blade using finite element analysis, and the relative stacking of the blade elements was manipulated to reduce the blade tip deflection and stress during design operating condition. Poulose and Hu (2010) evaluated strength of a wind blade through finite element modeling. Stress, deflection and major factor failure criteria were analyzed and compared for three blade configurations of different fiber orientations, and a best orientation was selected. Forcier and Joncas (2012) investigated that introduction of ribs would improve the rigidity of the structure and reduce the blade shell thickness. Ply specification and stacking sequence are important but yet to be studied. For emerging hydrokinetic applications, Bir et al. (2011) performed structural design of a horizontal-axis tidal turbine composite blade. They achieved optimal location of webs and minimum thickness requirement that would satisfy the ultimate-strength and buckling-resistance criteria. The design of these blades still mainly used trial and error method based on existing baseline designs. The method needed considerable amount of time investment and the results might not be satisfactory.

Recently, more and more researchers adopted advanced computational intelligence to conduct geometric/structural optimization work for wind turbine blades. Pirrera et al. (2012) investigated two blade design concepts: quadrilateral spar section conformed to the aerodynamic profile of the blade; and rectangular spar sections which were free to change. Genetic algorithm was applied to optimize the blade geometric configuration as well as spar section location to maximize strength and buckling efficiency. Hu et al. (2012) developed an automated evolutionary algorithm optimization

process to optimize the multi-objective structure of a horizontal axis wind turbine blade based on ultimate limit state analysis. Layer thickness, material type and layer orientation were optimized to reduce the cost and mass. However, optimization work conducted usually takes account of limited optimization parameters and no stacking sequence optimization was performed. A comprehensive study on blade structural performance, in terms of material type, number of layers, stacking sequence, ply thickness and ply orientation, need to be performed .

Particle swarm optimization (PSO), introduced by Eberhart and Kennedy (1995), can be applied to nonlinear combinatorial optimization problems with vast solution search spaces. Therefore, it is applied widely for composite structure design and analysis in recent years. Bloomfield et al. (2008) developed a two-level optimization approach for the composite optimization problem; in which gradient optimization was used at the first level to minimize the laminate weight, and a particle swarm optimization was used at the second level to determine the laminate stacking sequences. The PSO, under strength, buckling and lamination parameter constraints, was able to determine stacking sequence which closely matches the optimum lamination parameters. Chang et al. (2009) investigated the stack sequence optimization of composite laminates using permutation discrete PSO. It was found that the computational efficiency is comparable to other discrete PSO algorithms. Jiang et al. (2012) studied weight minimizing of a composite box structure using PSO and zero-order method. PSO is insensitive to the initial design sets and yielded better or equivalent results of zero-order method, and less number of finite element analyses was required. Manjunath et al. (2011) optimized ply stacking sequence of a composite drive shaft for a given torque, speed and length to minimize

weight using PSO. An optimal stack sequence was generated and it was found that PSO yielded better results than genetic algorthim. Chen et al. (2013) coupled PSO algorithm with a parametric finite element model of composite wind turbine blade (2MW) to optimize blade thickness and spar cap location and the optimization process leaded to significant weight saving. Among these researches, PSO is a favorable tool for composite structure optimization. However, little work was done on composite blades for emerging hydrokinetic turbine applications.

In the present work, a two-step online automated optimization methodology was developed to optimize structural performance of the composite hydrokinetic turbine blade. The optimization algorithm couples PSO with finite element analysis. A baseline parametric finite element composite blade model was formulated as the start to perform iterative structure optimization. As the first step, a standard particle swarm optimization (SPSO) model was developed to optimize weight of the composite blade. The model optimizes separate and independent design variables (ply thickness, layer number and ply orientation) and uses a global target function of weight minimization. As the second step, a novel permutation discrete particle swarm optimization (PDPSO) model, specifically for strengthening the out-of-plane load-carrying capacity of the composite blade with the optimal weight, was developed. Valid/invalid exchange check was introduced in PDPSO to exclude invalid exchanges in the search space. The concept of memory checking was applied to prevent premature convergence and improve the ability of global searching (Chang et al., 2009). After iterative weight and load-carrying capacity optimization, an optimized composite blade for hydrokinetic applications was presented.

2. BASELINE DESIGN OF THE COMPOSITE BLADE

The baseline turbine blade design for the current study was shown in Fig. 1. The blade length is 1 m and is divided into 8 stations, with circular station at the root area for easy installation (Li et al., submitted). The hydrofoil for blade tip station is EPPLER 395, which has a high ratio of lift to drag, and a high coefficient of lift at stall angle. The blade was designed with a twist angle 8.5 degree.

2.1 Structural configurations of the blade

Various blade structural configurations, like facesheet only, facesheet with core, and facesheet with shear web, were investigated to yield the baseline structure of the composite blade (Li et al., submitted). Previous study reveals that the baseline composite blade should consist of facesheet, shear web as well as foam core. E-glass/epoxy composite (Soden et al., 1998) was chosen as the material of facesheet and shear web. E-glass/epoxy composites are able to withstand highly repetitive hydrodynamic loadings and prevent corrosion (Anyi and Kirke, 2010) during operation of the composite hydrokinetic turbine under water. Shear web is required for the blade to carry the shear loading. The foam is resistive to buckling and water permeability, and also provides neural buoyance for the entire rotor. For the current study, the foam core was ignored for the optimization process, since the blade study involved no geometric optimization, and the weight of foam core was constant for all blade configurations. Also, presence of foam core significantly increased the time for each finite element simulation and optimization. Hence, the baseline composite blade, in the current study, consists of facesheet (E-glass/epoxy) and shear web (E-glass/epoxy). The baseline composite blade developed was shown in Fig. 2.

2.2 Structural evaluation of the blade

Structural evaluation of the composite blade requires calculation of the loading on blade during operation and the corresponding stress response. A comprehensive modified blade element momentum-finite element method (BEM-FEM) coupled model was thereby developed as explained in Section 3. Stress from each ply through the blade thickness was calculated. Three failure criteria were used as the indicator of composite failure, specifically maximum stress, Tsai-Hill and Tsai-Wu criteria. The first ply failure (FPF) was identified as the structural failure initiation of the composite blade (Zhang and Yang, 2009). The composite blade for being safe should not experience stress higher than FPF. Studies on the statistical distribution of the Missouri river indicate an average flow velocity of 1.74 m/s and a deviation of 0.25 m/s based on the river discharge data over 90 years at river station, Hermann, Missouri (Li et al., 2012). For a conservative design of the three-blade horizontal axis hydrokinetic turbine system, the blade was designed to withstand water velocity at 2.47 m/s, while operating under tip speed ratio of 3.

3. LOAD IDENTIFICATION AND STRESS ANALYSIS

The composite blade was treated as an encastre beam to perform structural analysis. All degrees of freedom were fixed at the root section. Loads including the weight of the blade $\{F_w\}$, the buoyancy force $\{F_b\}$ from water, the induced centrifugal force $\{F_{ce}\}$, and the coriolis force $\{F_{co}\}$ were considered (Young et al., 2010). The structural analysis of the composite blade in the rotating blade-fixed coordinate system was formulated as:

$$[K]\{u\} = \{F_h\}+\{F_w\} + \{F_b\} + \{F_{ce}\} + \{F_{co}\} \quad (25)$$

Where $\{F_h\}$ is the hydrodynamic force, $\{u\}$ is the structural nodal displacement vector and $[K]$ is the stiffness matrix. $\{F_h\}$ was calculated by the modified blade element momentum theory, and $\{u\}$ was identified by the three-dimensional parametric finite element blade model.

3.1 Modified blade element momentum theory

The blade element momentum (BEM) theory has been widely used in wind industry, and was transformed, in this paper, for the study of hydrokinetic turbine systems. The modified BEM incorporated Prandtl tip loss, Glauert correction and hub loss to improve solution accuracy. The algorthim is capable of yielding time-efficient and reliable solution at any specified hydrokinetic turbine configurations. Specific input variables include blade geometry, pitch, angular velocity and flow velocity. The solution from the developed model was validated with the commercial code-Tidal Bladed. Details regarding the model development can be found in reference Li et al. (submitted).

3.2 Finite element simulation of the composite blade

The finite element model of the composite blade was developed in ABAQUS version 6.10 (Dassault Systèmes, 2010) to perform stress analysis. As shown in Fig. 2, the composite blade was further partitioned for easy meshing. Facesheet and shear web were meshed using S4R 4-node shell elements with reduced integration and hourglass control. The distributed hydrodynamic loads $\{F_h\}$ (from BEM) was integrated and applied on the blade surface using the multi-point constraint (MPC) technique. Structural distributing coupling was used to interconnect degrees of freedom between the control point and the corresponding blade station. The material model used in simulation was listed in Table 1 (Soden et al., 1998).

The developed flowchart of the BEM-FEM model coupled with the PSO process is depicted in Fig. 3. The calculation of hydrodynamic loads on the blade was performed in MATLAB, while the finite element analysis of the blade model was conducted in ABAQUS. The block of PSO reads the stress/displacement data from finite element analysis results, serves as the decision box on particle disposal and provides updated structural parameters to the finite element model along with hydrodynamic loads. Through the iterative structural optimization process, PSO model would visit BEM-FEM model for each particle position until the optimal position was obtained.

4. STRUCTURAL OPTIMIZATION OF THE COMPOSITE BLADE

As discussed in Section 2, the facesheet and shear web form the baseline design of the composite hydrokinetic turbine blade studied (Li and Chandrashekhara, 2012). Symmetric and identical composite lay-up was assumed for both facesheet and shear web to improve convergence and achieve a balanced structural design. Three types of ply orientation $[0]_2$, $[\pm 45]$ and $[90]_2$ were chosen based on practical selections of ply orientation in industry. The shear web lay-up is fixed with $[0_4/(\pm 45)_2/90_4]_s$, and the lay-up configuration of facesheet was studied as the optimization target. PSO-based structural optimization is expected to have many invalid searches due to failure of the composite blade at some specified lay-up configuration and the extreme hydrodynamic loads. Three types of failure criterion (Agarwal et al., 2006), specifically maximum stress, Tsai-Hill and Tsai-Wu criteria were used to evaluate the blade performance and obtain a conservative blade design. As shown in Fig. 3, the value of keywords (lay-up information

and stacking sequence) in *inp file was modified in MATLAB to specify the particle position and hydrodynamic loads. The stress analysis job was then submitted to ABAQUS. *rep file would be generated and analyzed in MATLAB for failure data of the blade. Meanwhile, PSO optimization process was invoked for particle position evaluation. The online automated PSO iteration process coupling finite element analysis was supported by the developed automation code in MATLAB.

The focus of composite blade design always lies in material saving to reduce manufacturing cost while satisfying the performance requirements. In the first step, standard PSO (SPSO) was used to identify the effects of the separate parameters, namely ply thickness, number of layers and ply orientation and obtain the optimal blade design with significant material saving (weight reduction). In the second step, parameter like stacking sequence was also optimized to improve the loading performance of the blade with optimal weight. PSO algorithm was adapted to address the stacking sequence optimization of composite blades, as a discrete combinatorial optimization problem, similar as travelling salesman problems (Li et al., 2006). However, stacking sequence optimization problem is not identical to travelling salesman problems, and the exchange between two layers with the same ply orientation would not change the composite structural properties. A novel Permutation-based discrete PSO was developed to reach the design requirement.

4.1 Weight targeted particle swarm optimization

In the first step of the blade optimization process, independent parameters in terms of ply thickness (t), number of layers (N) and ply orientation (θ) were used as design variables, as shown in Equation (2). SPSO was adequate to perform weight optimization on these parameters.

$$t_{min} \leq \mathrm{t} \leq t_{max}$$
$$N_{min} \leq N \leq N_{max} \tag{2}$$
$$-90° \leq \theta \leq 90°$$

The design constraints were the three failure criteria: maximum stress, Tsai-Hill and Tsai-Wu. Qualified particle searches in SPSO were only limited to the lay-up configurations that survive in the proposed criteria, as shown in Equation (3). The maximum displacement of the blade is not intended as a design constraint; however, the value is recorded continuously during particle position moves.

Max. stress: $-S_L^- < \sigma_1 < S_L^+, -S_T^- < \sigma_2 < S_T^+, |\tau_{12}| < S_{LT}$

Tsai-Hill: $\sigma_1^2/S_L^2 - \sigma_1\sigma_2/S_L^2 + \sigma_2^2/S_T^2 + \tau_{12}^2/S_{LT}^2 < 1$

Use $S_L^+(S_T^+)$ if $\sigma_1(\sigma_2) > 0$, otherwise use $S_L^-(S_T^-)$

Tsai-Wu: $F_{11}\sigma_1^2 + F_{22}\sigma_2^2 + F_{66}\sigma_6^2 + F_1\sigma_1 + F_2\sigma_2 + 2F_{12}\sigma_1\sigma_2 < 1$ (3)

where $F_{11}=1/(S_L^+ S_L^-)$, $F_{22}=1/(S_T^+ S_T^-)$, $F_1=1/S_L^+ - 1/S_L^-$,

$F_2=1/S_T^+ - 1/S_T^-$, $F_{66}=1/S_{LT}^2$, $F_{12} = -\sqrt{1/(4S_L^+ S_L^- S_T^+ S_T^-)}$

The particle velocity and position were updated based on the following equation:

$$\mathrm{V_k^i} = \mathrm{w} \times \mathrm{V_{k-1}^i} + \mathrm{c_1} \times \mathrm{rand_1} \times \left(\mathrm{pbest^i} - \mathrm{X_{k-1}^i}\right) + \mathrm{c_2} \times \mathrm{rand_2} \times \left(\mathrm{gbest_{k-1}} - \mathrm{X_{k-1}^i}\right)$$
$$\mathrm{X_k^i} = \mathrm{X_{k-1}^i} + \mathrm{V_k^i} \tag{4}$$

where the superscript i denotes the particle number and subscript k denotes the iteration number; V and X denotes the particle velocity and position respectively; w is the inertia weight; $\mathrm{c_1}$ and $\mathrm{c_2}$ are acceleration constants, while $\mathrm{rand_1}$ and $\mathrm{rand_2}$ are random numbers in the interval [0,1]; $\mathrm{pbest^i}$ is the best position of particle i and $\mathrm{gbest_{k-1}}$ the global best position at iteration $\mathrm{k-1}$. Figure 4 illustrates particle parameters (Equation 4) in the form of vector.

The schematic of the weight targeted SPSO is shown in Fig. 5. The detailed procedures in the flowchart are as follows (Engelbrecht, 2007):

1. Initialize the swarm with random position values (lay-up information), random initial velocities, and normalized to fit in the range of [-1, 1].

2. Perform stress analysis (ABAQUS) and failure evaluation of the particular particle position and also calculate the fitness function (weight target).

3. If the particle passes the failure evaluation and weight comparison, store the particle position as pbest for gbest generation; otherwise, reject the particle for new position generation.

4. Determine the velocity vector for each particle in the swarm using the knowledge of the best position attained by each particle and the previous position of each particle in the swarm

5. Modify the position of each particle using the velocity vector and the previous position of each particle.

6. Repeat from step 2 until the fitness function (weight target) is satisfied.

7. Denormalization of the gbest position to generate the best structural design (optimal lay-up).

4.2 Stacking sequence optimization to improve blade structural performance

Altering stacking sequence of the composite lay-up is always beneficial to improve the structural performance of the composite blade. However, during the second step of the optimization process, the design parameter (stacking sequence) is discrete but interconnected on a layer-to-layer basis. Permutation-based method is valid and effective in solving such optimization problem. Therefore, permutation was introduced in DPSO and the calculating rules of DPSO were revised.

Only pairs of ply $[0]_2$, $[\pm45]$, $[90]_2$ used for the laminate tended to reduce the number of permutations and improve convergence. The composite lay-up was represented by a list of distinctive integers. For example, for a specified composite stacking sequence of $[0_4/(\pm45)_4/90_4]$s, the corresponding permutation code is [1/2/3/4/5/6/7/8] for layers above mid-plane, specifically code 1 and 2 belong to 0_2, code 3 to 6 belong to ±45 and code 7 and 8 belong to 90_2, as shown in Fig. 6.

The velocity vector and position value of each particle (specified stacking sequence as represented by permutation codes) in PDPSO were expressed in the same way as SPSO (Equation 4), but in different calculation algorithms (Chang et al., 2009). For this particular problem, to evaluate subtraction for $\mathrm{pbest}^{i} - X^{i}_{k-1}$ and $\mathrm{gbest}_{k-1} - X^{i}_{k-1}$ on element-to-element basis, for j th element of i th particle, the subtraction was given by:

$$\begin{aligned} \mathrm{pbest}^{i}_{j} - X^{i}_{k-1,j} &= \begin{cases} 0 & \text{if same} \\ \mathrm{pbest}^{i}_{j} & \text{else} \end{cases} \\ \mathrm{gbest}_{k-1,j} - X^{i}_{k-1,j} &= \begin{cases} 0 & \text{if same} \\ \mathrm{gbest}_{k-1,j} & \text{else} \end{cases} \end{aligned} \tag{5}$$

An array of random numbers corresponding to each element in velocity vector would be randomly generated in a range of [0, 1]. The multiple of the velocity vector was calculated:

$$\begin{aligned} c_1 \times \left(\mathrm{pbest}^{i}_{j} - X^{i}_{k-1,j}\right) &= \begin{cases} \mathrm{pbest}^{i}_{j} - X^{i}_{k-1,j} & \text{if rand} \geq c_1 \\ 0 & \text{else} \end{cases} \\ c_2 \times \left(\mathrm{gbest}_{k-1,j} - X^{i}_{k-1,j}\right) &= \begin{cases} \mathrm{gbest}_{k-1,j} - X^{i}_{k-1,j} & \text{if rand} \geq c_2 \\ 0 & \text{else} \end{cases} \end{aligned} \tag{6}$$

Similarly, the multiple of random number to the velocity vector was calculated with:

$$c_1 \times \mathrm{rand}_1 \times \left(\mathrm{pbest}_j^i - X_{k-1,j}^i\right) = \begin{cases} c_1 \times \left(\mathrm{pbest}_j^i - X_{k-1,j}^i\right) & \text{if } \mathrm{rand}_1 \geq 0.5 \\ 0 & \text{else} \end{cases}$$
$$c_2 \times \mathrm{rand}_2 \times \left(\mathrm{gbest}_{k-1,j} - X_{k-1,j}^i\right) = \begin{cases} c_2 \times \left(\mathrm{gbest}_{k-1,j} - X_{k-1,j}^i\right) & \text{if } \mathrm{rand}_2 \geq 0.5 \\ 0 & \text{else} \end{cases} \quad (7)$$

The summation of two velocity vectors was stated as:

$$V_{k,j}^i = \begin{cases} c_1 \times \mathrm{rand}_1 \times \left(\mathrm{pbest}_j^i - X_{k-1,j}^i\right) & \text{if rand} \geq 0.5 \\ c_2 \times \mathrm{rand}_2 \times \left(\mathrm{gbest}_{k-1,j} - X_{k-1,j}^i\right) & \text{else} \end{cases} \quad (8)$$

The final step was the new position updates for particles, which was in the form of:

$$X_{k,j}^i = X_{k-1,j}^i + V_{k,j}^i \quad (9)$$

If $V_{k,j}^i = 0$, $X_{k,j}^i = X_{k-1,j}^i$; otherwise, search $X_{k-1,l}^i$ in X_{k-1}^i which satisfy $X_{k-1,l}^i = V_{k,j}^i$, then swap $X_{k-1,l}^i$ and $X_{k-1,j}^i$ to form the $X_{k,j}^i$.

Assume for i th particle at iteration $k-1$, the coding for the composite laminate was [1/3/6/2/5/4/7/8], i.e. the lay-up $[0_2/(\pm 45)_2/0_2/(\pm 45)_2/90_4]$s. Using the proposed method, if the current status of i th particle is:

$$X_{k-1}^i = [1/3/6/2/5/4/7/8]$$
$$\mathrm{gbest}_{k-1} = [2/3/8/4/1/6/5/7] \quad (10)$$
$$\mathrm{pbest}^i = [2/3/1/7/5/6/8/4]$$

Then it can be inferred that:

$$\mathrm{pbest}^i - X_{k-1}^i = [2/0/1/7/0/6/8/4]$$
$$\mathrm{gbest}_{k-1} - X_{k-1}^i = [2/0/8/4/1/6/5/7] \quad (11)$$

There is a significant amount of invalid exchanges in stacking sequence optimization problem. Hence, the concept of memory checking was introduced to avoid invalid permutations. The generated stacking permutations in history were stored in

memory. The memory would be checked for each generated new string. If the position of a specific particle was found in the memory, the code would generate a new design string. Otherwise, took the string as a qualified string, and stored it into the memory.

As a comparison and also a validation process, DPSO using partially mapped crossover (PMX) was also applied to solve the stacking sequence optimization problem (Hu et al., 2003). The new velocity was normalized to represent the possibility that the particle changes. Each position randomly determined if there was a swap with a probability determined by the velocity. If a swap was required, the position would be set to the value of same position in pbest by swapping values. For example, if the integer assigned to particle seven is 6, the possibility of mutation is 0.75 (equal to 6/8, 8 is the total number of particles). The value is greater than 0.5 and indicates a mutation. Searching pbest, value 6 of current X position is with particle one. A swap between X values of particle one and seven was performed (as shown in Table 2). However, when the position was identical to pbest, X would stay in its current position forever. To overcome the shortcoming, the particle would randomly swap one pair of positions in the permutation if X equals to pbest. For example, values of particle two and six were swapped (as shown in last line, Table 2).

4.3 Case study and result analysis

4.3.1 Hydrodynamic loads on the blade

As stated in Section 2.2, the composite blade was designed to withstand water flow velocity of 2.47 m/s, while operating under tip speed ratio of 3. Based on modified BEM theory, the extreme hydrodynamic loads along the turbine blade span were obtained. Along with other loads (Equation 1), the hydrodynamic loads were applied on the blade surface through the three-dimensional parametric finite element model using MPC

technique. Both in-plane and out-of-plane hydrodynamic loads along the blade span are plotted in Fig. 7. While leaving the inner bound of the blade, the station tended to have higher RPM, which induce higher loads on the surface. However, because the decreasing blade surface area due to shorter chord length, the loads tended to drop at the outer bound of the composite blade. Out-of-plane loads were much higher than in-plan loads which provides the torque for power generation. Hence, out-of-plane hydrodynamic loads were the major source of blade breakage during operation.

4.3.2 Weight optimization

In the current study, the lay-up of the blade is symmetric with respect to the middle plane and three types of ply orientations $[0]_2$, $[\pm 45]$ and $[90]_2$ were used. The number of layers for each ply orientation above the middle plane was limited to 2~6 to maintain adequate but not excessive search space. Ply thickness of the E-glass/epoxy composites used was limited to 0.000125~0.00025m (Soden et al., 1998). For SPSO parameters, $w = 0.8$ was used for the inertia weight, and $c_1 = 2$, $c_2 = 2$ were used for two acceleration constants. Particle number was assumed 8 which give broad search space, quick convergence and reasonable results. It was observed that the solution converged to a final value after limited iterations, so iteration limit=20 was taken for data plot.

Figures 8 and 9 demonstrate the output of the composite blade weight and blade laminate thickness during SPSO iteration, respectively. Since the fitness function was to reduce weight of the composite blade, as shown in Figs. 8 and 9, the ply thickness decreased gradually, and the total blade weight decreased accordingly. Because blade laminate thickness is the indicator of blade weight, both curves followed the same trend during iteration process. The blade weight started from a high value of 4.3277 kg to a

much lower value of 2.4944 kg (weight saving of 42.36%), accordingly the laminate thickness reduced from 0.0052 m to 0.003 m. During the iteration process, only the blade designs (specific particle positions) which passed the failure evaluation were used for subsequent weight optimization process. For the current case, limited iterations (4 x 8 particle number) were required to converge to the minimized weight which was attributed to the relatively smaller range of ply thickness, ply number as well as controlled ply orientation. Table 3 lists the optimized composite lay-up based on three failure criteria. Each ply orientation reached its own lowest ply number (2 x 2 above middle plane), as defined by the optimization constraints. The baseline blade with $[0_4/(\pm 45)_2/90_4]_s$ configuration (i.e., the optimal lay-up) was adequate to survive the failure evaluation and tended to have the minimal weight (total: 2.495 kg, including 2.183 kg for facesheet and 0.312 kg for shear web) as compared to other blade configurations. The presence of shear web improved the stiffness of the composite blade, so less deflection was observed for the blade with shear web, as compared to the case without shearweb (0.022 m), under the same loading condition. For the accuracy of the failure index from the analysis, the failure index was extracted from the integration point of each element. The safety factor, as a reverse of failure index, was used to monitor the health of the blade and was listed in Table 3. The safety factor of the composite blade was around 1.54 after weight optimization, and showed only a slight variation to a magnitude of -4 was observed for the three criteria used.

4.3.3 Stacking sequence optimization

For stacking sequence optimization using permutation discrete PSO (PDPSO), initial value 0.9 was used for initial weight w, but linearly decreased to 0.45 to obtain broader search space and avoid premature convergence, and set c_1=0.4, c_2 =0.6 which

gave higher efficiency for iteration process (Chang et al., 2009). Optimized particle number 8 was also used to retain quick convergence with reasonable results. Same values of the parameters were applied to DPSO using PMX. The input to DPSO algorithm was the output from SPSO which provided the composite blade configuration with optimal weight, specifically $[0_4/(\pm45)_2/90_4]_s$. Pairs of ply $[0]_2$, $[\pm45]$, $[90]_2$ were free to alter positions with each other during DPSO iteration process.

Figures 10, 11 and 12 illustrate the comparison between PDPSO and DPSO-PMX for safety factor improvement based on the three failure criteria during stacking sequence iteration process. It was observed that within limited iterations (less than 20 x 8 particle number), the safety factor of the composite blade has been improved, as compared to the one from SPSO output. The limited improvement of safety factor was attributed to the relatively robust initial lay-up (symmetric, balanced) from SPSO, and constrained degree of freedom of ply alteration (3 pairs of ply). The varying initial lay-up information indicates wide search space. Depending on the initial blade lay-up to be optimized, more significant improvement of structure performance can be achieved. For both algorithms, identical ultimate safety factor and optimal stacking sequence were obtained for improved out-of-plane load-carrying capacity, which in turn validated the DPSO developed, as summarized in Table 4. An optimized stacking of $[0_2/90_4/0_2/(\pm45)_2]s$ was obtained for both Tsai-Hill and Tsai-Wu criteria. However, a different optimal blade lay-up configuration of $[90_2/0_4/(\pm45)_2/90_2]s$ was acquired for maximum stress criterion which can be attributed to the relatively less conservative of this failure criterion. Optimal safety factors close to 1.56 were attained for Tsai-Hill and Tsai-Wu criteria, which is less than the one for maximum stress criterion (1.5942). Tsai-Hill and Tsai-Wu criteria took

account of stress interaction, and tended to provide more conservative solutions. Therefore, there was less improvement of safety factor around 1.2% compared to 3.22% for the maximum stress criteria. Also, the corresponding deflections were slightly smaller.

The flapwise deflection of the composite blade with optimized stacking sequence ($[0_2/90_4/0_2/(\pm 45)_2]s$) is shown in Fig. 13a. Under extreme hydrodynamic loads, the blade tended to deflect and the maximum deflection was around the composite blade tip. The maximum deflection around 0.01916 was recorded during the iterative optimization process. Unbalanced deflections were observed due to the complex shape of the blade as well as unbalanced hydrodynamic loads. Minimal deflection was around the root section where the composite blade was fixed. The accompanying blade lay-up $[0_2/90_4/0_2/(\pm 45)_2]s$ is shown in Fig. 13b. Ply-up coordinate system 1 represents 0 degree of ply orientation, while 2 represents 90 degree of ply orientation. Accordingly, the Tsai-Hill failure index of the composite blade under same loading condition is displayed in Fig. 14. Compared to other regions throughout the entire composite blade, the vulnerable region was at the pressure side of the root section (highlighted). The maximum failure index monitored at the specific integration points was 0.6397, while the corresponding safety factor was 1.5633 as shown in Table 4. The dominated failure mode was matrix cracking in the transverse direction due to its lower strength under tension.

5. CONCLUSION

A two-step online automated structural optimization methodology was presented for composite hydrokinetic turbine blades using PSO. During the first step, irrelevant

composite lay-up parameters, in terms of ply thickness, layer numbers and ply orientation, were optimized for optimal blade weight using SPSO. In the second step, DPSO, in terms of PDPSO and DPSO-PMX, was used to optimize relevant variables (stacking sequence) to improve the blade structural performance. The weight targeted SPSO significantly reduced the composite blade weight up to 42.36%, and stacking sequence optimization improved the blade load-carrying capacity up to 3.22%. PSO tended to provide wide search space, and the introduction of valid/invalid exchange and memory checking into the algorithm successfully avoided trapping in local optimal solutions. It is predictable that if using a larger scale of composite blade with loose lay-up constraints, like more uncustomary ply orientations, more number of ply and more flexibility of sequence alteration, will induce much more value to the developed automated optimization algorithm. Potentially more significant weight savings and structural performance improvement with relatively less optimization time can be expected. Integrating PSO with composite blade structural design renders an effective and efficient solution for structural optimization of fiber reinforced composite blades with multiple design variables. The methodology, coupling advanced numerical method, provides experience for efficient blade structural design compared to traditional trial and error optimization methods.

REFERENCES

Agarwal, B.D., Broutman, L.J. and Chandrashekhara, K., Analysis and Performance of Fiber Composites (Third edition), Wiley, USA, 2006.

Anyi, M. and Kirke, B., "Evaluation of Small Axial Flow Hydrokinetic Turbines for Remote Communities," Energy for Sustainable Development, Vol. 14(2), pp. 110-116, June 2010.

Bloomfield, M. W., Herencia, J. E., and Weaver, P. M., "Optimization of Anisotropic Laminated Composite Plates Incorporating Nonconventional Ply Orientations," Proceedings of 49th AIAA/ASME/ASCE/AHS/ASC Structures, Structural Dynamics, and Materials Conference, Schaumburg, IL, 2008.

Bir, G. S., Lawson, M. J. and Li, Y., "Structural Design of a Horizontal-axis Tidal Current Turbine Composite Blade," Proceedings of the 30th International Conference on Offshore Mechanics and Arctic Engineering (OMAE ASME 2011), Vol. 5, pp. 797-808, Rotterdam, Netherlands, June 19-24, 2011.

Chang, N. , Wang W., Yang W., and Wang J., "Ply Stacking Sequence Optimization of Composite Laminate by Permutation Discrete Particle Swarm Optimization," Structural and Multidisciplinary Optimization, Vol. 41, pp. 179-187, 2009.

Chen, J., Wang, Q., Shen, W., Pang, X., Li, S. and Guo, X., "Structural Optimization Study of Composite Wind Turbine Blade," Materials and Design, Vol. 46, pp. 247-255, 2013.

Dassault Systèmes, ABAQUS Version 6.10 User Documentation, 2010.

Eberhart, R. C., and Kennedy, J., "A New Optimizer Using Particles Swarm Theory," Proc. Proc. 6th International Symposium on Micro Machine and Human Science, pp. 39-43, Nagoya, Japan, 1995.

Engelbrecht, A. P., Computational Intelligence – An Introduction (Second Edition), Wiley, USA, 2007.

Forcier, L. C. and Joncas, S., "Development of a Structural Optimization Strategy for the Design of Next Generation Large Thermoplastic Wind Turbine Blades," Structural and Multidisciplinary Optimization, Vol. 45(6), pp.889-906, 2012.

Hu, X., Eberhart, R. C., and Shi, Y., "Swarm Intelligence for Permutation Optimization: A Case Study on N-queens Problem," IEEE Swarm Intelligence Symposium 2003 (SIS2003), Indianapolis, Indiana, pp. 37-44, 2003.

Hu, W., Han, I., Park, S. and Choi, D., "Multi-objective Structural Optimization of a HAWT Composite Blade based on Ultimate Limit State Analysis," Journal of Mechanical Science and Technology, Vol. 26(1), pp. 129-135, 2012.

Jiang, P., Lin, Z., Xu, J. and Sun, J., "A Particle Swarm Optimization Algorithm for Minimizing Weight of the Composite Box Structure," Proceedings of International Conference on Frontiers of Advanced Materials and Engineering Technology (FAMET 2012), Vol. 430-432, pp. 470-475, Xiamen, China, January 4- 5, 2012.

Li, X., Tian, P., Hua, J., and Zhong, N., "A Hybrid Discrete Particle Swarm Optimization for Travelling Salesman Problem," Lecture Notes Computer Science, Vol. 4247, pp. 181–188, 2006.

Li, H., Chandrashekhara, K. and Mishra, R., "Fatigue Life Investigation for a Medium Scale Composite Hydrokinetic Turbine Blade," pp.1-15, Proceedings of Society for the Advancement of Material and Process Engineering (SAMPE), Baltimore, Maryland, May 21-24, 2012.

Li, H. and Chandrashekhara, K., "Structural Optimization of Laminated Composite Blade Using Particle Swarm Optimization," Proceedings of ASME 2012 International Mechanical Engineering Congress & Exposition (IMECE), pp. 1-7, Houston, Texas, November 9-15, 2012.

Li, H., Hu, Z., Chandrashekhara, K., and Du, X., "Reliability-based Fatigue Life Investigation for a Medium-scale Composite Hydrokinetic Turbine Blade," submitted to Journal of Ocean Engineering

Manjunath, K., Kumar, S. M. and Channakeshava, K. R., "Optimization of Ply Stacking Sequence of Composite Drive Shaft using Particle Swarm Algorithm," Journal of Engineering Science and Technology, Vol. 6(4), pp. 493-502, 2011.

Pierson, S. H., , "Composite Rotor Design for A Hydrokinetic Turbine," University of Tennessee Honors Thesis Projects, University of Tennessee – Knoxville, http://trace.tennessee.edu/utk_chanhonoproj/1311/, 2009

Poulose, P. and Hu, Z., "Strength Evaluation and Failure Predication of a Composite Wind Turbine Blade using Finite Element Analysis," Proceedings of ASME International Mechanical Engineering Congress and Exposition, IMECE 2010, Vol. 3, pp. 295-301, Vancouver, BC, Canada, November 12-18, 2010.

Pirrera, A., Capuzzi, M., Buckney, N. and Weaver, P. M., "Optimization of Wind Turbine Blade Spars," Proceedings of 53rd AIAA/ASME/ASCE/AHS/ASC Structures, Structural Dynamics, and Materials Conference, Honolulu, HI, United states, April 23-26, 2012.

Soden, P., Hinton, M. and Kaddour, A. "Lamina Properties, Lay-up Configurations and Loading Conditions for a Range of Fiber-reinforced Composite Laminates," Composite Science and Technology, Vol. 58, pp. 1011-1022, 1998.

Sale, D., Jonkman, J. and Musial.,W., "Hydrodynamic Optimization Method and Design Code for Stall-regulated Hydrokinetic Turbine Rotors," Proc. ASME 28th International Conference on Ocean, Offshore, and Arctic Engineering, Honolulu, Hawaii, NREL/CP-500-45021, 2009.

Young, Y.L., Motley, M.R. and Yeung R.W., "Three-dimensional Numerical Modeling of the Transient Fluid-structural Interaction Response of Tidal Turbines," Journal of Offshore Mechanics and Arctic Engineering, Vol. 132, 011101-1-12, February, 2010.

Zhang Y. and Yang C., "Recent developments in finite element analysis for laminated composite plates," Compos Structure, Vol. 88, pp. 147–157, 2009.

Zhu, S. and Rustamov, I., "Structural Design and Finite Element Analysis of Composite Wind Turbine Blade," 11th International Conference on Fracture and Damage Mechanics, FDM 2012, Vol. 525-526, pp. 225-228, Xian, China, September 18-21, 2012.

Table 1 Material model used for facesheet and shear web

Property	Young's Modulus (GPa)	Poisson's Ratio	Shear Modulus (GPa)	Inplane Shear Strength (MPa)
Value	E_1= 45.6, E_2=E_3= 16.21	ν_{12}=ν_{13}= 0.278, ν_{23}= 0.4	G_{12}=G_{13}=5.83, G_{23}= 5.786	s_{LT} = 73
Property	Longitudinal Tensile Strength (MPa)	Longitudinal Compressive Strength (MPa)	Transverse Tensile Strength (MPa)	Transverse Compressive Strength (MPa)
Value	s_L^+ = 1280	s_L^- = 800	s_T^+ = 40	s_T^- = 145

Table 2 Particle update and mutation in DPSO using PMX

Particle parameter	Particle one	Particle two	Particle three	Particle four	Particle five	Particle six	Particle seven	Particle eight
V	7	3	1	4	5	2	6	8
|V |	0.8475	0.375	0.125	0.5	0.625	0.25	0.75	1.0
pbest	6	2	4	8	1	5	3	7
X	3	4	2	5	1	7	6	8
X+V	6	4	2	5	1	7	3	8
X=pbest	6	5	4	8	1	2	3	7

Table 3 Optimized lay-up of the composite blade

Lay-up	$[0_4/(\pm 45)_2/90_4]_s$		
Lamina thickness (m)	0.000125		
Blade thickness (m)	0.003		
Blade weight (kg)	Facesheet: 2.183 Shear web: 0.312 Total: 2.495		
Blade deflection (m)	With shear web: 0.019 < Without shear web: 0.022		
Safety factor (reverse of failure index, with shear web)	Failure criterion		
	Maximum stress	Tsai-Hill	Tsai-Wu
	1.5445	1.5444	1.5438

Table 4 Optimized stacking sequence for improved load-carrying capacity

Failure criteria	Optimized Stacking	Optimal safety factor	Improvement of safety factor	Deflection (m)
Maximum stress	$[90_2/0_4/(\pm45)_2/90_2]s$	1.5942	3.22%	0.0191609
Tsai-Hill	$[0_2/90_4/0_2/(\pm45)_2]s$	1.5633	1.22%	0.0191589
Tsai-Wu	$[0_2/90_4/0_2/(\pm45)_2]s$	1.5629	1.24%	0.0191589

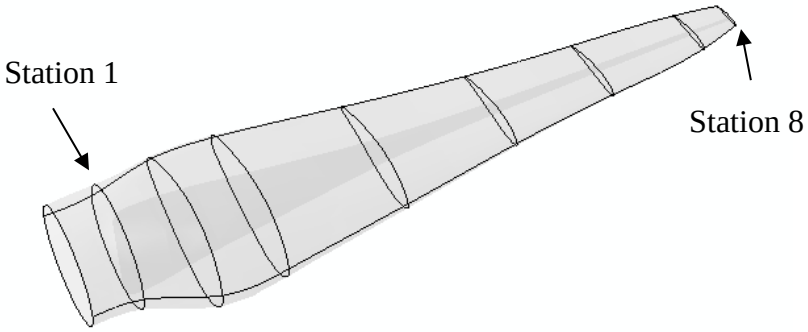

Fig. 1 Geometry layout of the hydrokinetic composite blade

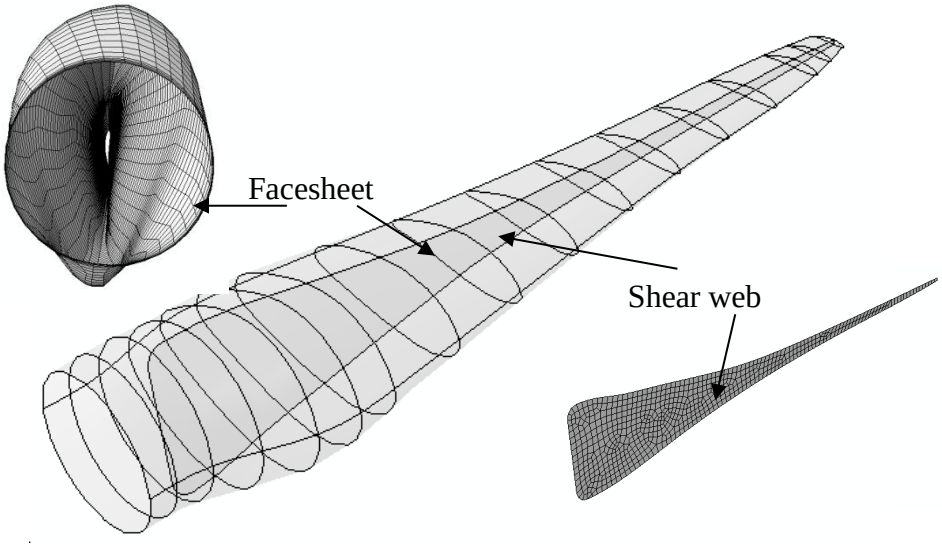

Fig. 2 Design concept of the composite blade

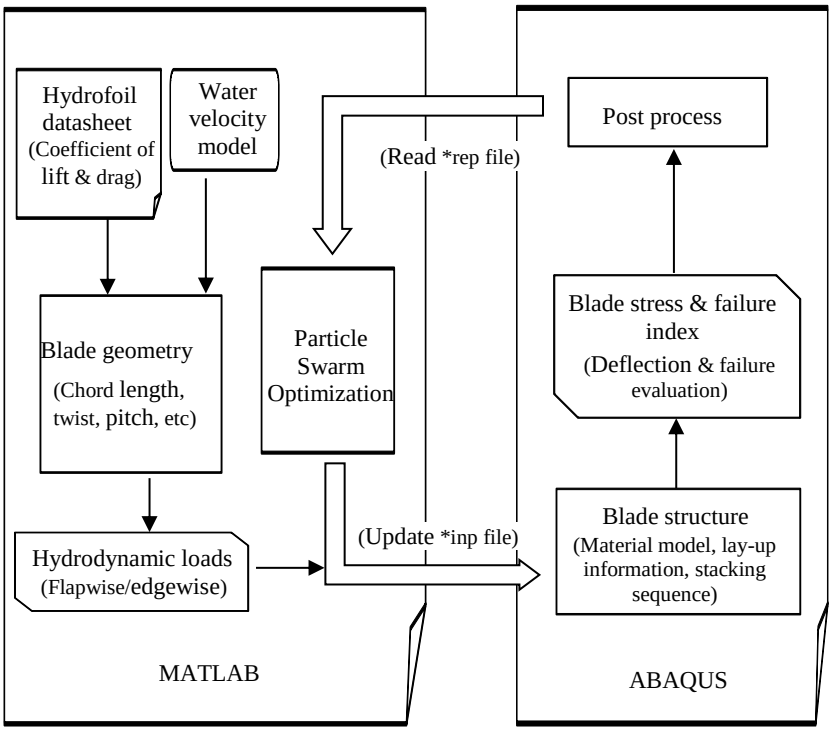

Fig. 3 Flowchart of the BEM-FEM model coupled with PSO process

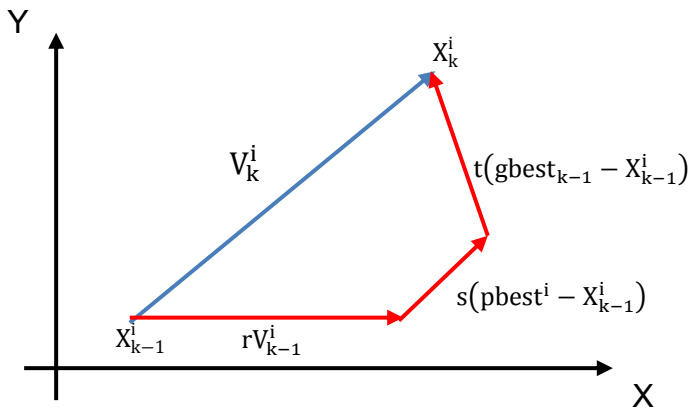

Fig. 4 Particle position updates in SPSO

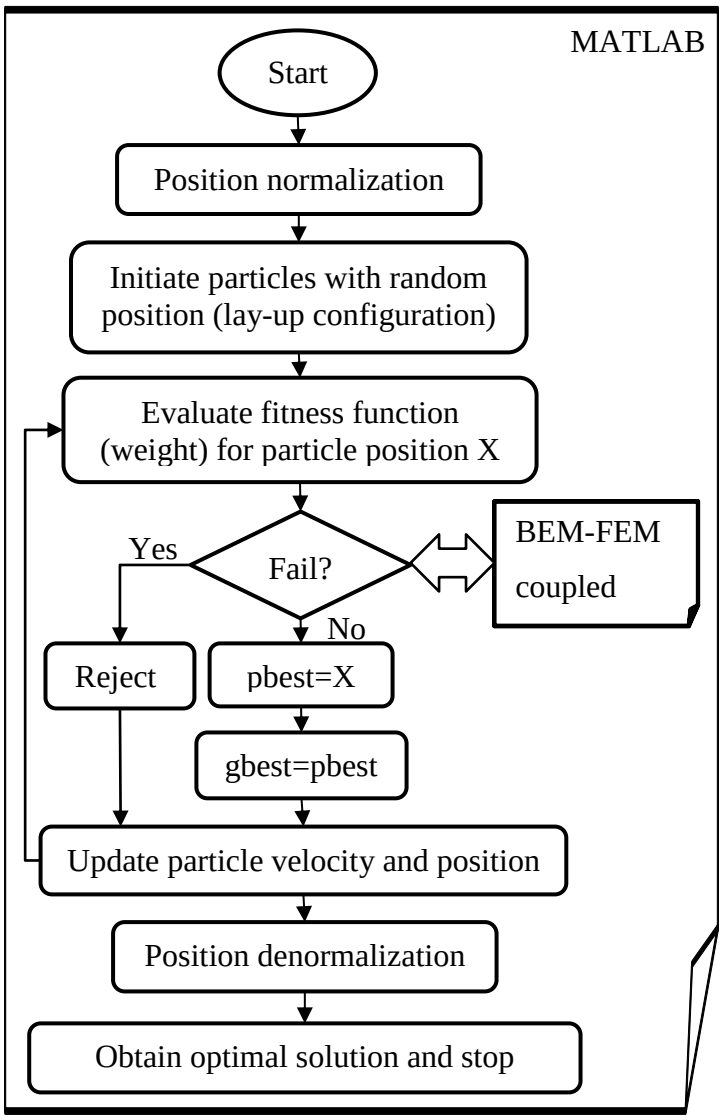

Fig. 5 Flowchart of SPSO for composite blade with optimal weight

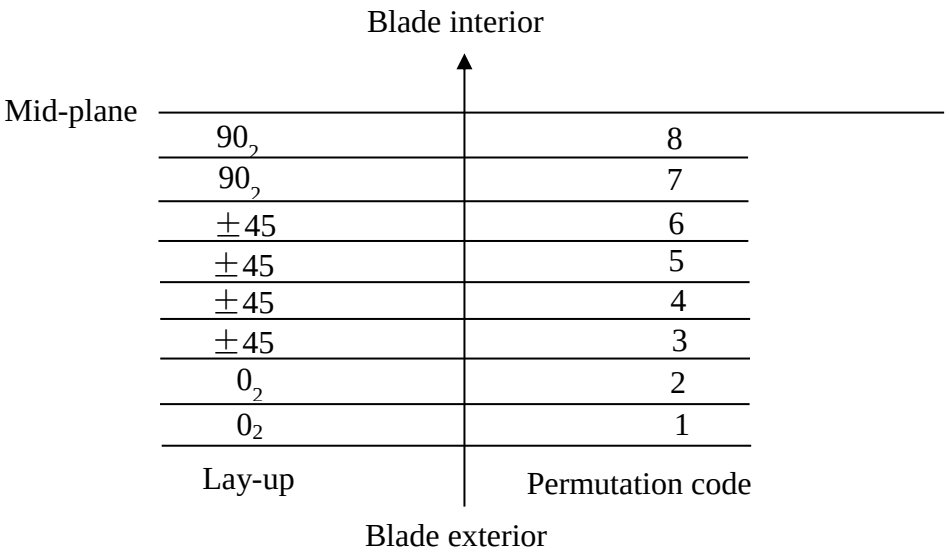

Fig. 6 Schematic of permutation codes corresponding to stacking sequence

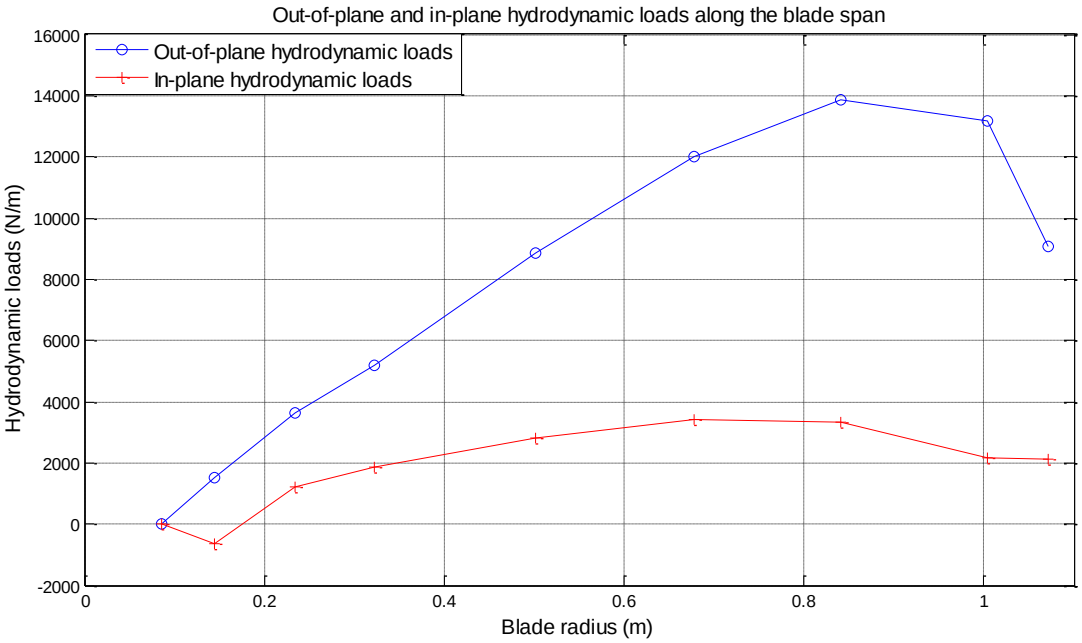

Fig. 7 Hydrodynamic loads along the turbine blade span (flow velocity: 2.47 m/s)

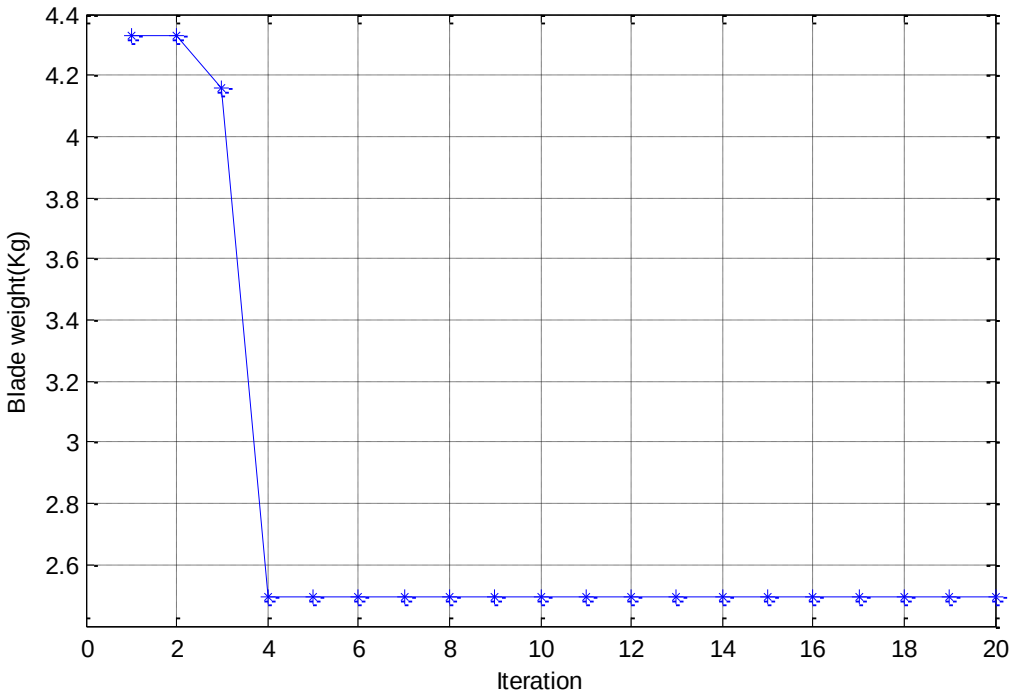

Fig. 8 Composite blade weight during SPSO iteration

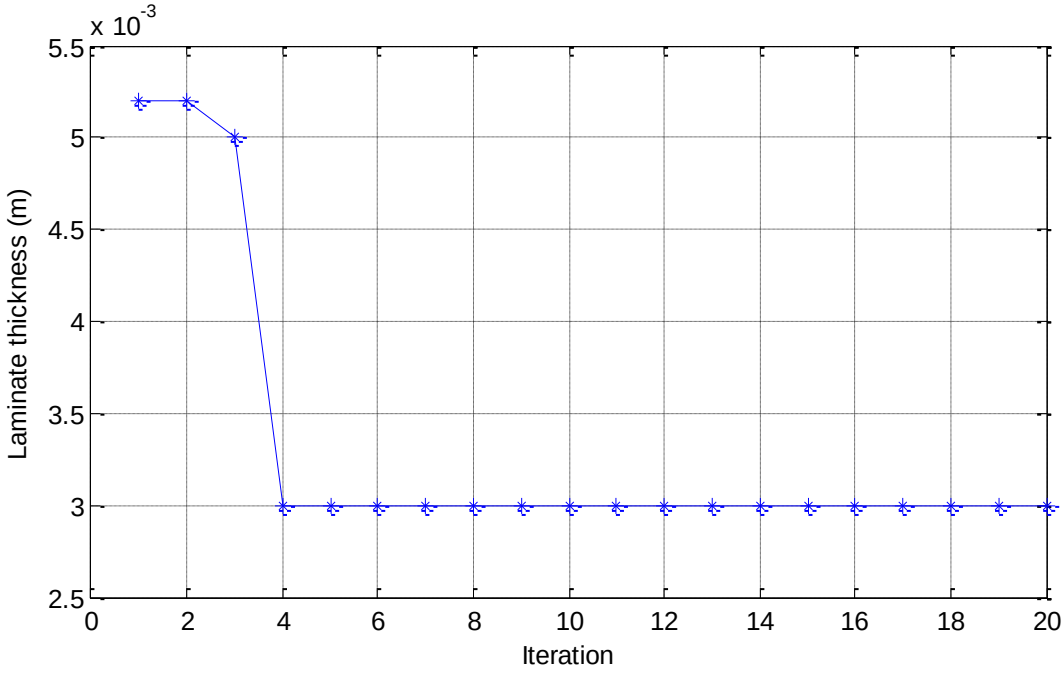

Fig. 9 Composite laminate thickness during SPSO iteration

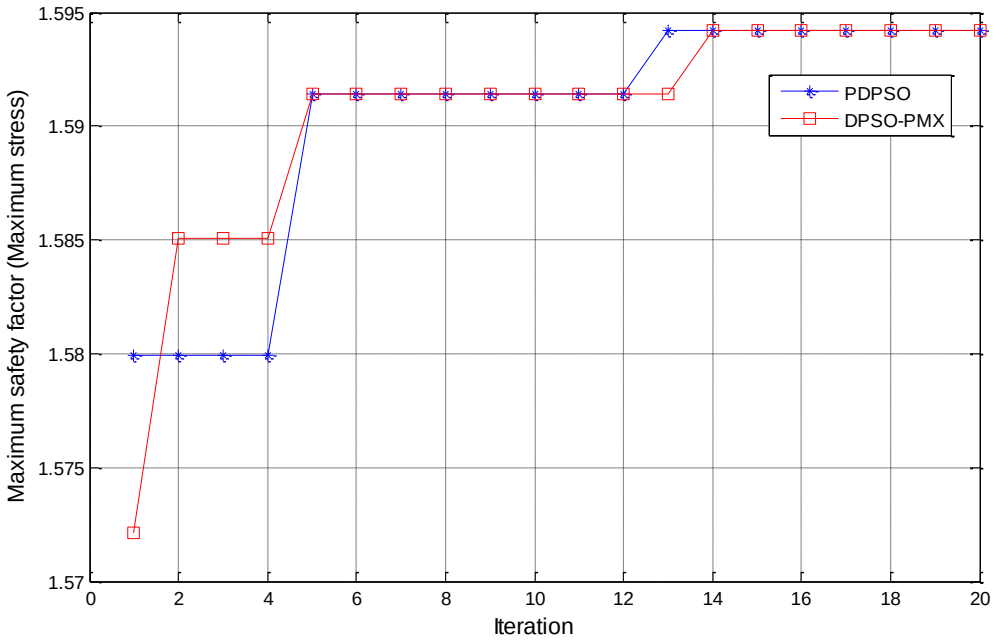

Fig. 10 Maximum safety factor vs. iteration (Maximum stress)

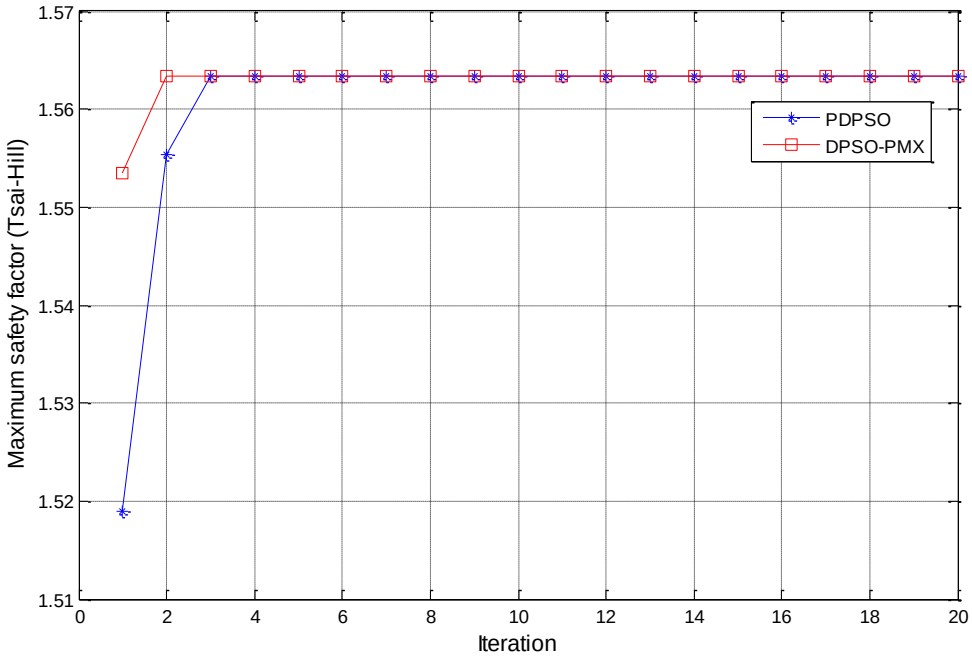

Fig. 11 Maximum safety factor versus iteration (Tsai-Hill)

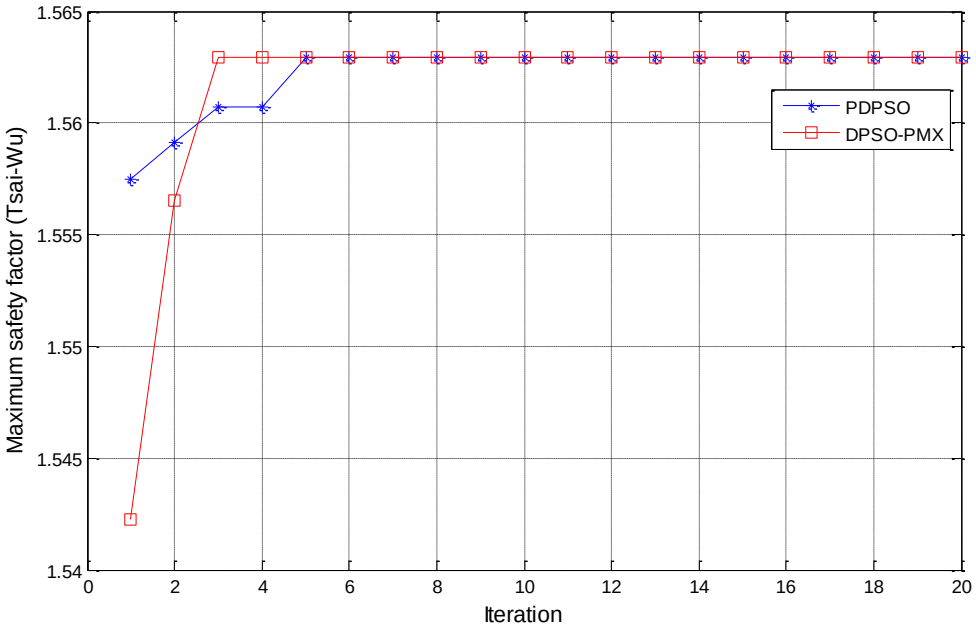

Fig. 12 Maximum safety factor versus iteration (Tsai-Wu)

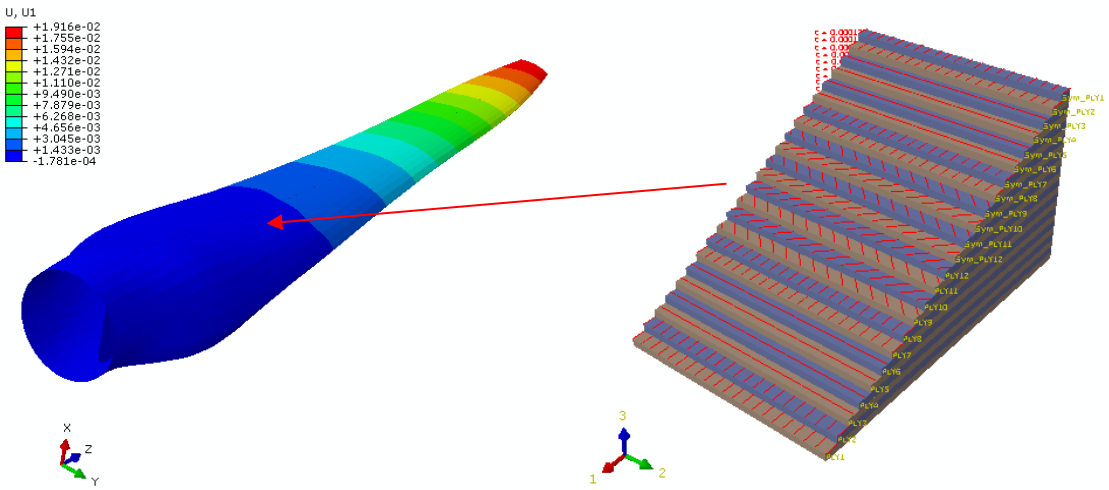

Fig. 13 Flapwise deflection of the composite blade with lay-up $[0_2/90_4/0_2/(\pm 45)_2]s$

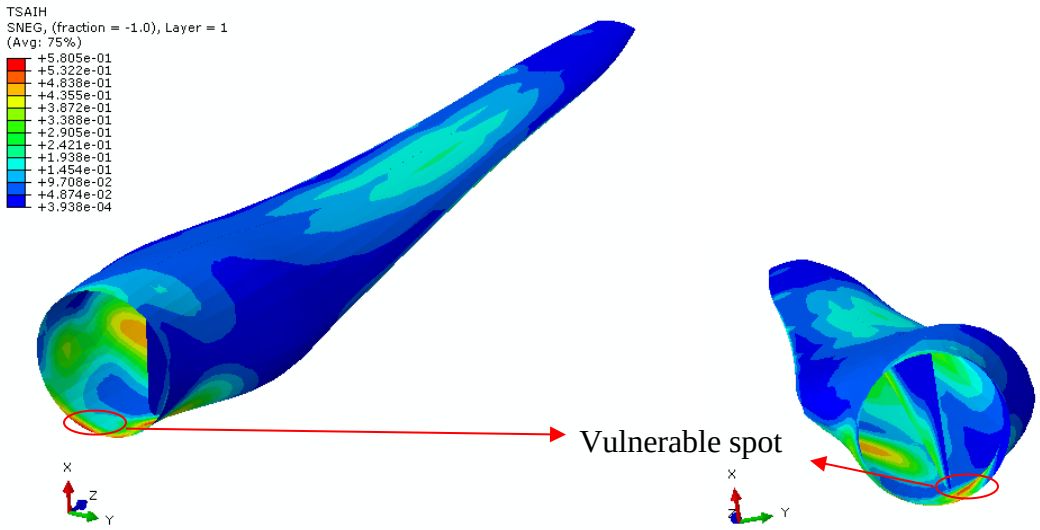

Fig. 14 Tsai-Hill failure index of the composite blade with lay-up $[0_2/90_4/0_2/(\pm 45)_2]s$

III. DESIGN AND PERFORMANCE EVALUATION OF A HYDROKINETIC COMPOSITE TURBINE SYSTEM

H. Li, G. A. Taylor, A. M. Abutunis, J. L. Rovey and K. Chandrashekhara

Department of Mechanical and Aerospace Engineering

A.R. Kashyap and J. W. Kimball

Department of Electrical and Computer Engineering

Missouri University of Science and Technology, Rolla, MO 65409

ABSTRACT

As an attractive alternative to existing renewable energy resources, the utilization of kinetic energy from the river is promising. Hydrokinetic turbine systems with "zero-head" and great mobility are advantageous over traditional dam based hydropower systems. Although sharing similar design principles as wind turbine systems, hydrokinetic turbine systems have significant differences in terms of free surface effects and cavitation. In this work, a three-blade horizontal axis hydrokinetic composite turbine system (12 inch diameter) was designed and tested in a water tunnel. Computational fluid dynamics (CFD) simulation was conducted for the chosen hydrofoil and to characterize hydrodynamic performance and wake flow of the hydrofoil. The result was validated with particle image velocimetry (PIV) measurements. A numerical model to predict performance of the turbine system was developed based on the modified blade element momentum (BEM) theory and a comparison between experiment and simulation were performed. The comparison indicated that the developed numerical model provided satisfactory prediction of the performance of the hydrokinetic composite turbine system.

1. INTRODUCTION

A hydrokinetic turbine system is an integrated turbine generator for electricity generation in free flows. No dam or diversion is required for such construction. The system offers multiple benefits, as compared to conventional dam based hydropower, such as less environmental and ecological impact, less initial cost of dam construction, and lower maintenance in operation. If the viable river and estuary locations for turbine installation are developed into hydroelectric power sites, the rivers and estuaries in US could provide up to 130, 000 gigawatt-hours per year which equals to half the annual production of the US dams (Sofge, 2009). Due to huge resources of hydroelectric power sites, the development of hydrokinetic turbine systems is promising.

In recent years, a few experiment and simulation combined research have been conducted on hydrokinetic turbine systems in prospective applications, including rivers, tides, ocean currents and wave. McCann et al. (2006) discussed the development of GH Tidal Bladed regarding tidal device modeling and standards development, a European design tool for tidal current turbines transformed from wind industry. To validate the code, Bahaj et al. (2007) conducted experimental hydrodynamic performance of a model 800 mm diameter turbine in a cavitation tunnel and a towing tank. Shaft power and thrust generated by the turbine at a series of blade pitches and speeds were obtained and compared with GH-Tidal Bladed. It was demonstrated that the experimental turbine performance can be adequately represented by the numerical code. Clarke et al. (2007) designed and tested a contra-rotating tidal current turbine, and power coefficient prediction is in good agreement with numerical prediction using modified blade element modeling theory. To improve power coefficient, Cecile et al. (2009) introduced the

concept of ducted turbine, and a power coefficient of 55% was obtained at a tip speed ratio (TSR) of 7. Apart from prototype level study, studies regarding operational parameters (Myers and Bahaj, 2004), effect from onset turbulence (Milne et al., 2010) and inertia (Whelan et al., 2009a), and free-surface/blockage correction (Whelan et al., 2009b) were performed. A complete summary of simulation based optimization methodology of tidal turbine blades can be found in Nicholls-Lee et al. (2008).

However, the study on hydrokinetic turbine systems is very limited and the mechanism of hydrokinetic turbine system operation is still not fully understood. With respect to the design and manufacturing consideration, different from conventional molded aluminum alloy/steel blades used in literature studies, composite rotors for marine/river applications are attractive and amounting to a promising new market sector (Marsh, 2009; Li and Chandrashekhara, 2012). Hence, in current efforts, a prototype of three-blade hydrokinetic composite turbine system was designed and evaluated in a water tunnel. The set of composite blades was manufactured using out of autoclave (OOA) process. The hydrofoil as blade elements was selected after conducting computational fluid dynamics (CFD) analysis and particle image velocimetry (PIV) testing. Based on the blade elemental study, an in-house code using modified blade element momentum (BEM) theory was developed to predict the performance of the turbine system. To validate numerical results, experimental testing of the turbine system was performed and torque/power outputs were obtained at various tip speed ratios (TSR) and blade pitches.

2. BLADE DESIGN AND MANUFACTURING

The composite blade designed has a length of 6 in. (152.4 mm, except root) and a width of 0.66 in. (16.76 mm). It has a constant cross section with blade elements of Eppler 395 (hydrofoil). No twist of the blade was introduced to better quantify design parameters and evaluate corresponding turbine performance using both experimental and simulation tools. A detailed discussion of hydrofoil selection as the element of the composite rotor is discussed in Section 3. Figure 1 shows the mold (ULTEM 9085) from Stratasys for manufacturing three identical composite blades. Two half molds were used for manufacturing the upper and bottom half blades. The composite blades manufactured were intended to be assembled as part of the three-blade horizontal axis turbine system.

Out of autoclave (OOA) manufacturing technique was employed in the manufacturing of the composite blades. The process begun with sanding the tool (ULTEM 9085) with Aluminum oxide 120/220 grit sandpaper and applying 4-5 coats of the sealant (FREKOTE B15) five minutes apart which was followed by the application of 3-4 coats of the release agent (FREKOTE 700nc). Once ready, the ULTEM mold was placed on an aluminum mold (a layer of breather was applied on the aluminum mold beforehand for easing trapped air removal). Three layers of unidirectional carbon prepreg (AS4/Cycom 5320) was cut to dimension and laid onto the ULTEM mold in the order of $90^{\circ}/0^{\circ}/90^{\circ}$ (Fig. 2a). Sufficient care was taken to ensure no trapped air was present between the layers. A layer of Fluorinated ethylene propylene (FEP) was placed on the laid out prepreg to ensure easy removal of the part after curing, after which an additional layer of breather was applied. After providing an outlet for the air, the entire mold was

vacuum bagged (Fig. 2b). Vacuum (28 in. of Hg) was applied and the sample was cured according to the manufacturer recommended cure cycle.

The manufactured upper and bottom half prepreg composite blades were matched and glued together. Additional machining steps were used to trim extra edges and boundaries before polishing the blade surface to achieve desired surface quality and dimensional accuracy, as shown in Fig. 3.

3. WATER TUNNEL EXPERIMENTAL SETUP

3.1 Hydrokinetic turbine system

The composite turbine system developed consisted of a three-blade rotor, transmission shafts and the generator (Fig. 4). The rotor hub had two halves that clamp three blades at root sections. Blade pitch was adjustable as per requirement, and was defined as the angle between blade tip chord and rotor plane. The mechanical power generated by the rotor was transmitted to the generator through the horizontal and vertical shafts which were interconnected by a pair of bevel gear. A hollow tube with small diameter was used to protect the vertical shaft while minimizing disturbance to the flow. A gear system was used to increase rpm from the shaft as input to the generator at a ratio of 1~5. The two parallel supporting beams housed the generator on top and were also used to hang the entire system into the water tunnel for testing.

3.2 Water tunnel test facility

The structural performance of a hydrokinetic turbine system was mainly characterized through power/power coefficient measurement. In this study, measurement

of torque and associated power output of the composite turbine system was carried out in a laboratory 1520HK water tunnel. Figure 5a shows the test section of the water tunnel with the turbine system installed. The center of horizontal shaft was aligned with the center of the cross section of water body, which avoids excessive boundary and free surface effects. The test section has a dimension of 60 in. x15 in. x20 in. (1524 mm x 381 mm x 508 mm), and a maximum water velocity of 1 m/s. A controlled environment of parametric testing was provided through manipulating the frequency of the motor which energized the water tunnel. To visualize and characterize flow of interest, particle image velocimetry (PIV) as a complete-flow-field technique with instantaneous velocity vector measurement in the cross-section of the flow was applied. A YAG laser sheet/ LaserPulse synchronizer along with a high resolution PowerView Plus 4M camera system were used (Fig. 5b). Accompanying Insight 4G PIV software was used for optical image processing. A summary of experiment setup is illustrated in Table 1.

4. HYDRODYNAMIC CHARACTERISTIC OF BLADE ELEMENT

4.1 Computational fluid dynamics analysis

Lift and drag coefficient data of blade elements along the blade span were required to calculate numerical torque and power generated by the turbine at given flow velocity and rotor rpm. Computational fluid dynamics (CFD) analysis was conducted in ANSYS CFX 12.0 to obtain the hydrodynamic coefficients of the blade elements (hydrofoil Eppler 395). The hydrofoil tends to provide a high ratio of C_l/C_d (Li et al., 2012). To get accurate results, coefficients of drag/lift at a low range of angle of attack

(0 º- 20 º) were calculated at the Reynolds number of turbine operation in the water tunnel. Fig. 6a shows the mesh of the flow field with finer mesh around the hydrofoil and wake region to better capture flow characteristics in these regions of interest. Totally 9350 quad-4 elements were used, and the K-Epsilon model was utilized to solve this fluid problem. A sample velocity contour around the hydrofoil at flow velocity 0.42 m/s and angle of attack (AOA) 6 º, which demonstrates much higher velocity (less pressure) at the suction side as compared to the pressure side, is shown in Fig. 6b. Lift and drag coefficients (C_l and C_d) versus varying AOA at different Reynolds numbers were obtained and shown in Fig. 7. Result indicates similar tendency of C_l and C_d at different Reynolds numbers. Linear and almost same C_l values are observed at low AOA below 8 °, and the hydrofoil stalls around 12 °, after which C_l decreases as AOA increases above 12 °. In this particular case, increasing Reynolds number tends to have lower lift coefficient in stall region which may be due to increasing separation area over the hydrofoil under such small Reynolds numbers. C_d increases gradually as AOA increases, and a higher slope is observed at higher AOA above 12 ° due to stall. Reynolds number has limited effect on C_d, although C_d seems high in all cases due to the low Reynolds number (viscous forces are dominant over inertial forces of flow). Viterna method (Viterna and Janetzke, 1982) was used to extend the hydrofoil datasheet obtained from CFD analysis into large AOA namely [-180 °, 180 °]. The complete hydrofoil datasheet generated served as the input to the numerical model developed for power prediction of the turbine system.

4.2 Particle Image Velocimetry (PIV)

PIV was used in this research to validate the CFD model developed for the blade elements. Flow behind the hydrofoil trailing edge was visualized and instantaneous 2D velocity measurement and related properties in the wake region were obtained. The wake region was selected for characterization of the flow around the hydrofoil due to the inability of the laser to see through the hydrofoil. The experiment started with the composite blade submerged into the water tunnel and fixed vertically at a specified pitch angle using a fixture. Seeding particles, same density as water, were dispersed in the running water tunnel for camera tracking/capturing. The laser was used to produce a laser sheet intersect the flow region of interest (parallel to the bottom of water tunnel, across the blade). The digital camera was positioned upwards to capture the laser lighted flow (Fig. 8). The synchronizer was used to control the laser, camera, and images shifter so that each component operated in the correct sequence. A computer with the Insight 4G software was connected to the camera synchronizer, and appropriate time step was set to have best particle tracing.

4.3 Validation of hydrodynamic characteristic of blade element

During PIV testing, a total of 100 digital images in time series were captured and processed in the Insight 4G software accompanied with the Tecplot 360 software. The 2D vector field was averaged and compared with CFD simulation results at the same condition for validation.

The scaled composite blade for testing has 2 in. chord and 10 in. length with a constant cross section of Eppler 395. The scaled blade was tested at flow velocity 0.35 m/s and AOA 12 º. A 4 in. x 6 in. (101.6 mm x 152.4 mm) block of the contour field was extracted with the trailing edge of the hydrofoil located at the center of the left edge (Fig.

9). Using a same color scale, the CFD result (Fig. 9b) showed a similar flow pattern as the PIV result (Fig. 9a). Due to the fact that the PIV result was from the averaged vector field over 100 images while the CFD result was only based on a static case (not dynamically averaged), a slight difference on the flow distribution was observed.

To better compare the flow velocity field, a line centered 2 in. (50.8 mm) away from the trailing edge of the hydrofoil was identified (Fig. 9), and the corresponding flow velocity vector (U) was monitored along the line and compared between CFD and PIV results (Fig. 10). The average flow velocity of the adjacent region for both results was around 0.35 m/s, although in the wake region close to the trailing edge, CFD analysis predicted less velocity (0.21 m/s) as compared to PIV testing (0.3 m/s). In addition to the "averaging" of vector field in PIV, the mismatch could also be attributed to the surface roughness of the composite blade and disturbance of freestream in the experiment.

5. PERFORMANCE EVALUATION OF THE TURBINE SYSTEM

Power output and power efficiency are the two key parameters of interest while characterizing turbine performance (Bahaj et al., 2007). In this section, an in-house code based on modified blade element momentum (BEM) theory was developed to predict the power and power coefficient of the composite turbine system. Meanwhile, water tunnel experiments on the built composite turbine system were conducted at various pitch angles and flow velocities to evaluate the performance.

5.1 Numerical power prediction

The BEM theory coupled the momentum theory and the blade element theory and was typically an iterative process to find the axial and tangential induction factors at every blade element (Hansen, 2008). When the variation of axial and tangential induction factors for a specific blade element in the subsequent iteration was less than an allowed tolerance (0.0001), the solution converged and the iteration process stopped. To improve solution accuracy, Prandtl tip loss, Glauert correction and hub loss were incorporated in the algorithm (Sale et al., 2009), the details of which can be found in Li et al. (2012). In the present work, only the calculation methods of torque, power and power coefficient of interest were discussed. As the lift and drag coefficients (C_l and C_d) of blade elements (hydrofoil) were extrapolated from the hydrofoil datasheet developed in Section 4, the lift L and drag D per unit blade station length can be computed:

$$L = \frac{1}{2}\rho V_{rel}^2 c C_l$$
$$D = \frac{1}{2}\rho V_{rel}^2 c C_d \quad (1)$$

where c is the hydrofoil chord length, ρ is flow density and V_{rel} is the relative flow velocity to the hydrofoil (defined in Fig. 11). The force normal (F_N) to and tangential (F_T) to the rotor plane, as shown in Fig. 11, can be obtained by using the angle ϕ between V_{rel} and the rotor plane:

$$F_N = Lcos\phi + Dsin\phi$$
$$F_T = Lsin\phi - Dcos\phi \quad (2)$$

These loads was integrated over the blade elements, assuming a linear load variation between blade radius r_i and r_{i+1}. For tangential loads,

$$F_T = \frac{F_{T,i+1}-F_{T,i}}{r_{i+1}-r_i}\mathrm{r}+\frac{F_{T,i}r_{i+1}-F_{T,i+1}r_i}{r_{i+1}-r_i} \quad (3)$$

The torque dM for each element dr can be calculated by:

$$\mathrm{dM} = (\frac{F_{T,i+1}-F_{T,i}}{r_{i+1}-r_i}r^2 + \frac{F_{T,i}r_{i+1}-F_{T,i+1}r_i}{r_{i+1}-r_i}r)dr \quad (4)$$

Upon integrating over the entire blade span, the total shaft torque for three composite blades was the sum of individual contribution from each blade element:

$$\mathrm{M} = 3\sum_{1}^{N-1}\left[\frac{1}{3}\frac{F_{T,i+1}-F_{T,i}}{r_{i+1}-r_i}(r_{i+1}^3-r_i^3)+\frac{1}{2}\frac{F_{T,i}r_{i+1}-F_{T,i+1}r_i}{r_{i+1}-r_i}(r_{i+1}^2-r_i^2)\right] \quad (5)$$

where N is the total blade station number. The power was calculated by $P = \omega\mathrm{M}$ and the corresponding power coefficient is $C_p = \frac{\omega\mathrm{M}}{0.5\rho\pi R^2U^3}$, where TSR=ωR/U, ω is the angular velocity of the rotating blade, R is the rotor radius, and U is the freestream velocity.

5.2 Turbine testing and data acquisition/processing

The composite turbine system built was tested in the water tunnel (Fig. 12). On top of the platform was the FUTEK reaction torque sensor (maximum torque 50 oz-in, 0.353 N·m) aligned with a C2 magnetic particle clutch (maximum torque 32 oz-in, 0.226 N·m) applied on top of the vertical shaft. The torque sensor was wired to a FUTEK USB device which continuously stored torque data and transported them to a LabVIEW interface program. The clutch was powered by a changeable current power supply which was used to adjust load/torque on the turbine and hence controlled the turbine rpm. The turbine rotation (rpm) was measured by a digital photo sensor tachometer (RPM range: 6-99999, accuracy: ± 0.05% plus 1 RPM) orthogonal to the vertical shaft. Pitch variation was achieved manually by adjusting the angle between rotor plane and blade tip chord. A protractor was used to measure the pitch angle. Frequency of the motor energizing the water tunnel was controlled to reach the aimed flow velocity. Data from continuous

monitoring of the torque/rpm measurement was post-processed in the LabView program. A summary of the data acquisition system is shown in Table 2.

5.3 Comparison of the performance of the turbine system with numerical simulation

The performance of the composite turbine system was evaluated in terms of power output and power coefficient at various pitch and flow velocity combinations. Table 3 illustrates the details of test matrix. Seven flow velocities (V1-V7, range: 0.222 - 0.422 m/s) and three pitch angles (10°, 12° and 15°) were used. Plots with TSR as the x-axis, were adopted to illustrate the performance of the turbine system. The turbine performance plots were generated from both the in-house numerical model and experimental data. The starting torque of the turbine system generally required flow velocity greater than V3, so the incomplete dataset for flow velocity V1 and V2 were not recorded. Figure 13 shows the power and TSR relationship at a fixed pitch angle 15 ° with increasing flow velocity (V3-V7). As a small scale turbine system, a power output less than 1 W was obtained, however, increased water velocity enhanced power output. A close correlation between simulation and experimental results was observed. Both power curves exhibited same tendency with increasing TSR. With the 15 ° pitch angle, the turbine had an optimal TSR of around 4.5 where the turbine had the maximum power output for specific flow velocities. Due to experimental restrictions (overcoming starting torque of the turbine system), experimental data was limited to the upper region of TSR and fewer data points was available at lower flow velocities.

The corresponding power coefficient curves under the identical condition as Fig. 13 is plotted in Fig. 14. In simulation results, almost identical C_p versus TSR curves (maximum C_p around 0.35) were obtained for various flow velocities. The identical C_p

versus TSR curve herein served as a representative curve available to characterize the performance of the turbine system. Deviation observed in the experiment results could be attributed to statistical variance. Due to less experimental power as shown in Fig. 13, accordingly lower experimental C_p was obtained at the same TSR as compared to simulation results. The turbine system with the 15 ° pitch angle tended to be operated near the stall condition thus reducing the power yield.

Figures 15 and 16 show the power and power coefficient versus TSR at varying pitch angles (10 °-15 °) but fixed flow velocity (V6: 0.4 m/s). With decreasing pitch angle, higher power output and power coefficient were generated in the experiment. It was inferred that the optimal operating pitch of the turbine system should be around 10 ° to prevent stall phenomena of the turbine system at higher pitches. However, in simulation results, there was no significant difference in power and power coefficient at low TSR (less than 4). Although at high TSR (greater than 4), there was slight difference between 10 ° and 12 ° and higher for 15 °. The difference between simulation and experimental results indicated that the effect of free surface and blockage in water tunnel testing that could influence the turbine performance. These factors were applicable for the current test setup, given limited cross section (15 in. x20 in. or 381 mm x 508 mm) of the tunnel and large sweeping area of the turbine (R=6 in. or 152.4 mm). Reduced pitch angles in experiment resulted in enlarged blockage to the cross section of the water tunnel, which in turn enhanced the power output/performance of the turbine system. A correction to the power/power coefficient and flow velocity obtained from experiment would be necessary to improve the performance prediction of the turbine system. In the current phase, a blockage correction was applied through reduction in C_p by 30% (Fig. 16) with P

unchanged (Fig. 15), and better results were illustrated. A detailed study of free surface and blockage effect in the numerical model would also benefit the performance prediction of the composite turbine system operated in a small scale water tunnel.

6. CONCLUSION

A small scale three-blade horizontal axis hydrokinetic composite turbine system was designed, manufactured and tested in a water tunnel. To characterize the hydrodynamic coefficients of the chosen hydrofoil Eppler 395, CFD analysis and PIV testing were conducted and both showed a close matching with each other in terms of flow vector field. An in-house numerical simulation model, based on the hydrofoil datasheet generated from CFD analysis, was hereby developed to predict the performance of the composite turbine system. To validate the numerical model, the composite turbine system was operated in the water tunnel at a series of flow velocities and pitches with rpm and torque monitored. A close correlation of power and power coefficient between simulation and experimental results was observed. The study provides a helpful tool for understanding operating principles of hydrokinetic turbine systems and conducting parametric studies from both simulation and experiment point of view. To better characterize the hydrokinetic composite turbine system, the numerical simulation model requires incorporating free surface and blockage effects and a broader range of TSR and flow velocities needs to be tested.

REFERENCES

Bahaj, A., Battern, W. and McCann, G., "Experimental verifications of numerical predictions for the hydrodynamic performance of horizontal axis marine current turbines," Renewable Energy, Vol. 32(15), pp. 2479-2490, Oct. 2007.

Clarke, J., Connor, G., Grant, A. and Johnstone, C., "Design and testing of a contra-rotating tidal current turbine," Proceedings of the Institution of Mechanical Engineers, Part A: Journal of Power and Energy, Vol. 221(2), pp. 171-179, 2007.

Cecile, M., Marcel, V., Joao, G., Romain, L., Paul, G. and Francois, A., "Design and Performance Assessment of a Tidal Ducted Turbine," 3rd IAHR International Meeting of the Workgroup on Cavitation and Dynamic Problems in Hydraulic Machinery and Systems, pp. 571-581, Brno, Czech Republic, Oct., 2009.

Hansen, M., "Aerodynamics of Wind Turbines," UK: Earthscan, 2008

Li, H., Chandrashekhara, K. and Mishra, R. S., "Fatigue Life Investigation for a Medium Scale Composite Hydrokinetic Turbine Blade," Society for the Advancement of Material and Process Engineering (SAMPE) 2012. Baltimore, Maryland, May 21-24, 2012.

Li, H. and Chandrashekhara, K., "Structural Optimization of Laminated Composite Blade Using Particle Swarm Optimization," Proceedings of ASME 2012 International Mechanical Engineering Congress & Exposition (IMECE 2012). Houston, Texas, November 9-15, 2012.

Marsh, G., "Wave and Tidal Power—an Emerging New Market for Composites," Reinforced Plastics, Vol. 53(5), pp. 20-24, 2009.

McCann, G., Rawlinson-Smith, R. and Argyriadis, K., "Load Simulation for Tidal Turbines using Wind Turbine Experience," Garrad Hassan and Partners Ltd & Germanischer Lloyd WindEnergie GmbH, 2006.

Milne, I., Sharma, R., Flay, R. and Bickerton, S., "The Role of Onset Turbulence on Tidal Turbine Blade Loads," Proceedings of the 17th Australasian Fluid Mechanics Conference, Auckland, New Zealand, Dec. 5-9, 2010.

Myers, L. and Bahaj, A. "Basic Operational Parameters of a Horizontal Axis Marine Current Turbine," Proceedings of 8th World Renewable Energy Congress, Denver, USA, November, 2004.

Nicholls-Lee, R., Turnock, S. and Boyd, S., "Simulation based Optimization of Marine Current Turbine Blades," Proceedings of the 7th International Conference on Computer and IT Applications in the Marine Industries (COMPIT'08), pp. 314-328, Liege, Belgium, April 21-23, 2008.

Sale, D., Jonkman, J. and Musial, W., "Hydrodynamic Optimization Method and Design Code for Stall-Regulated Hydrokinetic Turbine Rotors," ASME 28th International Conference on Ocean, Offshore, and Arctic Engineering, American Society of Mechanical Engineers (ASME), NREL/CP-500-45021, Honolulu, Hawaii, May 31-June 5, 2009.

Sofge, E., "Underwater Wind Turbines Tap River Energy," (Magazine Website), Popular Mechanics, Oct., 2009.

Viterna, L. and Janetzke, D., "Theoretical and Experimental Power from Large Horizontal-Axis Wind Turbines," No. DOE/NASA/20320-41; NASA TM-82944, National Aeronautics and Space Administration, Cleveland, OH, Lewis Research Center, 1982.

Whelan, J., Graham, J. and Peiro, J., "Inertia Effects on Horizontal Axis Tidal-Stream Turbines," Proceedings of the 8th European Wave and Tidal Energy Conference, Uppsala, Sweden, 2009a.

Whelan, J., Graham, J. and Peiro, J., "A free-surface and Blockage Correction for Tidal Turbines," Journal of Fluid Mechanics, Vol. 624(1), pp. 281-291, 2009b.

Table 1 Summary of water tunnel experimental testing setup

Experimental testing components	Specification
1520HK water tunnel	Test section: 60 in. x15 in. x20 in. (1524 mm x 381 mm x 508 mm), up to 1 m/s
Laser synchronizer	YAG laser sheet/ LaserPulse synchronizer
High resolution camera system	PowerView Plus 4M camera system with 28-mm F/2.8 Af Nikkor lens
Optical image processing software	Insight 4G and Tecplot 360 software

Table 2 Summary of the testing data acquisition system

Data acquisition system components	Specification
FUTEK reaction torque sensor	Maximum torque 50 oz-in, 0.353 N·m
Turbine rpm control	C2 magnetic particle clutch
Digital photo sensor tachometer (turbine rpm measurement)	RPM range: 6-99999, accuracy: ± 0.05% plus 1 RPM
Blade pitch control	Manual adjustment with protractor
Water tunnel (flow velocity control)	Motor frequency adjustment (range: 0 - 1 m/s)

Table 3 Test matrix of the turbine testing

Test parameters	Values
Pitch angle	10°, 12°, 15°
Flow velocity	V1: 0.222 m/s, V2: 0.312 m/s, V3: 0.334 m/s, V4: 0.356 m/s, V5: 0.378 m/s, V6: 0.400 m/s, V7: 0.422 m/s

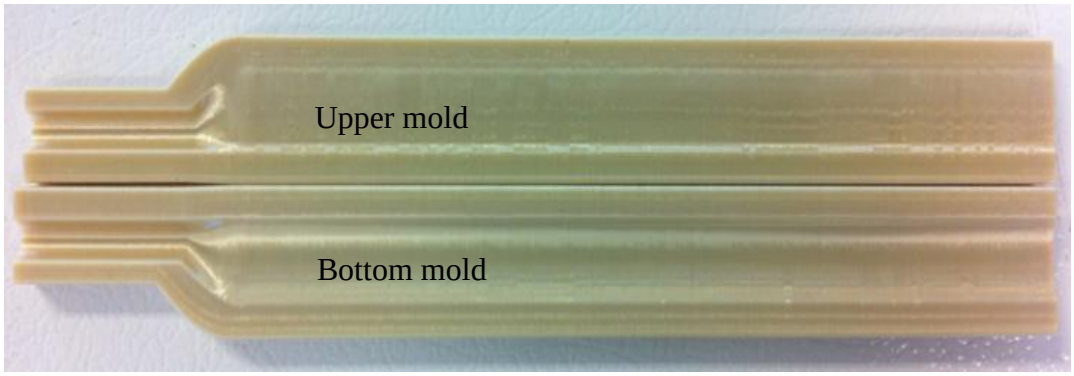

Fig. 1 Blade mold (upper/bottom half mold)

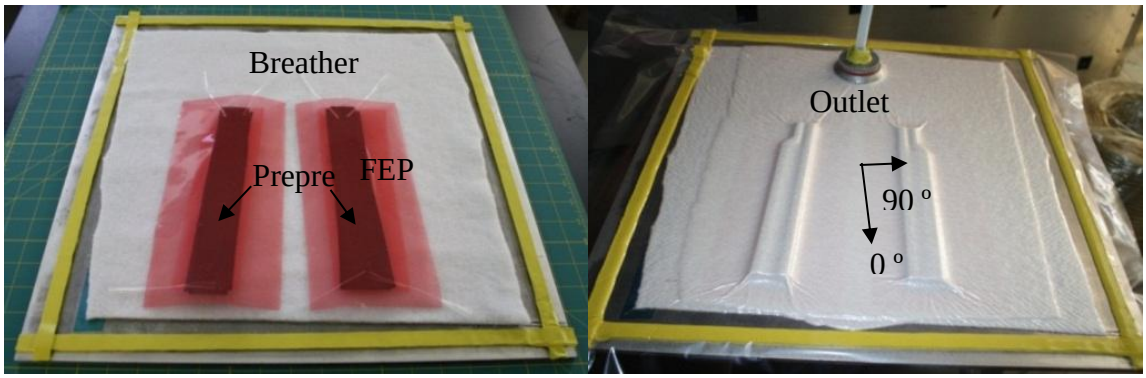

(a) (b)

Fig. 2 The manufacturing process of composite blades using carbon prepreg (a) out of autoclave setup process (b) vacuum bagged for curing

Fig. 3 Manufactured AS4/Cycom 5320 composite blades

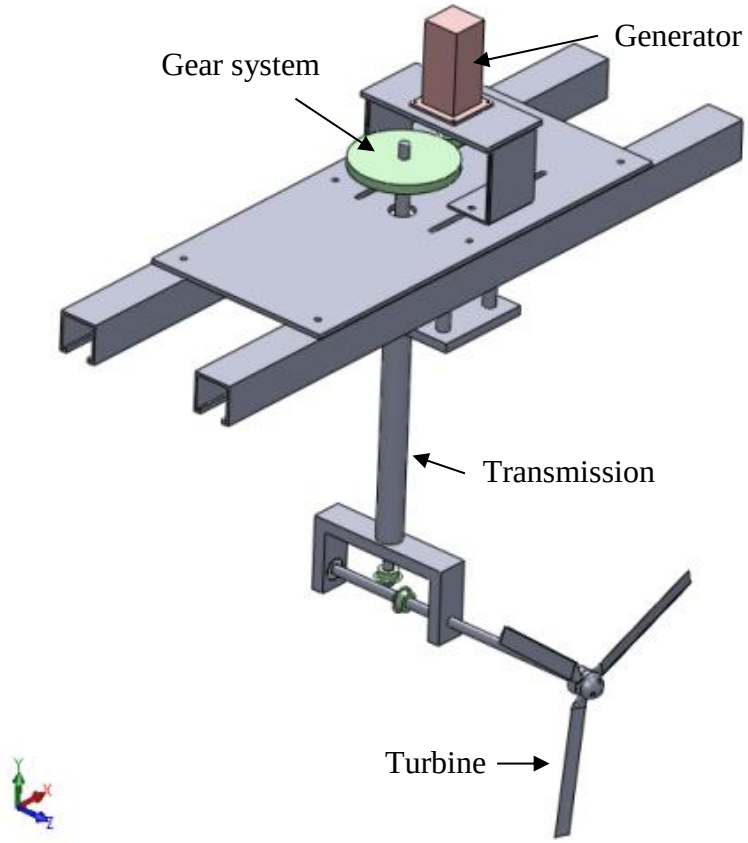

Fig. 4 The CAD model of the hydrokinetic turbine system

(a) (b)

Fig. 5 Test section of the water tunnel (a) composite turbine system installed (b) components of particle image velocimetry

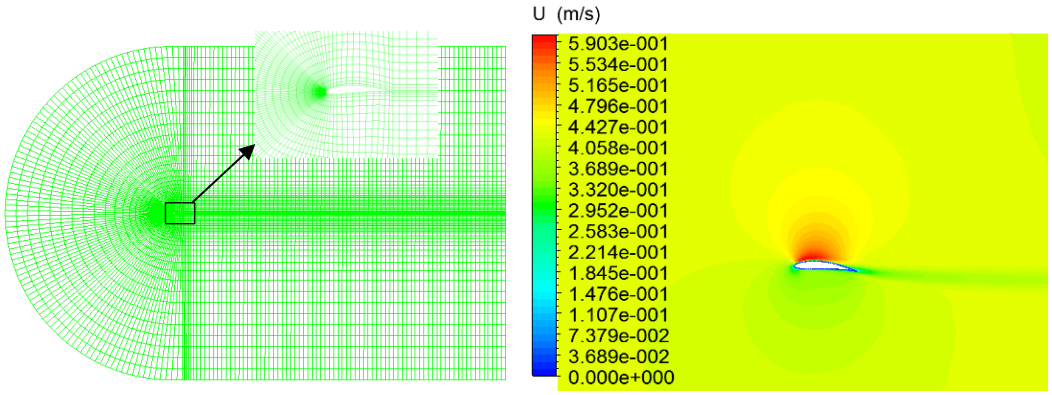

(a) (b)

Fig. 6 CFD model of flow field around the hydrofoil (a) mesh of the flow field (b) velocity contour around the hydrofoil (flow velocity 0.42 m/s, angle of attack 6 ٩)

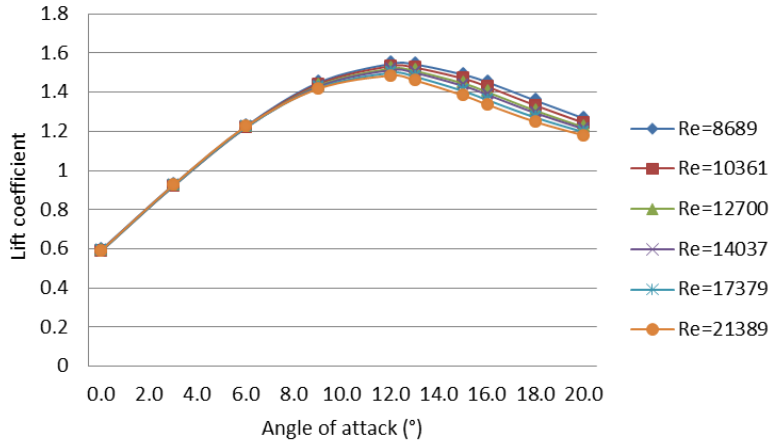

(a)

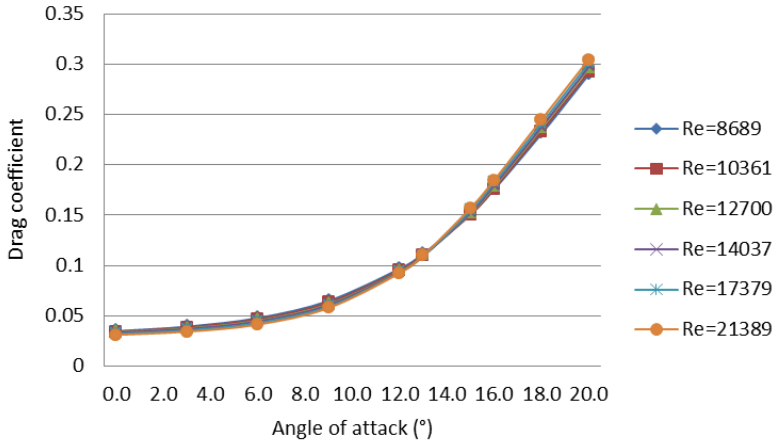

(b)

Fig. 7 Hydrodynamics of the hydrofoil at different AOA and Reynolds numbers (a) C_l versus AOA (b) C_d versus AOA

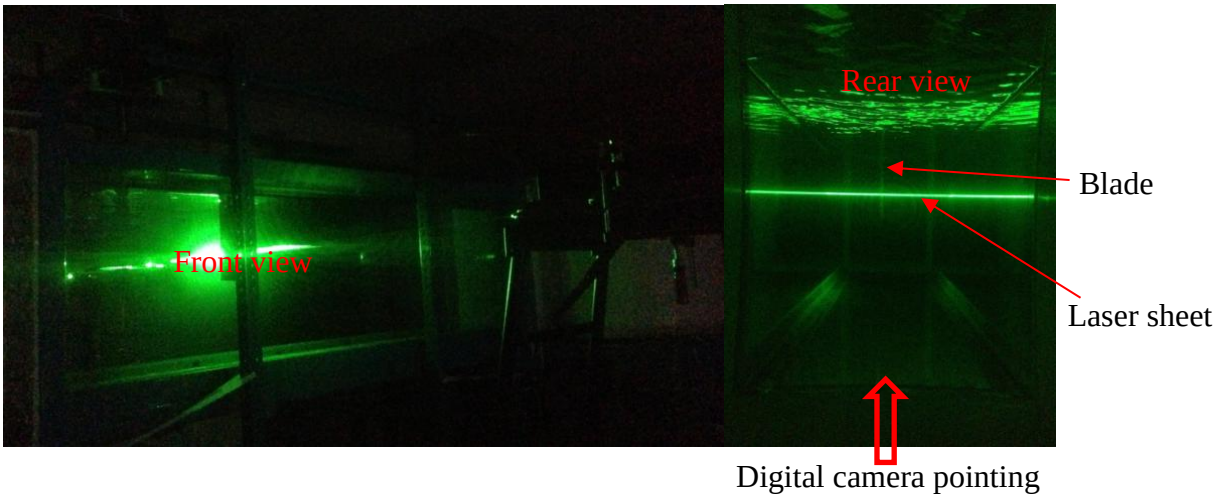

Fig. 8 Operation of the PIV system

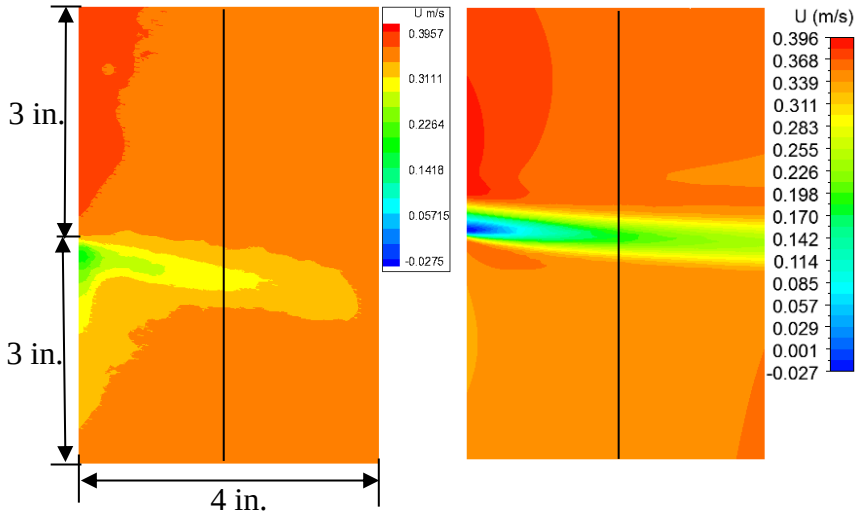

(a) (b)

Fig. 9 Flow velocity field (U) behind the hydrofoil obtained by a) PIV b) CFD

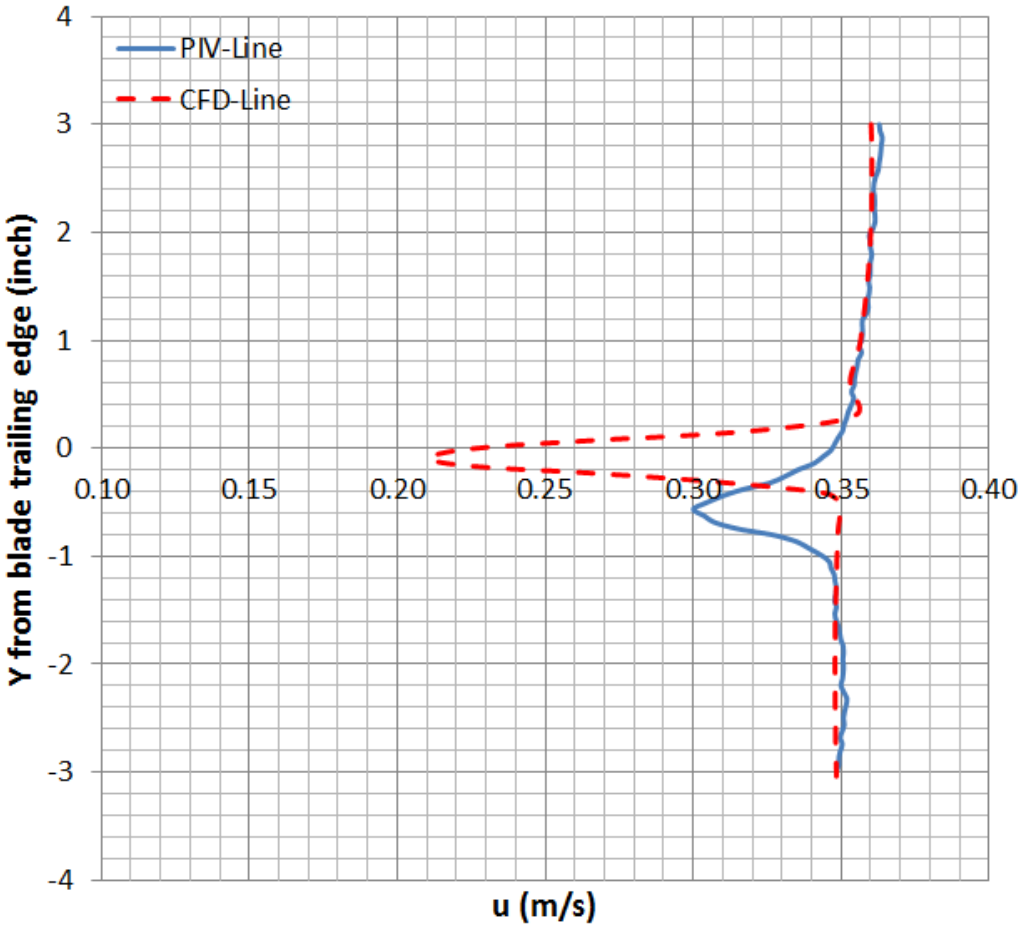

Fig. 10 Velocity vector field (U) along the line 2 in. away from the trailing edge

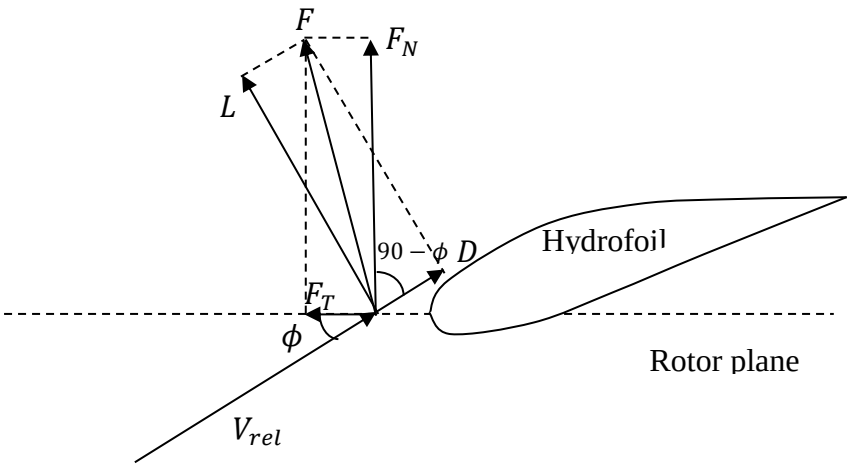

Fig. 11 Load integration on a typical hydrofoil

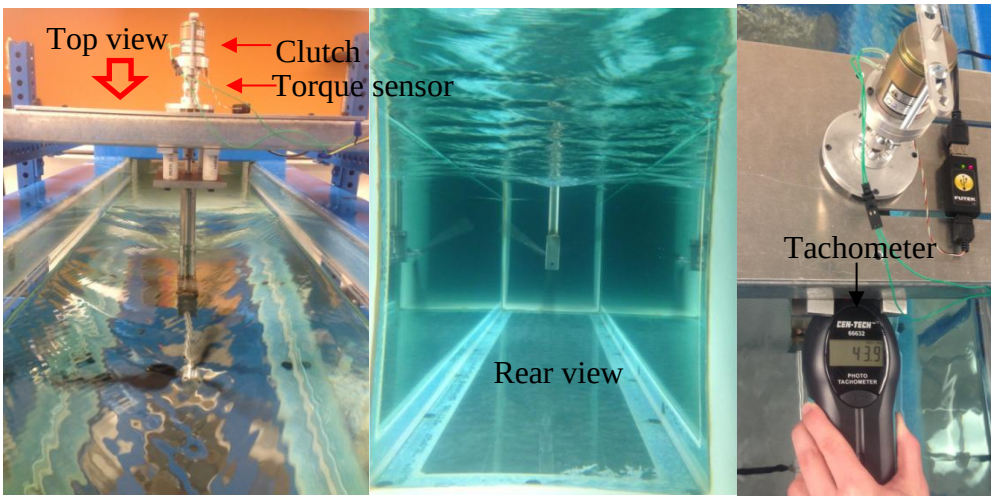

Fig. 12 Turbine in operation and testing in water tunnel

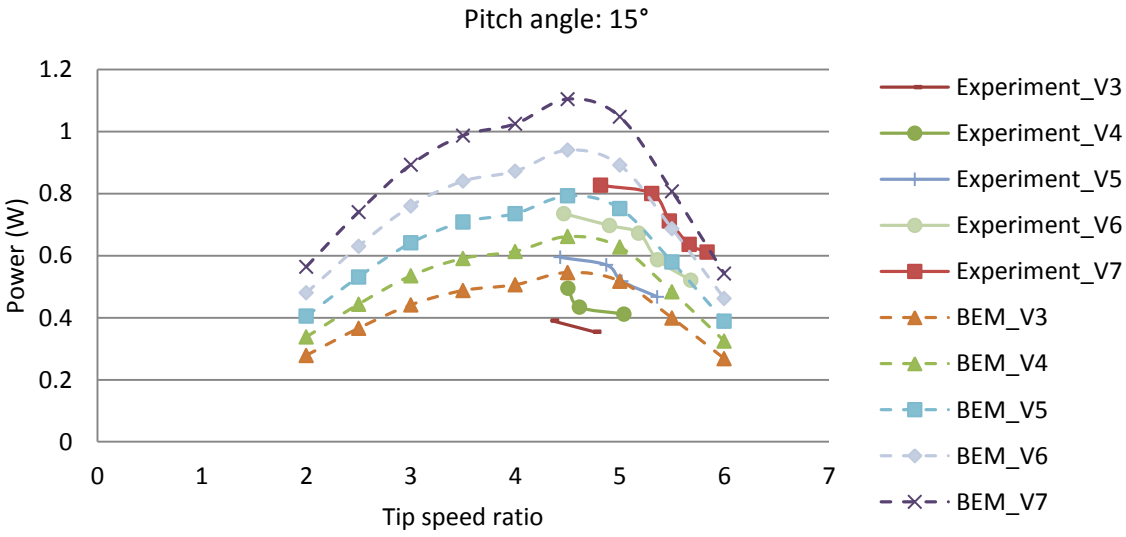

Fig. 13 Power versus TSR at fixed pitch (15 °) and various water velocities (V3-V7)

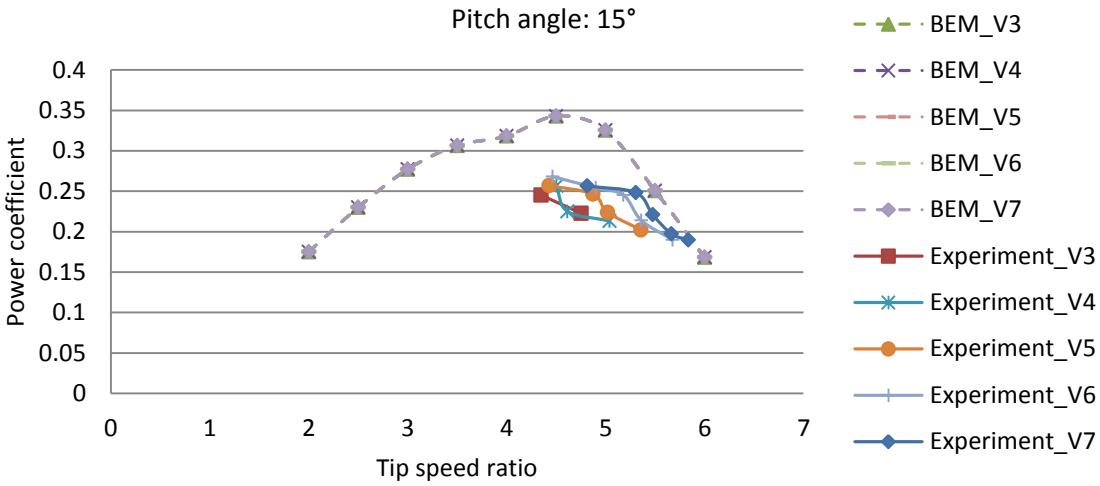

Fig. 14 Power coefficient (C_p) versus TSR at fixed pitch (15 ٩) and various water velocities (V3-V7)

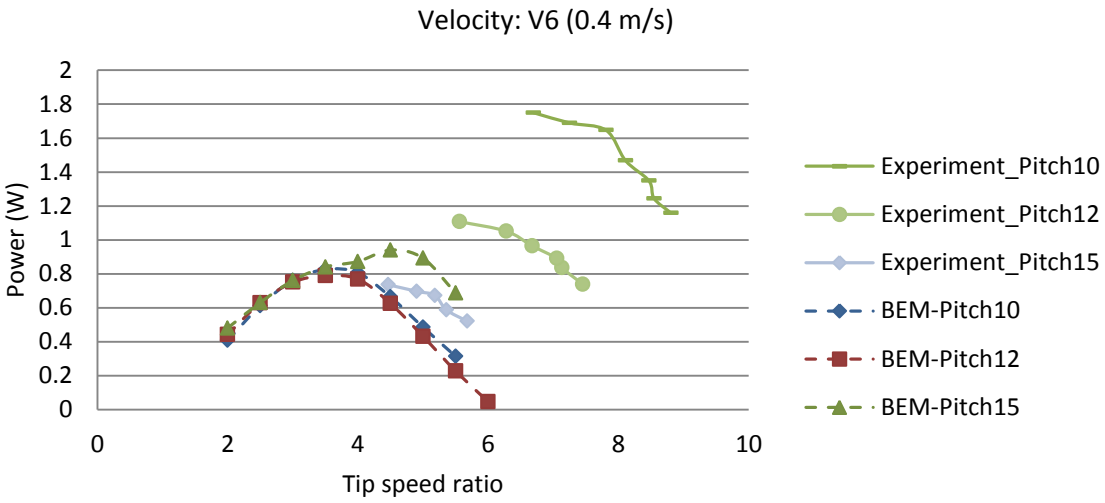

Fig. 15 Power versus TSR at fixed flow (V6) and various pitch angles (10 °-15 °)

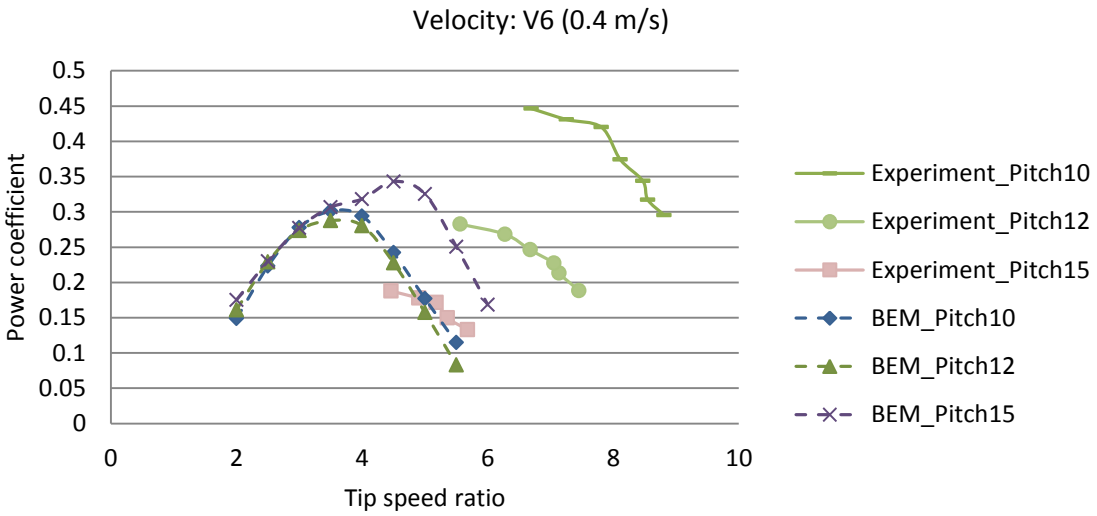

Fig. 16 C_p versus TSR at fixed flow (V6) and various pitch angles (10 °-15 °)

SECTION

4. CONCLUSIONS

The first paper of this work offers a methodology for the reliability-based fatigue life investigation of a median scale composite hydrokinetic turbine blade. A modified BEM-FEM coupled method was developed and implemented to determine the stress response of the composite turbine blade under varying hydrokinetic loads. The model was derived from the MSU/DOE fatigue database and a constant life diagram was hereby developed. A metamodel with respect to stress response was established to study effects of scatter in S-N data on fatigue life distribution and sensitivity of composite stiffness and ply orientation on probability of fatigue failure. The composite blade was capable of operating for more than 20 years. The probability of fatigue failure is most sensitive to E_{22} (the blade transverse direction). The second ply and third ply, among four plies, contributed more positively to the probability of fatigue failure. Also, the river velocity model only slightly influenced the fatigue failure probability. The model developed here can be used to study the fatigue life and probability of fatigue failure of various composite hydrokinetic turbine blade designs.

The second paper developed a two-step online automated structural optimization algorithm for composite hydrokinetic turbine blades using PSO. During the first step, ply thickness, layer numbers and ply orientation were optimized for optimal blade weight using SPSO. In the second step, Discrete PSO was used to optimize stacking sequence to improve the blade structural performance. The introduction of valid/invalid exchange and memory checking successfully avoided trapping in local optimal solutions. The modified

BEM-FEM method was implemented to find the failure index of the composite blade under extreme hydrokinetic loads. The particle position update and optimal position search process was automated in MATLAB coupling the nonlinear finite element blade model in ABAQUS. The weight targeted SPSO significantly reduced the composite blade weight, and stacking sequence optimization improved the blade load-carrying capacity. The developed model is applicable to a larger scale of composite blade with loose lay-up constraints in terms of more number of uncustomary ply orientations and plies, and more flexible sequence alteration. More significant weight savings and structural performance improvement with relatively less optimization time can be achieved.

The third paper extended the developed mathematic model to design and test a three-blade horizontal axis hydrokinetic composite turbine system in a water tunnel. CFD analysis and PIV testing were conducted to characterize the chosen hydrofoil Eppler 395. A close matching of flow vector field between CFD analysis and PIV experimental testing was demonstrated. An in-house simulation model predicting the performance of the turbine system, based on the modified BEM, was developed. The hydrodynamic characterization of blade hydrofoil was performed using CFD, and served as an input to the simulation model for turbine performance prediction. The prototype hydrokinetic turbine system was tested in water tunnel at various flow velocities and pitches. The rotational speed and torque were monitored during operation. The power and power coefficient of the prototype composite turbine system were studied. A close correlation between the simulation model and experimental results was observed. Also, the effect of pitch angle, water velocity and tip-speed ratio on the performance of the turbine system

performance were studied. The model and experimental testing provide a means to study and characterize prototype level composite hydrokinetic turbine systems.

The research presented here can be extended in several ways. Future research could use the modified BEM-FEM algorithm to design and analysis various blade shapes and structures. The reliability-based fatigue life and probability of fatigue failure can be used to study other different scale blade configurations. The PSO algorithm developed exclusively for the composite blade can be used to optimize different baseline blade structures accounting for detailed composite lay-up information. The automated analysis and optimization algorithm coupling MATLAB and ABAQUS can be used to quicken the composite blade design process, and can be extended to study other composite structures as well. The validated model and experimental testing for performance evaluation of composite turbine systems can be extended to study other types of composite hydrokinetic turbine systems, like turbines with six blades or co-axial multi-turbine systems.

BIBLIOGRAPHY

Bahaj, A., Battern, W. and McCann, G.,"Experimental Verifications of Numerical Predictions for the Hydrodynamic Performance of Horizontal Axis Marine Current Turbines," Renewable Energy, Vol. 32(15), pp. 2479-2490, Oct. 2007.

Bir, G. S., Lawson, M. J. and Li, Y., "Structural Design of a Horizontal-axis Tidal Current Turbine Composite Blade," Proceedings of the 30th International Conference on Offshore Mechanics and Arctic Engineering (OMAE ASME 2011), Vol. 5, pp. 797-808, Rotterdam, Netherlands, June 19-24, 2011.

Cecile, M., Marcel, V., Joao, G., Romain, L., Paul, G. and Francois, A., "Design and Performance Assessment of a Tidal Ducted Turbine," 3rd IAHR International Meeting of the Workgroup on Cavitation and Dynamic Problems in Hydraulic Machinery and Systems, pp. 571-581, Brno, Czech Republic, Oct., 2009.

Clarke, J., Connor, G., Grant, A. and Johnstone, C., "Design and Testing of a Contra-rotating Tidal Current Turbine," Proceedings of the Institution of Mechanical Engineers, Part A: Journal of Power and Energy, Vol. 221(2), pp. 171-179, 2007.

Degrieck, J. and Paepegem, W.V., "Fatigue Damage Modeling of Fibre-reinforced Composite Materials: Review," Applied Mechanics Reviews, Vol. 54(4), pp. 279-300, 2001.

Forcier, L. C. and Joncas, S., "Development of a Structural Optimization Strategy for the Design of Next Generation Large Thermoplastic Wind Turbine Blades," Structural and Multidisciplinary Optimization, Vol. 45(6), pp.889-906, 2012.

Lange, C. H., "Probabilistic Fatigue Methodology and Wind Turbine Reliability," Sandia National Laboratory report: SAND96-1246, 1996.

Mandell, J.F. and Samborsky D.D., "DOE/MSU Composite Material Fatigue Database," Sandia National Laboratories, SAND97-3002, Vol. 19, http://windpower.sandia.gov, March 31, 2010.

McCann, G., Rawlinson-Smith, R., and Argyriadis, K., "Load Simulation for Tidal Turbines using Wind Turbine Experience," Garrad Hassan and Partners Ltd & Germanischer Lloyd WindEnergie GmbH, 2006.

Nijssen, R.P.L., "Fatigue Life Prediction and Strength Degradation of Wind Turbine Rotor Blade Composite," Graduate Thesis, November, 2006.

Poulose, P. and Hu, Z., "Strength Evaluation and Failure Predication of a Composite Wind Turbine Blade using Finite Element Analysis," Proceedings of ASME International Mechanical Engineering Congress and Exposition, IMECE 2010, Vol. 3, pp. 295-301, Vancouver, BC, Canada, November 12-18, 2010.

Sofge, E., "Underwater Wind Turbines Tap River Energy" (Magazine Website), Popular Mechanics, Oct., 2009.

Sutherland, H.J. and Mandell, J.F., "Optimized Constant-life Diagram for the Analysis of Fiberglass Composites Used in Wind Turbine Blades," Journal of Solar Energy Engineering, Vol. 127, pp. 563-569, November 2005a.

Sutherland, H.J. and Mandell, J.F., "The Effect of Mean Stress on Damage Predictions for Spectral Loading of Fibreglass Composite Coupons," Wind Energy, Vol. 8, pp. 93-108, 2005b.

Shokrieh, M.M. and Rafiee, R., "Simulation of Fatigue Failure in a Full Composite Wind Turbine Blade," Composite Structures, Vol. 74, pp. 332-242, 2006.

Samborsky, D.D., Wilson, T.J., Agastra, P. and Mandell, J.F., "Delamination at Thick Ply Drops in Carbon and Glass Fiber Laminates Under Fatigue Loading," Journal of Solar Energy Engineering, Vol. 130, pp. 031001-1-8, August 2008.

Young, Y. L., Baker, J.W. and Motley, M.R., "Reliability-based Design and Optimization of Adaptive Marine Structures," Composite Structures, Vol. 92(2), pp. 244-253, January 2010.

Zhu, S. and Rustamov, I., "Structural Design and Finite Element Analysis of Composite Wind Turbine Blade," 11th International Conference on Fracture and Damage Mechanics, FDM 2012, Vol. 525-526, pp. 225-228, Xian, China, September 18-21, 2012.

VITA

Mr. Haifeng Li was born in Zhoushan, Zhejiang, the People's Republic of China. He was admitted to Chongqing University, Chongqing, China in 2003 and received his B.S. degree in Mechanical Engineering in 2007. After that, he began his graduate study in Chongqing University, Chongqing, China and received his M.S. degree in Mechanical Engineering in 2010.

Since August 2010, Mr. Haifeng Li has been enrolled in the Ph.D. Program in Mechanical Engineering at Missouri University of Science and Technology (formerly University of Missouri-Rolla), Rolla, Missouri, USA. He has served both as Graduate Research Assistant and Graduate Teaching Assistant between August 2010 and July 2014 in the Department of Mechanical and Aerospace Engineering. In December 2014, he received his Ph.D. degree in Mechanical Engineering from Missouri University of Science and Technology, Rolla, Missouri.